Distinct patterns of overlapping neural representation of sensorimotor variables in primary and associative motor areas: Insights from chronic intracortical recordings in the human brain

Thesis by

Kelly Kadlec

In Partial Fulfillment of the Requirements for
the degree of
Doctor of Philosophy

CALIFORNIA INSTITUTE OF TECHNOLOGY
Pasadena, California

2025
(Defended July 23, 2024)

Kelly Kadlec
ORCID: 0000-0002-8765-7253

ACKNOWLEDGEMENTS

The work in this thesis happened because of three individuals who dedicated more to this research than I ever could. Thank you, participants and BCI pioneers, JJ, RD, and NS. Thank you for your endless patience as I learned how to be a scientist. Thank you for letting me listen to– and even see!– your brains. And thank you for your generosity and kindness. Each of you has had more of an impact on my life than you could ever know, and I am so grateful to you for everything.

I would also like to thank the Andersen lab, my family, and friends, and my partner. Thank you for supporting and inspiring me.

ABSTRACT

Although many of the movements we make are produced without much conscious thought, motor control requires the coordination of multiple brain areas and several complex processes to occur as seamlessly as it does, two of which are primary motor cortex (MC) and posterior parietal cortex (PPC). Traditional views of the organization of these areas have mapped separate parts of the body, or effectors, onto separate areas of cortex. However, recent findings that show extensively overlapping representations of different effectors within small populations of neurons in both motor and posterior parietal cortices have reignited a debate over the organization of each area. The studies in this thesis aim to reconcile these conflicting records through a unique opportunity to directly compare between single neuron recordings in both areas in human participants chronically implanted with intracortical electrode arrays. The functional organization of these areas was investigated during movement of different parts of the body in different contexts. In the first study, I found that the entire body is represented within small patches of both MC and PPC, but with a clear emphasis on a single part of the body in MC. In PPC, although single neurons showed specialization for particular effectors, there were an equal number of neurons specialized for every effector resulting in an equal strength in representation of the population across effectors. In the second study, I investigated how spatial information was represented across different effectors. In particular, it has previously been reported that some areas within PPC represent location of an object in space relative to the position of one's eyes, or in an eye-centered coordinate frame, while other areas represent location in space as relative to the position of one's body, for example a hand-centered coordinate frame. We find that the population in PPC flexibly changes the coordinate frame it encodes the location of a visual

target in from hand centered during a reach paradigm to eye-centered during a delayed saccade paradigm. In contrast to the multiple coordinate frames coded by the population in PPC, in MC the population predominantly encoded spatial location in hand-centered coordinates during reaches. The flexibility seen in the population results in PPC motivate the study of Chapter 4, where I explore these changing coordinate frames in more detail at the single neuron level. I found that the distinct coordinate frames are encoded by almost entirely separate sets of neurons, with very few neurons engaged in both task. Overall, these results show clearly distinct organization of motor variables within MC and PPC, and offer important insights into the possible functions of each region both within and beyond motor control. In addition, they highlight a need to continue exploring how neurons within a defined region respond beyond their traditionally associated functional roles.

TABLE OF CONTENTS

LIST OF ILLUSTRATIONS AND/OR TABLES

Number *Page*

NOMENCLATURE

BMI: brain-machine interface, also known as a brain-computer interface (BCI)

contralateral: side of the body on the opposite side of the implant

coordinate frame: the way position is spatially described by a reference point, for example to describe a position by its location relative to the position of the eyes would be an eye-centered coordinate frame (also called: reference frame)

cortical map: A segmenting of different functions to different anatomical locations in the brain

crossnobis: cross-validated Mahalanobis distance

effector: part of the body (e.g. right ankle)

fixation: maintaining eye position at a focus point

fMRI: functional magnetic resonance imaging

G-T: a vector that describes the position of a visual target relative to gaze position (eye position)

H-G: a vector that describes the position of the hand relative to the position of the gaze

H-T: a vector that describes the position of a visual target relative to hand position

implant: an intracortical electrode array that is inserted into the a brain

ipsilateral: side of the body same as the implant or condition

IPS: intraparietal sulcus

JJ: one participant in our studies

M1: primary motor cortex

MC: motor cortex

NHP: non-human primate

NS: one participant in our studies

neural representations: neural responses to variables of interest

overlap: When multiple functions are represented by individual neurons/ populations of neurons

PC-IP: junction of the postcentral (PC) and intraparietal (IP) sulci.

population: a group of related neurons, often the group being recorded

PPC: posterior parietal cortex

preference: The variable that causes the largest response in a neuron or population of neurons

RD: one participant in our studies

Reference frame: see coordinate frame

saccade: a short eye movement

SCI: spinal cord injury

SD: standard deviation

SEM: standard error of the mean

SMG: Supramarginal gyrus

SPL: Superior parietal lobule

somatotopy: organization of different parts of the body into different anatomical locations of cortex

spike: action potential

spike sort: identify and cluster action potentials into putative single neurons

tetraplegia: paralysis affecting all four limbs (also tetraplegic, an individual with tetraplegia)

tuning: when a neuron's firing rate changes in response to a particular variable

unit: neuron

Chapter 1

INTRODUCTION

1.1 Overview

How the brain controls our movements has been a central question in neuroscience since the origin of the field of neuroscience. Some neuroscientists have even argued that our ability to control our movements was fundamental to the evolution of our conscious minds (Graziano, 2019; Schwartz, 2016). Whether or not this is true, many of us can agree that movement is an important part of our experience in the world. Perhaps further supporting the idea that the brain exists mainly for movement is that there are several regions in the brain recruited for motor control. The extensive nature of the motor network in the brain has led to many questions about the different contributions each of these different regions makes, and this is commonly addressed by assessing what movement variables are represented/controlled by the neurons in each region. Early work suggested that different parts of the body, or effectors, were controlled by largely separate anatomical patches of cortical motor areas. This led to the adaptation of somatotopic maps as the organizing principle for at least primary motor (M1) and somatosensory cortices (S1), but also to an extent premotor (PM), supplementary motor (SMA), and posterior parietal cortex (PPC) (Fulton, 1935; Penfield & Boldrey, 1937; Seelke et al., 2012; Woolsey et al., 1952). As one reverses upstream from primary motor cortex, this map was anticipated to become less granular and much more overlapping, until at the level of PFC only the goal itself is encoded in a largely effector agnostic capacity.

After over a century of examining the organization of motor areas, we have come to appreciate a complexity that challenges and at times directly conflicts with the notion of a truly topographic mapping of the body to cortex. Long train intracortical stimulation in nonhuman primates revealed

multi-limb movements could be evoked from small patches of primary M1, PM, SMA, and PPC (Baldwin et al., 2018; Graziano et al., 2002, 2005). Overlapping effector representations have also been found in humans, first with functional magnetic resonance imaging (fMRI) and more recently with single neuron recordings in both M1/PM and PPC (Heed et al., 2016; Meier et al., 2008a; Sanes et al., 1995; Willett et al., 2020; Zhang et al., 2017). These findings seem at odds with the traditional hierarchical view of effector specification in the motor system, and the expectation that M1 and PPC would have different patterns of overlapping effector representations. In addition, they call into question the classic consideration of M1 as a "low-level" movement code and PPC as a "high-level" one, referring to the higher-cognitive positioning of PPC in the pathway for movement.

Understanding how motor areas of the brain are organized and their different functional roles is not only important for building a more complete picture of how the brain controls our behavior, but also for developing tools to improve quality of life for individuals where movement is impaired. One example of such a device is a brain-machine interface (BMI), which can be used in cases where the cause of motor impairment is in the ability of motor signals to reach their respective muscle outputs (Andersen et al., 2019). While there are many types of BMI, the most cutting edge to this end utilize recordings from intracortically implanted electrode arrays. These arrays only cover small patches of cortex, which has led to implant location being guided largely by the prioritized application of the BMI and the most functionally relevant brain area. As a result, most work has focused on BMIs for similar functions, which may be a limitation of topography-based expectations rather than one imposed by the neural populations themselves. This motivates the need to explore more diverse functional applications both to improve BMI technology and reevaluate our attempts to characterize brain areas by their function.

This dissertation presents results from three tetraplegic participants chronically implanted with intracortical electrode arrays as part of an ongoing BMI clinical trial. Recordings were made from what would be considered "hand" areas of M1 and PPC based on the traditional views of these areas. In three studies, I compare these neural populations in how they represent movements of different parts of the body across differing contexts. These are among the first works to compare between single neuron activity recorded simultaneously in primary and associative motor areas in human cortex allowing for a unique opportunity to explore questions about the way motor variables are represented in each.

In the remaining sections of Chapter 1, I will present relevant background information on motor areas of the brain and brain-computer interfaces. The following chapters will compare how motor variables in MC and PPC are encoded in the human during different behavioral paradigms designed to test different components of sensorimotor processes.

Chapter 2 will compare how movements of the full body are encoded in small patches (~4mm x 4mm) in human MC and PPC. Traditionally, both MC and PPC were thought to have at least some broad level of anatomical separation between neural representations for different parts of the body, or effectors. In our recordings from "hand" areas of each area, we saw responses to every effector tested from head to foot, including both contralateral and ipsilateral sides of the body. The pattern of this full-body representation in each region was distinct, with more responses in MC being driven by movements of the hand than any other effector, but no such emphasis of a single effector in PPC.

In Chapter 3 I will explore how spatial information is represented for these overlapping effector representations. Previously it was thought that areas of PPC specialized for hand movements would also represent spatial information relative to the body, while areas specialized for eye movements

would represent spatial location relative to the position of the eyes. Given that we found both hand and eye movements overlapping in the same population, is the relative coding of spatial information also changing? We found that at the population level, PPC flexibly changes whether it represents the location of a target as being relative to the eyes or the hand depending on whether the movement instructed for interacting with the target was a saccade or imagined reach respectively.

The study in Chapter 4 seeks to extend our understanding of the results from Chapter 3 further by recording from an additional participant. For this experiment, we focused on exploring whether the flexible coding of spatial information for reaches or saccades was driven by single neurons changing their responses or by different subpopulations of neurons responding during the different movements. In addition, this chapter compares between two different regions with PPC, and shows distinct patterns of spatial representation.

Finally, Chapter 5 will provide a summary that ties together the results across these three studies in the context of sensorimotor literature. I will also discuss the broader impact of these results in how they align with fieldwide neuroscience findings and how they can guide future work in brain machine interfaces.

1.2 Brain areas for motor control

1.2.1 The pathway for voluntary movements

To illustrate the pathway information takes in the brain, in particular in the cortex, when we make voluntary movements, I will give an example of walking and noticing a wad of gum on the sidewalk in your path. While in some unfortunate instances attention may be elsewhere, if you are luckier, you will see the wad of gum and divert your step so that you don't end up with a sticky shoe. Although a relatively minor action, this recruited areas across the entirety of the brain (Luo, 2016). The visual information of an object in your path first passes from your retinas to the visual cortex. From there,

the ventral stream carries information about that object to the temporal cortex to identify it as gum. The dorsal stream carries the information to the parietal cortex, where it is computed that the location of the object is dangerously close to the likely location your foot will strike next. This is then passed on to the prefrontal cortex, where the object's identity as gum, and its location in your walking path, are weighed together to determine the different action/outcome combinations (or to distract you from the alert altogether in the mentioned unlucky version of events). The decision is passed to subcortical areas for action selection, as well as to the parietal cortex and premotor cortex where the movement plan is formed and integrated with other current sensory information. Finally, this plan reaches the primary motor cortex which sends a motor command to the spinal cord. It should be noted that many of the processes I just listed as hierarchical are most likely happening in parallel and not as fully discretized steps. The following sections will detail primary motor cortex and posterior parietal cortex and their contributions to motor control. Much of our understanding of these areas comes from nonhuman primates (NHPs), which will be discussed alongside results from human studies.

1.2.2 Motor Cortex

The motor cortex (MC) is made up of three main regions: primary motor cortex (M1), premotor cortex (PM), and the supplementary motor area (SMA). MC occupies a fairly large portion of the frontal lobe and includes the anterior edge of the central sulcus and extends forward onto the precentral gyrus. The exact boundaries between each region of MC is still unclear in the human cortex, but generally M1 is the most posterior of these regions, and PM and SMA sit anterior and superior to M1 respectively. Early work that established a large output from M1 to the spinal cord led many researchers to the area with some expectation that this would provide an area in cortex where variables coded by single neurons were directly related to variables we can measure outside the brain, for example muscle activity. It seemed reasonable that M1 would encode specific muscle parameters that when combined would correspond to an identifiable movement. This intuition was further fueled

by stimulation studies which seemed to suggest that M1 was organized in a map of the body (Beevor & Horsley, 1887; Penfield & Boldrey, 1937; Woolsey et al., 1952). Neither of these initial hypotheses, however, have been supported by experimental evidence, and today a more complex picture has emerged regarding the function and organization of M1 (Scott, 2008). This has ultimately led to the organization of the entire MC to be debated. In the following sections I will go over evidence of topographic organization of M1 and how it compares with the other main areas of MC.

1.2.2a Topographic organization

Although a body map in M1 was first proposed in the late 1800s (e.g. Beevor & Horsley, 1887), the work that made it a part of neuroscience textbooks occurred a few decades later. Penfield and Boldrey electrically stimulated M1 in patients undergoing surgery for epilepsy and brain tumors (Penfield & Boldrey, 1937). They reported the movements elicited as they stimulated different locations, and found that the most medial parts of M1 evoked movements of the feet and legs, while the most ventral evoked movements of the mouth and jaw. Stretched in-between these they found the largest portion of cortex evoked movements of hand and fingers. They drew their results as a homunculus and showed how the cortical surface of M1 could be mapped from head to toe, ventrally to medially (Figure 1.1a). Importantly, they emphasized that this was only a gross level, with greater separation in stimulation sites associated with greater differences in the effectors for which movements were evoked. At the finer resolution, they reported a high degree of overlap between the different parts of the body and emphasized gradual rather than discrete shifts from areas coding for one body part or another.

This was further confirmed in nonhuman primates (NHPs), with almost all reporting some level of overlap rather than a segmented map (Fetz & Cheney, 1980; Leyton & Sherrington, 1917; Schieber & Hibbard, 1993; Woolsey et al., 1952). This included work by Woolsey who seemed to predict that

maps meant to be guides would be taken as a fact rather than a simplified illustration, saying "It must be emphasized, however, that (the motor map) is an inadequate representation of the localization pattern since (it) cannot indicate the successive overlap which is so characteristic a feature of cortical representation," (Woolsey et al., 1952). Despite these warnings against over-applying the motor map, some insisted on fine grain architecture in particular for the hand (Asanuma & Arnold, 1975). This extreme take was poorly supported, however, and the debate over overlap within a limb was more or less settled when it became established that even single motor neurons could innervate multiple muscle groups, meaning there had to be some overlap of representation at least within a limb (Fetz & Cheney, 1980; Rathelot & Strick, 2006, 2009). Ultimately, a gradient style body map has been the most widely adapted take on organization of M1 (Figure 1.1b) (Schieber, 2001).

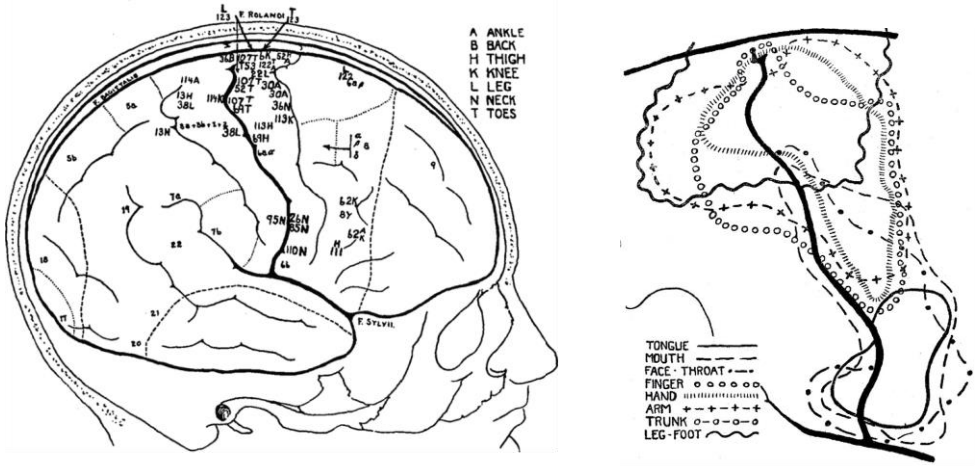

Figure 1.1 Somatotopic organization of primary motor cortex
Figures from the original report of Penfield and Boldrey in 1937. Left: Summary of their results showing that stimulating different areas along the central sulcus and pre and postcentral gyrus evoked the movements of different effectors with a general organization of effectors from head to toe as one moved the stimulation site from more lateral to more medial . Right: A more detailed look at the high degree of overlap of different effectors that were evoked at the different stimulation sites reported by Penfield and Boldrey (Figure 25B).

Adapted from Penfield, W., & Boldrey, E. (1937). Somatic motor and sensory representation in the cerebral cortex of man as studied by electrical stimulation. Brain, 60(4), 389–443 and Schieber, M. H. (2001). Constraints on Somatotopic Organization in the Primary Motor Cortex. Journal of Neurophysiology, 86(5), 2125–2143.

In addition to the extent of overlap between neighboring effector representations, whether the map is truly somatotopic in nature has also been debated. The first evidence to directly contradict the body

map was from (Kwan et al., 1978) where a center surround type organization was found for the fingers, hand, and arm. Control of the digits was encapsulated in a central region that was both ventrally and medially surrounded by a hand region, and an arm region ventral and medial to each hand region (Kwan et al., 1978; M. C. Park et al., 2001). This deviation from the typical body map was confirmed again in NHPs as well as with fMRI in humans. Initial work in humans only reported a center surround organization for the hand, but not other effectors (Meier et al., 2008a). Recently, however, this was seen for the foot and head as well, with for example the leg bordering either side of the foot representation (Gordon et al., 2023).

Another feature of the initial body maps drawn for MC was division of the sides of the body between the two hemispheres. A contralateral relationship was observed early on in stimulation studies, and further supported by anatomical evidence showing upper motor neurons crossing at the brain stem (Leyton & Sherrington, 1917; Penfield & Boldrey, 1937). Although most lesion and stimulation work support contralateral organization, electrophysiology and fMRI results reveal bilateral activation of MC during unimanual movements (Cramer et al., 1999; Hanakawa et al., 2005; Heming et al., 2019). Most work to this end suggests these responses are largely driven by different neural populations within a hemisphere, and the exact role of observed bilateral activation is still unknown.

Although the views I have discussed vary in their placement of different body part representations across cortex, they all generally support a low level movement code. More recent work suggests that small patches of MC can actually encode complex multi-effector movement. This was first hinted at by long train intracortical stimulation studies. Early stimulation work that had led to the drawing of somatotopic maps had been short 50ms injections of current. Some researchers began to consider that very few movements occur in brief isolations, and tried to evoke naturalistic movements using longer stimulation periods of 500ms (Graziano et al., 2005). This caused multiple parts of the body to be

moved from stimulation at a single site. Interestingly, these movements were not random, but rather could be described in terms of ethologically relevant movements (Graziano et al., 2002). For example, one site caused the monkey to bring both hands to his mouth and open his mouth, as if to eat. Another site caused a defensive posture. It can be difficult to fully interpret stimulation studies in terms of attributing the resulting behavior to the site stimulated or the larger network engaged by that area. Using fMRI, the same researchers who found a behavioral map using stimulation in NHPS chose to investigate this same question in humans (Meier et al., 2008a).

The most recent findings of overlap in MC have been the most extreme and have led to labels of cognitive and associative- previously reserved for "higher-level" motor areas. One study recorded intracortically from the hand knob of precentral gyrus in humans found neural responses to movements of effectors from the head to the feet (Willett et al., 2020). Here the authors suggest that precentral gyrus may be considered more premotor than primary motor cortex, and hypothesize that deeper within the central sulcus, a more granular body map would emerge. However, both high resolution fMRI and stereoelectroencephalography (sEEG) that examined the sulcal representations of the body both found highly overlapping patches (Gordon et al., 2023; Jensen et al., 2023). Interestingly, in the fMRI study they found three patterns of organization within MC (Gordon et al., 2023). First, they identified a transition from foot to head when moving medially to ventrally. Next, they found the same previously reported center-surround patterns of activity within each limb sub section. Third, and most novel, they report that this body map is not continuous. Rather between limb groups (i.e. between the legs and arm and between the arm and head) there are patches of full body representation. In this organization, proximal effectors are most represented in the overlapping patches and distal effectors occupy the more specialized regions.

One interpretation of the recent findings in humans and their conflict with findings in NHPs is that the organization of M1 in humans is more complex than that in NHPs. If this is the case, it brings up the question of whether the MC of humans is more in line with higher level motor areas in NHPs, like PPC. Directly comparing between results in human and NHP MC has often uncovered anatomical differences. It has been proposed that as a result of our increasingly complex behavioral repertoire, the motor cortex was divided into subregions not possessed by NHPs in order to accommodate specialized motor function such as fine digit control for tool use (T. N. Aflalo & Graziano, 2006; Geyer et al., 1996; Graziano & Aflalo, 2007). The increase in the number of subregions combined with what appears to be a decrease in the functional distinctions between each region have led to the analogous areas between NHP and human motor cortex to be debated. The more evidence reported for overlapping effectors in M1, the more it has been argued that the currently defined M1 in humans is more analogous to the premotor cortex of NHPs (Willett et al., 2020). The next section will touch on the general thought of how M1 and the two main other subregions within MC both share and differ in function and organization.

1.2.2b Premotor areas

There are at least six subdivisions of premotor cortex that are recognized today. Despite there being clear segmentation, the exact differences in function of these regions has remained unclear (Graziano & Aflalo, 2007; Matelli et al., 1985; Meier et al., 2008a). It is important to bring up premotor cortex, because in humans there has been some recent debate over where the premotor cortex becomes primary motor cortex, with some suggesting that M1 includes parts of the precentral gyrus, and others suggesting M1 is buried deep within the central sulcus (Graziano et al., 2002; Willett et al., 2020). Some have even posited that there are multiple subregions within M1 in man and dexterous primates (Geyer et al., 1996).

The premotor cortex is directly anterior to M1. In most mammals, M1 is thought to be restricted within the sulcus. In primates however, the boundary between PM and M1 is thought to lie somewhere within the precentral gyrus, and it remains unclear how far M1 extends beyond the sulcus. This boundary has in part been difficult to establish because of a lack of clear transition in functional roles of each area. Traditionally, the PM is thought to be involved in motor planning and action selection, and has been observed to encode contextually relevant information for a movement, like a reward. The idea of PM as a higher level movement code than M1 also led to the expectation that there would be more overlapping effector representation in PM than M1 (Campbell, 1904; Fulton, 1935). When mapping between regions, as mentioned no distinct border is observed and instead, the two areas seem to share a map that includes some overlapping effector areas that are sub grouped more by action than body part alone (Graziano et al., 2002). It should be noted that despite M1 receiving inputs from PM, the relationship is not purely hierarchical. PM does connect to the spinal cord as well as M1, and it was found that lesions to both but not only one area resulted in abolished movement (Fulton, 1935).

The other most notable premotor area is less often confused with M1 and is the supplementary motor area, or SMA. Penfield originally labeled this M2, and actually did not include PM in his drawings of a homunculus (Penfield & Boldrey, 1937). Both Woosley and Penfield reported that M2 exhibited a sort of squashed body map (Penfield & Boldrey, 1937; Woolsey et al., 1952). Again it was thought that perhaps a distinguishing feature between SMA and M1 would be the extent of overlap between effectors, because the first studies to stimulate SMA showed full body movements could be evoked, although we now know similarly complex movements can be evoked from M1 given longer bursts of stimulation (Graziano et al., 2002). Additionally, like for M1 and PM, we now know that SMA also projects directly to the spinal cord, further confusing the functional lines between primary and

premotor areas. Once again, this argues against a hierarchical progression from high to low level representation of movement.

1.2.3 PPC

PPC is part of the parietal cortex that is posterior to the postcentral gyrus, adjacent to the primary somatosensory cortex. PPC has been studied extensively for its role in sensorimotor integration as the meeting point between the dorsal visual stream and the somatosensory and motor cortex. In addition to its role in coordinating visual and proprioceptive information, PPC also has been found to be involved in motor planning, attention, and visual awareness. Recently as PPC in humans has been explored more, we have seen a rich variety of functions that begin to suggest an even higher cognitive role for the area (T. Aflalo et al., 2020; T. Aflalo, Zhang, et al., 2022; Zhang et al., 2017). This has long been suspected, as damage to PPC can result in a wide array of different deficits ranging from motor to memory (Andersen et al., 2014; Cleret de Langavant et al., 2009; Li & Malhotra, 2015; Vallar & Perani, 1986).

The PPC in humans is far more extensive than that in nonhuman primates (Figure 1.2) (Bruner et al., 2023; Caminiti et al., 2015; Kastner et al., 2017). This is hypothesized to have been driven by tool use, and indeed there are areas of PPC activated by actions relevant for tool use. Visual information about objects regarding both object identity and location are both passed to areas in PPC that are able to translate this into the proper hand shape and direction of arm movement for one to reach out and grasp said object. The roles for PPC in spatial reasoning and attention can also not be understated. Perhaps the most profound outcome of damage to PPC that can occur is neglect (Li & Malhotra, 2015; Vallar & Perani, 1986). This manifests as a complete lack of awareness of one half of the visual field despite intact vision. The nature of this deficit also implicates some role in spatial memory for PPC. Examination of PPC in humans has yielded even more functional processes in which the area

is involved including semantics, speech, and individual digit movements (T. Aflalo et al., 2020; Guan et al., 2022; Wandelt et al., 2024). This variety in representation and hypotheses as to how PPC achieves such a rich representation space is discussed in the PPC BMI section to follow.

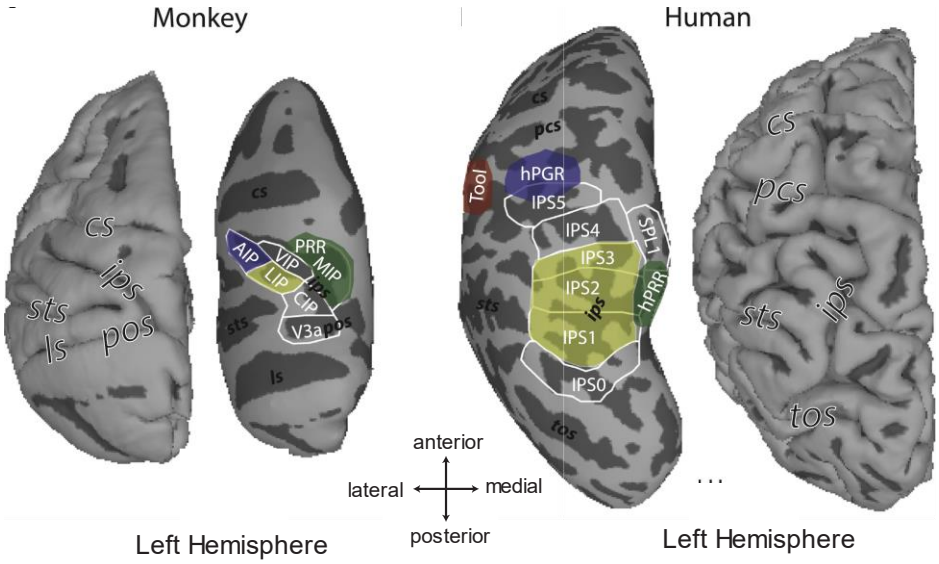

Figure 1.2 The expansion of the posterior parietal cortex in humans.
Areas thought to be functionally analogous between NHPs (left) and humans (right) are depicted. Areas with saccade related responses are shown in yellow, those with grasp-related responses in blue, and reach-related responses are shown in green. Most notable is the extension of regions within the IPS of NHPs to areas outside the sulcus. hPGR denotes the "human parietal grasp area" thought to be functionally equivalent to AIP in NHPs. hPRR shows the human parietal reach region, thought to be outside the sulcus in comparison to PRR in NHPs which lies within the IPS.

Adapted from Kastner, S., Chen, Q., Jeong, S. K., & Mruczek, R. E. B. (2017). A brief comparative review of primate posterior parietal cortex: A novel hypothesis on the human toolmaker. Neuropsychologia, 105, 123–134.

Although today we have come to understand that role of PPC, at least in humans, extends beyond motor to higher cognitive functions as well, it has most extensively been studied for its critical for visuomotor transformations. Damage to different areas within PPC resulted in deficits in hand movements or eye movements depending on their locations, which seemed to mimic the somatotopy seen in MC (Duhamel et al., 1992; Gréa et al., 2002; Jakobson et al., 1991; Karnath & Perenin, 2005;

Purves et al., 2001). The findings that first led to this organization to be proposed as well as the more recent findings that seem in direct conflict with those findings are discussed in the following sections.

1.2.3a Separation of effector representations for hand, eye, and arm movements

Much like the full body map seen in MC, results from PPC have shown different subregions emphasize a single effector. In NHPs, this has corresponded to the lateral intraparietal area coding for saccades, the anterior intraparietal area coding for grasps, and the parietal reach region coding for reaches (Andersen et al., 2007; Konen et al., 2013; Vingerhoets, 2014). Thus, for an action like reaching and grasping an object, it was initially thought that the processes for reach and grasp were separated by effector as early as PPC. It was hypothesized that the dorsal stream brought the location of the object to PRR, where it was integrated with somatosensory information before being sent to the dorsal part of PM and then the arm region of M1 (Milner & Goodale, 2008). The ventral stream in contrast delivers the relevant information about an object's identity to AIP to convert this identity into a grasp shape that is then passed to the ventral part of PM and then the hand area of M1. In addition to electrophysiology studies, lesion studies in NHPs reveal deficits to either saccades, grasps, or reaches depending on the location of the damage (Gallese et al., 1994; Hwang et al., 2014; Wardak et al., 2002; Wilke et al., 2012). Interestingly, one study in PRR, damage to which is associated with reaching deficits, found that while isolated saccade movements were not impaired, saccades during coordinate movements of the arm and eyes were impacted (Hwang et al., 2014).

In humans, separation of hand and eye movements in PPC has been less clear (Heed et al., 2011; Jastorff et al., 2010). Most fMRI studies report a gradient from more eye responsive to more hand responsive regions from posterior to anterior regions in IPS, however this gradient includes extensive overlap between the two effectors in the regions between the most anterior and posterior points

(Vingerhoets, 2014). Some fMRI work suggests that reach and grasp areas exist in multiple areas of PPC, including actually outside of the sulcus in humans, although the actual extent of effector segregation by neurons in these areas is not known (Bruner et al., 2023; Kastner et al., 2017). It has been unclear whether the lack of evidence for effector specific coding in human PPC is actually interpretable as a divergence from NHP literature or a result of difficulty resolving between areas with fMRI. The areas that make up the parietal reach network are interconnected, and this adds to the channel in distinguishing hemodynamic responses for each region.

There is also evidence for lateralization with the contralateral side of the body being more emphasized within a hemisphere. In LIP, inactivation of one hemisphere results in an increase in ipsilesional eye movements thought to reflect impairment in making contralateral movements (Wardak et al., 2002; Wilke et al., 2012). Recordings from PRR in NHPs show predominantly contralateral reach representation and although there is bilateral activation observed within IPS, there is a reported preference for contralateral movements (Mooshagian et al., 2022). Electrophysiology results from humans show much more overlap between contra- and ipsilateral representations within a hemisphere (Kagan et al., 2010). Notably, it was also reported that during simultaneous movements of digits on the contra and ipsilateral hand, only the contralateral digit is encoded. Cases of damage to PPC generally impact the contralateral limb, with additional lateralization of visual deficits that will be expanded on in the next section (Binkofski et al., 1998; PERENIN & VIGHETTO, 1988).

The focus on understanding hand, arm, and eye representations in PPC has been driven in part by the knowledge that damage to PPC can cause deficits in visually guided reaching and grasping interactions with objects. This led to the understanding that PPC was critical for hand eye coordination. Although a less studied area of investigation, researchers have also asked how coding for movement in PPC may be organized for the rest of the body. In NHPs, a long train ICMS study

found complex multi-effector movements evoked when stimulating certain regions of PPC (Baldwin et al., 2018; Thier & Andersen, 1998). This topic has also been investigated in humans, where as early as 1999, one study proposed an action-based rather than effector-based organization of motor maps in PPC after having subjects make signing motions with their finger and their toe (Rijntjes et al., 1999). Further fMRI work comparing hand, eye, and foot movements found that while they could to an extent separate the areas for hand and eye activity, those for hand and foot activity were entirely overlapping (Heed et al., 2011). The idea of an action-based or functional organization within PPC is also supported by the finding that pointing-type movements with the hand and feet for writing seem to activate overlapping regions in the superior parietal lobule (SPL), and another study finding this even extends to action observation.

This has been researched more extensively in the context of both bi- amputees and individuals born without arms, who often use their feet to perform many of the functions we would normally do with our hands. Although the primary sensory and motor areas show little divergence from traditional body maps, fMRI shows the same areas that would be active for arm and hand movements are active for leg and foot movements when they are the effectors performing the reaching and grasping (Striem-Amit et al., 2018). It remains unknown, however, whether these movements are activating the same neurons, or different neurons that share a space too small to be resolved with fMRI.

1.2.3b Separation of gaze-centered and body-centered coordinate frames in PPC

For proper hand-eye coordination, as information about the location of an object moves through the dorsal stream, it must at some point be integrated with proprioceptive information for us to accurately interact with that object. Several pieces of evidence have implicated PPC as the site of that integration and subsequent transformation of spatial location from gaze-centered to hand-centered coordinates (Andersen et al., 1985, 1993). Initially, much like for hand and eye movements, it was thought that

more rostral areas would implement hand-centered coding and more caudal areas would use gaze-centered coding. While as expected, gaze-centered coding was found in regions that corresponded to control of saccades, like LIP, it seemed that regions for hand and arm movements, like PRR and AIP, were also implementing gaze-centered coding (Batista et al., 1999; Cohen & Andersen, 2002). A dorsal portion of BA5 was identified as one of the few areas in PPC that implemented mostly hand-centered coding.

While the transition from gaze-centered to hand-centered didn't seem to align as expected with areas controlling eye vs. hand movements, there did still seem to be separation to an extent between the different coordinate systems. However, as these coordinate frames were examined across further contexts, and considered as possibly dynamic processes, it was found that body hand- and gaze-centered coding could exist within shared patches of cortex (Bernier & Grafton, 2010; Bremner & Andersen, 2014; Leoné et al., 2015). This was demonstrated both in NHPs with electrophysiology and in humans with fMRI. In both, BA5 seems to demonstrate flexibility, leaving a question of whether the population level response seen in human fMRI is maintained by the same patterns of single unit activity seen in NHPs. Identifying homologous regions in PPC of humans and NHPs has proven more difficult than some other more well-preserved areas.

Much like the different sides of the body, the different halves of the visual field have also been hypothesized to be lateralized to an extent in their representation in PPC (Barash et al., 1991; Kagan et al., 2010). Although the lateralization appears to be more pronounced in NHPs, evidence in humans has come from cases of optic ataxia, where patients demonstrated more difficulty reaching targets in the visual field contralateral to the lesion (PERENIN & VIGHETTO, 1988) . This is also true for visual attention as in cases of visual neglect, which arises from extensive damage to one hemisphere of PPC and results in loss of awareness of the contralateral visual field (Vallar & Perani, 1986).

Finally, some argument has also been made that this same visuomotor transformation occurs for other parts of the body as well, for example visual coordination for locomotion. It has been proposed that the evolution of the pathway for the visuomotor control needed for locomotion coincided with that for the upper limbs, possibly resulting in shared pathways that did not fully diverge until at the spinal cord (Georgopoulos & Grillner, 1989). The importance of PPC beyond encoding spatial location of the eyes, head, hand, and arm is also illustrated by disorders in body representation or body schema, for example autotopagnosia where subjects with damage to left PPC cannot point to a requested part of their body (i.e. pointing to the hand when asked to point to the elbow) (Cleret de Langavant et al., 2009; Corradi-Dell'Acqua et al., 2008; Razmus, 2017).

1.3 Brain Machine Interfaces

The information presented in the previous sections has practical applications in the field of brain machine interfaces. Explaining this motivation in the study is important because the context of the clinical trial through which these data were collected played a part in shaping the locations of recordings and the scientific questions asked. In the next sections I will introduce BMIs for motor applications, briefly review MC and PPC BMI work, and touch on cortical remapping in cases of disrupted sensorimotor control.

1.3.1 Background

BMIs attempt to restore an impaired function for an individual. In a BMI for motor control, neural signals are decoded in order to allow the user to control an external device in place of their own body. Although there are several means of recording neural signals, the most cutting edge BMI work has been with ECoG and intracortical arrays. Intracortical arrays have been particularly promising and also allow for an exciting opportunity for interrogation of single neurons in the human brain. The

main downside of these arrays is a combination of the invasive nature of the implant procedure and the small size of the array. Taken together, this means a careful selection of brain area must be made. The division of functions across the brain means that an implant in one area may also limit the device to a specific application. Although we regularly discuss the plasticity of the brain, there is substantial evidence to suggest that this plasticity is not limitless, and certain neural populations will be constrained within certain functional spaces. (Of course, within functional spaces remapping and reorganization has been observed in many cases, and this will be expanded on in a future section.)

The hypothesis that intracortical BMIs would be functionally constrained by the brain area controlling them has meant that particular functions that are considered "most important" have been the main focus of this research to date. Because of the risky nature of this experimental work, only individuals with the most severe cases of motor impairment are currently eligible for enrollment in BMI clinical trials. This includes patients with cervical level spinal cord injury, ALS, or stroke. For this patient group, among the most highly desired restorations is hand function. The topographic view of motor areas organization led experimenters to target "hand areas" of MC and later PPC. This proved very successful and much work was done to understand the function of the neural populations in these small patches with respect to hand function. As a consequence, however, little work was done to understand how and if these "hand areas" may represent other parts of the body. Is somatotopy in motor areas preserved at this fine scale? I have already gone over the scientific motivation for this question, but in the context of BMI control, this question could have great implications for understanding functional advantages of implanting in different brain areas. What if the applications for BMIs using arrays implanted in "hand areas" didn't have to be limited to hand movements, but could instead be used to fulfill a full-body movement repertoire?

1.3.2 Motor cortex BCIs

Much work in intracortical BMIs has focused on MC. More specifically, because of the priority for hand function restoration, an area called the hand knob on the precentral gyrus has been targeted (Hochberg et al., 2006). Up until recently, the focus of these studies has been constrained to understanding hand and arm movements. In 2019, Willet et al. found that they were able to decode speech related signals from that hand knob implant. The small size of the array makes it unlikely that this was due to electrodes covering both mouth and hand areas. Rather, it seemed to suggest extensive overlap in effector representations within the hand knob. This went on to be confirmed in a following study that examined movement of the entire body and found effectors from head to toe represented in the hand knob. BMIs that use MC are driven by a biomimetic approach, where the subjects must attempt to make a movement to control the device (Collinger et al., 2013). In the next section I will discuss PPC based BMIs which have been hypothesized to be more flexible in the ways they may be able to facilitate a users control.

1.3.3 PPC BCIs

A more limited body of work has investigated the viabilities of intracortical recordings from PPC for the control of BMIs, but the results are promising. Although PPC also contains movement trajectory information like MC, it has also been demonstrated that the location of a movement goal can be decoded (T. Aflalo et al., 2015). This could be advantageous for BMIs because this means of control would allow for a more intuitive use of a BMI, as many movements we make don't require us to think about the exact motor plan needed for our body to be able to execute. In addition, PPC-based BMIs have been controlled using motor imagery (T. Aflalo et al., 2015; Andersen et al., 2019). Like in MC BMIs, hand function restoration has also been prioritized in PPC, with targeted areas including AIP and SPL. In humans, PPC shows much more variability between individuals in its anatomy than in

NHPs, and so functional imaging to identify areas active during grasping has been implemented to further guide choice of array location.

Perhaps the greatest surprises to come from this work have not been with regards to action goals, but the great variety of other information encoded in small patches of PPC. For example, the same population was seen to encode both grasping imagery as well as internal speech (Wandelt et al., 2022, 2024). Additionally, movements of the left and right shoulders and hands, semantics, and sensory mirror neurons have all been observed within the same neural population of only a few hundred neurons (T. Aflalo, Chivukula, et al., 2022; T. Aflalo et al., 2020; Zhang et al., 2017). A question that has come up is how one area does so many things while still maintaining a coding scheme that is interpretable to downstream targets. One hypothesis has been that the neurons in PPC are implementing partially mixed selectivity, in which single neurons responses to different variables are nonlinearly mixed in order for small populations to occupy high dimensional response spaces (Rigotti et al., 2013; Zhang et al., 2017). In doing so, response spaces for different combinations of variables are orthogonal to each other and can thus be easily linearly read out. This is advantageous in decoding for brain machine interfaces as well because it allows for us to decode multiple degrees of freedom without the need for nonlinear decoding methods which can have heavy computational costs.

1.3.4 Stability and remapping of cortical areas

The previous two sections reviewed BMIs controlled by decoding signals from MC and PPC. Although these areas are known to be involved in motor control in motor intact individuals, it is not clear to what extent the lack of sensorimotor control and feedback after paralysis may impact the functional properties of these areas. For example, in the case of a tetraplegic individual who instead of using their hand to control a traditional computer mouse, now uses their mouth to control a

tetramouse (i.e. computer mouse adapted to mouth control), has the representation of the mouth begun to infringe on that of the hand? And if so, is this the case in all motor areas?

Varying studies have reported evidence both supporting and against cortical remapping (Jain et al., 2008; Makin & Bensmaia, 2017; Muret & Makin, 2021; Pons et al., 1991). It has been especially debated whether primary areas like M1 and primary somatosensory cortex exhibit remapping, although most studies suggest that this reorganization does not occur in the adult brain (Makin & Bensmaia, 2017). Whether or not this is the case for PPC is less well understood. This is in part because it has been debated whether human PPC exhibits the same effector specific regions as NHPs or whether there is less separation of effectors in human PPC (not due to reorganization). While some fMRI work has reported extensive activation of hand regions in PPC during foot movements for individuals without arms, further investigation of PPC in individuals with arms also found such overlapping activation of hand and foot movements (Heed et al., 2016; Striem-Amit et al., 2018). Although it remains unclear to what extent remapping may or may not occur, it has been hypothesized that a neural population's ability to learn is not limitless but rather confined within the function of that population (Sadtler et al., 2014). This would imply that "remapping" in PPC would be more akin to uncovering hidden representation subspaces than the creation of entirely new ones.

1.3.5 Limiting factors in BMI applications

As discussed in the sections on MC and PPC BMIs, current strategies have generally revolved around the understanding of effector-based organization in the brain. This expected specialization of neural activity has resulted in a lack of understanding what other functional properties the brain areas we target may have that could be leveraged to improve BMIs. For example, overlapping effector representations could offer a higher dimension of BMI controls and thus a broader range of indications. This has begun to be explored with speech decoding from grasping areas, but has yet to

be seen for full-body decoding applications. There is a need to re-examine the boundaries of current BMI devices to determine whether they are rooted in actual constraints of the brain regions implanted, or perhaps were imposed limitations guided by researcher's expectations of an area's function. The implications for the results in these studies for future BMI work will be expanded on in Chapter 5.

Chapter 2

DISTINCT PATTERNS OF WHOLE-BODY CODING IN HUMAN MOTOR CORTEX AND POSTERIOR PARIETAL CORTEX

Summary

Traditional views of the organization of motor areas describe that movements of different parts of the body, or effectors, are represented in distinct anatomical locations. The extent to which representations of effectors overlap has been a topic of debate for decades. We recorded from single neurons in "hand areas" of motor and posterior parietal cortex of tetraplegic humans while they attempted movements from head to foot. We found every movement tested evokes a population level response from each area; however, in motor cortex there was a clear emphasis on movements of the hand while no one effector was emphasized in posterior parietal cortex. Single neurons in motor cortex were mostly tuned to a single effector or to two effectors within a shared limb. In contrast, neurons in posterior parietal cortex were tuned to seemingly random combinations of effectors. Although the extent of overlap seen in both areas was a surprise, the distinct patterns between the two areas support the long held hypothesis of a transition from more to less effector specific as one moves from primary to associative motor areas.

2.1 Introduction

Even simple movements rely on the recruitment of multiple brain areas. Understanding the functional organization of these brain areas is a classic problem in motor control. The fundamental question of how different brain regions contribute to the control of different parts of the body has been used as a framework to understand how information is arranged on the cortical surface more generally. In motor cortex (MC), results are summarized by the homunculus, an orderly representation of the body that

is topographically arranged from head to toe (Penfield & Boldrey, 1937). In posterior parietal cortex (PPC), results are summarized as distinct cortical regions responsible for the sensory-motor guidance of distinct effectors, such as the eye in the lateral intraparietal area, the arm in parietal reach region, and the hand in anterior intraparietal area (Andersen et al., 2007; Cui & Andersen, 2011; Grefkes & Fink, 2005; Premereur et al., 2015).

However, a number of recent results challenge this conventional wisdom. In MC, these include results from functional magnetic resonance imaging (fMRI), sEEG, and intracortical recordings in humans, all of which show extensive overlap in effector representations (Gordon et al., 2023; Jensen et al., 2023; Meier et al., 2008a; Willett et al., 2020). Although the original topographic organization proposed did include some overlap between neighboring effectors (e.g. the fingers (Schieber & Hibbard, 1993)), the overlapping effectors in more recent findings are from head to toe. For example, single unit recordings in humans from the hand knob of precentral gyrus found a compositional code for moving the entire body rather than only the hand as expected. Additionally, coding for both the ipsilateral and contralateral arm/hand are found to overlap in a single hemisphere (and even within a single neuron) (Alkadhi et al., 2002; Ames & Churchland, 2019; Heming et al., 2019; Steinberg et al., 2002). In non-human primates (NHPs), long train intracortical microstimulation (LT-ICMS) studies have also revealed overlapping effector representations, leading to the proposal of an ethological organization of behaviorally relevant effectors to be proposed (Graziano et al., 2002, 2005; Graziano & Aflalo, 2007).

In PPC, several recent studies in humans using fMRI show overlapping representations for different effectors for similar types of movements, suggesting a functional organization of movement (Heed et al., 2016; Leoné et al., 2014; Medendorp & Heed, 2019; Striem-Amit et al., 2018). Previously, we recorded from human PPC and found that in addition to expected contralateral hand movements, shoulder movements and ipsilateral movements of the hand and shoulder were all encoded using a

strategy called partially mixed selectivity (Zhang et al., 2017, 2020). Additionally, like in MC, LT-ICMS studies in NHPs show stimulating single patches in certain areas of PPC can evoke multi-effector movements (Baldwin et al., 2018; Thier & Andersen, 1998).

A comparison of the organization of effector representations in MC and PPC has been elusive. Because of the similarities in recent findings of overlapping effector representations in human recordings, it is natural to ask how coding for movements of the full body compares between the two areas. Due to differences in tasks, as well as subjects, it is difficult to evaluate these studies alongside each other to answer this question. In the current study, we record from 4 x 4 mm patches of cortex in human PPC and MC during attempted movements from the head to the feet in two human participants. Given that there is previous evidence for coding of multiple effectors in small populations of both PPC and MC, we can examine their responses during these movements to understand how control of different effectors are organized in each area. We also examine how combining two effectors in simultaneous movements impacts this representation in each area.

Despite targeting areas of both MC and PPC that have been classically associated with representing hand movements, the neural populations respond to movements of effectors across the body. The pattern of this overlapping representation, however, varied between the two regions. In MC, the population response for the wrist and thumb was two to three times stronger than other effectors. A majority of neurons were tuned to the contralateral hand, followed by the ipsilateral hand, with the fewest number of neurons being tuned to the proximal effectors including the legs and shoulders. The population in PPC was found to represent the whole body as well, however, unlike in MC, there is equivalent tuning strength across effectors both at the population and single neuron level. There was no relationship observed between the effectors coded by a single neuron in PPC, and instead each neuron was tuned to seemingly random combinations of effectors. We also sought to understand whether this overlapping representation has functionally useful characteristics, for example shared

spatial information between effectors, which has been suggested could facilitate transfer of learned motor skills from one limb to another. The extent to which information is shared is expected to vary between lower and higher cognitive areas, leading to a prediction that in MC spatial coding would be shared between specific effectors while in PPC arbitrary effectors would be able to share information (Zhang et al., 2017, 2020). Our results show evidence for specialized sharing in MC and arbitrary sharing in PPC, further emphasizing their functional differences.

Finally, we tested how simultaneous movements of two effectors were encoded. In MC, when a second effector was moved alongside the contralateral thumb, only the direction of the contralateral thumb is encoded, and the representation of that secondary effector was suppressed. In PPC there was not as clear of a linear relationship between individual and simultaneous movements, suggesting that the area may instead be implementing a more complicated nonlinear combination of movements of each effector to represent coordinated movements. These results point to clearly distinct organization of effector representations in MC and PPC, and allow for greater understanding of the different functional roles of each area and how each area contributes to motor control.

2.2 Results

As part of an ongoing clinical study, two participants were implanted with microelectrode Utah arrays. Participant RD is tetraplegic (C3/C4) and was implanted with two 64-channel arrays in the left hemisphere of the hand knob of precentral gyrus (RD-MCL and RD-MCM) a 64-channel array in the superior parietal lobule (SPL) of PPC (RD-PPC), and another in the supramarginal gyrus (RD-SMG) (Figure 2.1a) . Participant JJ is also tetraplegic (C4/C5) was implanted with two 96-channel intracortical arrays in the left hemisphere, one in the hand knob of precentral gyrus (JJ-MC) and the other in SPL (JJ-PPC, Figure 2.1b). Implant locations within each brain area were selected by asking

the participants to perform motor imagery for hand and arm movements during functional magnetic resonance imaging.

In the current study, to understand neural coding for body movements, we asked the participants to attempt to move each of twelve effectors to five target locations (Supplemental Figure 2.1a). This was done using a center-out paradigm where the effector to be moved was instructed on the screen. For each movement, the direction was indicated by one of five targets arranged 72 degrees apart in the center of the screen changing color from gray to red. Each movement was followed by an inter-trial interval (ITI) where the subject was at rest. The arrays were recorded from simultaneously as the subjects attempted movements of twelve total effectors (eyes, head, right/left shoulder, wrist, thumb, leg, and ankle). Attempted movements for both subjects result in overt movement for the eyes, head, and shoulders, but not for any other effectors (below the level of injury).

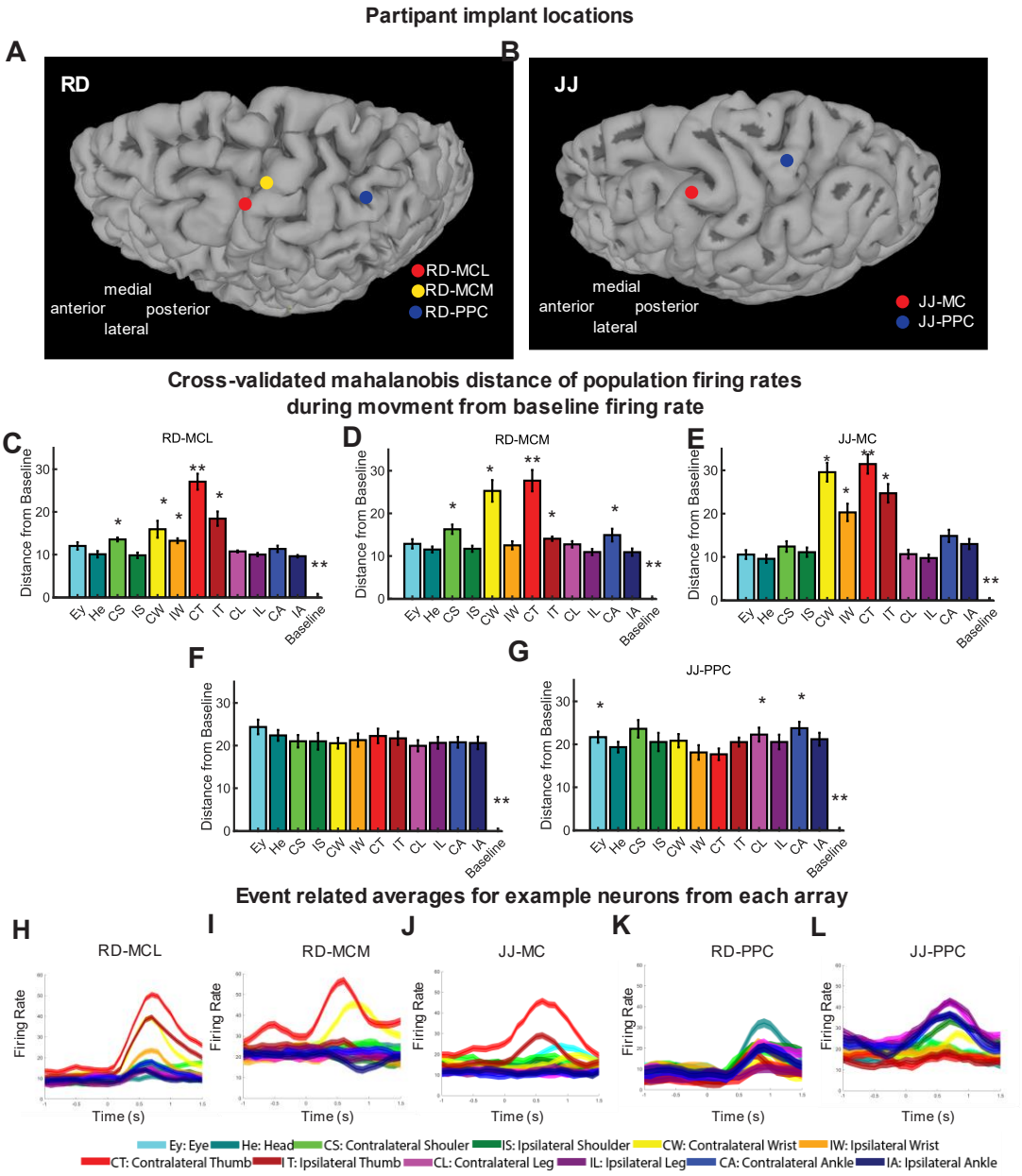

Figure 2.1 Fully body coding with distinct population responses in MC and PPC
1A: RD Implant locations: RD has two 64-channel Utah arrays located in the left hemisphere near the hand knob of precentral gyrus. The array that is located more medially is referred to as RD-MCM and the array that is more lateral is denoted RD-MCL. RD has another 64-channel array in the left hemisphere located slightly medial and posterior to the junction of the postcentral and intraparietal sulcus, denoted RD-PPC. Finally, RD has one 64-channel array in the left hemisphere of the supramarginal gyrus (RD-SMG).
1B: JJ Implant locations: JJ has one 96-channel Utah array located in left hemisphere near the hand knob of precentral gyrus, denoted JJ-MC. Additionally, JJ has one 96-channel array

in the left hemisphere that is located slightly medial and posterior to the junction of the postcentral and intraparietal sulcus, referred to as JJ-PPC. 1C-G: Cross-validated mahalanobis distance of population firing rates sampled from a 500ms window during movement execution and firing rates sampled from 500ms window during rest. Error bars show standard error of the mean. Significance was tested using a permutation test. Two stars indicate that the distance from baseline for that condition was significantly different from the distance from baseline for all other conditions. One star indicates that the distance from baseline for that condition was significantly different from that for select other conditions listed below. $p<0.05$ 1C: Results for RD-MCL. CT>all, IT>EY,HE,CS,IS,IW,CL,IL,CA,IA, CW, CW > HE, IS, CL, IL, IA IW > HE, IS, CL, IL, IA, CS> HE, IS, CL, IL, CA, IA 1D: RD-MCM. CT>all, CW>EY,HE,CS,IS,IW,IT,CL,IL,CA,IA CS> HE, IS, IW, CL, IL, IA, IT>HE,IS,IL,IA, CA>IL 1E: JJ-MC. CT>all, CW> EY,HE,CS,IS, IW,IT,CL,IL,CA,IA, IT>EY,HE,CS,IS,CL,IL,CA,IA, IW>EY,HE,CS,IS,CL,IL,CA,IA, CA>EY, HE, IS, IL 1F: RD-PPC. No significant differences other than all conditions from baseline. 1G: JJ-PPC, CA> HE, IW, CT; CS> IW, CT, CL>CT, EY>CT. 1H-L: Event related averages for an example neuron from each brain area. Neurons selected are representative of the population. Colors show responses to different effectors. Mean and 95% confidence intervals are shown. H: RD-MCL, I: RD-MCM, J: JJ-MC, K: RD-PPC, L: JJ-PPC.

MC represents the full body with a preference for the contralateral hand. PPC represents the full body with equal strength across effectors.

Is there an effector-specific movement code implemented in MC or PPC? We examined the population responses for any preference across effectors. The strength of representation across the body was determined by finding the cross-validated Mahalanobis distance (crossnobis) between the population firing rates during movements for each condition and the firing rate during an inter-trial-interval when the participant was at rest. Recorded signals were spike sorted. In both participants, all arrays in both MC and PPC showed population responses that were distinct from the baseline for all 12 effectors (Figure 2.1c-g, permutation test, $p<0.05$ for MC and PPC), however the relative strength of these representations across effectors were different between the two brain areas.

In RD-MCL, RD-MCM, and JJ-MC, the contralateral thumb was significantly more strongly encoded than other effectors (aside from the contralateral wrist in RD-MCM and JJ-MC, permutation test $p<0.05$) (Figure 2.1c-e). In RD-MCL, although still weaker than the contralateral side, the ipsilateral thumb showed responses significantly stronger than all non-hand effectors (Figure 2.1c; permutation test $p<0.05$). In RD-MCM the contralateral wrist evoked a stronger response than every effector other

than the contralateral thumb (Figure 2.1d). In addition, in JJ-MC, the contralateral wrist, ipsilateral thumb and ipsilateral wrist all evoked responses stronger than any of the non-hand effectors (Figure 2.1e; permutation test $p<0.05$).

The population responses from both RD-PPC and JJ-PPC showed each effector is coded with an equal strength of response relative to the baseline (with a few minor exceptions noted in figure caption, permutation test $p>0.05$) (Figure 2.1f-g). Only participant RD has an implant in SMG, and thus these results are presented in the supplemental figures. In RD-SMG, there is a significant population response to each effector, and the head was represented more strongly than several, although not all, effectors (Supplemental Figure 2. 2).

To get a qualitative sense of the single neuron activity that contributed to the population results, we computed event related averages for example neuron firing rates grouped by effector. In the single neuron examples for RD-MCL, RD-MCM, and JJ-MC shown, generally the neurons respond strongly to the contralateral thumb, followed by the ipsilateral thumb and contralateral wrist (Figure 2.1h-j). For the example neurons from RD-PPC and JJ-PPC, they respond to one, two, several, and even all effectors, making it difficult to choose as representative neuron as was chosen for the arrays in MC. The chosen examples show a neuron in RD-PPC that is tuned across all twelve effectors, and one in JJ-PPC that is tuned to half of the effectors (Figure 2.1k-l, more examples in Supplemental Figure 2.3).

Single neurons respond to multiple effectors in both MC and PPC, but with distinct patterns of overlap

The tuning preferences of individual neurons provides initial insight into the function of a cortical area, but it is not sufficient to understand how a cortical area contributes to behavior. For example, equivalent tuning across effectors could be consistent with PPC coding an effector agnostic spatial

code, or spatially inter-mixed but highly effector specific representations, amongst others. We therefore sought to better understand the neural architecture that supports coding for multiple body-parts in each area. Here we focus on two aspects of functional organization at the single neuron level. First, was there evidence for a systematic relationship between different effectors, e.g. if the preferred effector was the contralateral wrist, is it more likely that the ipsilateral wrist would be the second preferred effector. Second, if a neuron codes for multiple effectors, are the spatial tuning preferences similar?

We found the strength of modulation of single neuron firing rates during movements of each effector. The strength of a neuron's response was determined by subtracting a neuron's firing rate during its worst tuned direction from the firing rate in its best tuned direction. Only neurons that were significantly tuned to at least one effector were included in the final results (shuffle test, $p < 0.05$). First, we found each neuron's most preferred effector by finding the effector that had the maximum difference in firing rate between best and worst directions (Figure 2.2a-e). In each of the three MC arrays, around 40% of units were best tuned to the contralateral thumb, in line with the population results (Figure 2.2a-c, RD-MCL: 53%, RD-MCM: 40%,JJ-MC: 38%). Additionally, just over 20% of neurons in RD-MCM and JJ-MC preferred the contralateral wrist while just over 15% of neurons in RD-MCL and JJ-MC preferred the ipsilateral thumb.

In the PPC arrays, neural preferences were spread across effectors comparably, with between 4 and 18% of neurons best tuned to each effector (Figure 2.2d,e). In both arrays the eyes stand out as being slightly more preferred than other effectors, and likewise for the contralateral ankle in JJ-PPC, however this is only a significant difference for a few of the conditions (one-way anova, $p<0.05$). All effectors were preferred with roughly equal frequency in RD-SMG (Supplemental Figure 4a).

Next, we found the strength of single neuron responses across all effectors. The normalized strength of each neuron's response is plotted with neurons sorted by two characteristics: their most preferred effector (from eyes to ankle); and the number of other effectors coded (shuffle test, $p<0.05$; Figure 2.2f-j). The qualitative difference in pattern that can be observed in this analysis for MC and PPC is stark, and suggests there should be quantifiable differences between the effectors coded by a single neuron. To better understand the different effectors a single neuron coded for, we separated the neurons by their most preferred effector and then summarized the effectors coded by those neurons in pie charts (Figure 2.2k-o; supplemental Figure 2.5). As shown in Figure 2.2d and e, there are a similar number of neurons that prefer each effector in PPC (~30 neurons per effector), but in MC there are very few neurons that prefer an effector other than the contralateral thumb or wrist. Thus, the contralateral wrist and thumb were chosen as the most meaningful of these pie charts for the purpose of comparing between the arrays because a similar number of neurons preferred these effectors across all five arrays (all other pie charts in supplemental).

In all three arrays in MC most neurons are tuned to an individual effector, but there are a portion of single neurons that are tuned to multiple effectors (Figure 2.2f-g & Supplemental Figure 2.6a-c). In the RD-MCL and RD-MCM arrays, less than 10% of neurons are tuned to multiple effectors (Supplemental Figure 2.6a & b). In RD-MCL only a single neuron that preferred the contralateral thumb was tuned to another effector and was tuned to the contralateral shoulder (Figure 2.2k). There were only 7 total neurons that preferred the contralateral wrist in RD-MCL, with one of these neurons also coding for the contralateral shoulder, and another for the contralateral thumb. In RD-MCM, less than 15% of neurons that prefer the contralateral thumb were tuned to additional effectors, and this included the ipsilateral thumb and contralateral wrist (Figure 2.2l). In RD-MCM only four neurons that preferred the contralateral wrist were tuned to other effectors, and two of these were tuned to the contralateral thumb (Figure 2.2l).

In JJ-MC, the most apparent effector overlap for single neurons is between corresponding ipsilateral and contralateral effectors, in particular the wrist and thumb (f Figure 2.2 h, m). Around 40% of the neurons that were best tuned to the contralateral thumb were tuned to additional effectors. Of these, just under 50% are tuned to the ipsilateral thumb. Two of the three neurons that prefer the contralateral wrist and are tuned to multiple effectors are tuned to the ipsilateral wrist, with the third neuron tuned to the contralateral thumb (Figure 2.2 m). As a whole, overlap for single neurons across all three MC arrays were largely restricted within a single limb with only a few exceptions.

In both RD-PPC and JJ-PPC, a large portion of neurons code for multiple effectors (Figure 2.2i, j and Supplemental Figure 2.6 d & e- 49% in RD-PPC, 35% in JJ-PPC). Additionally, there is no clear consistent relationship between the effectors to which a single neuron is tuned (Figure 2.2i-j). Rather, neurons show clear preferences for specific, but random appearing, sets of effectors. In both RD-PPC and JJ-PPC, neurons that preferred either the contralateral wrist or contralateral thumb were tuned to the full range effectors from head to ankle (Figure 2.2n-o). This was also true for additional effectors which the MC arrays did not have enough units for comparison (Supplemental Figure 2.5). In RD-SMG only 2 neurons were significantly tuned to more than one effector (Supplemental Figure 2.4b,c). One was tuned to the head and contralateral shoulder. The other was tuned to the ipsilateral shoulder and ipsilateral thumb (Supplemental Figure 2.4d).

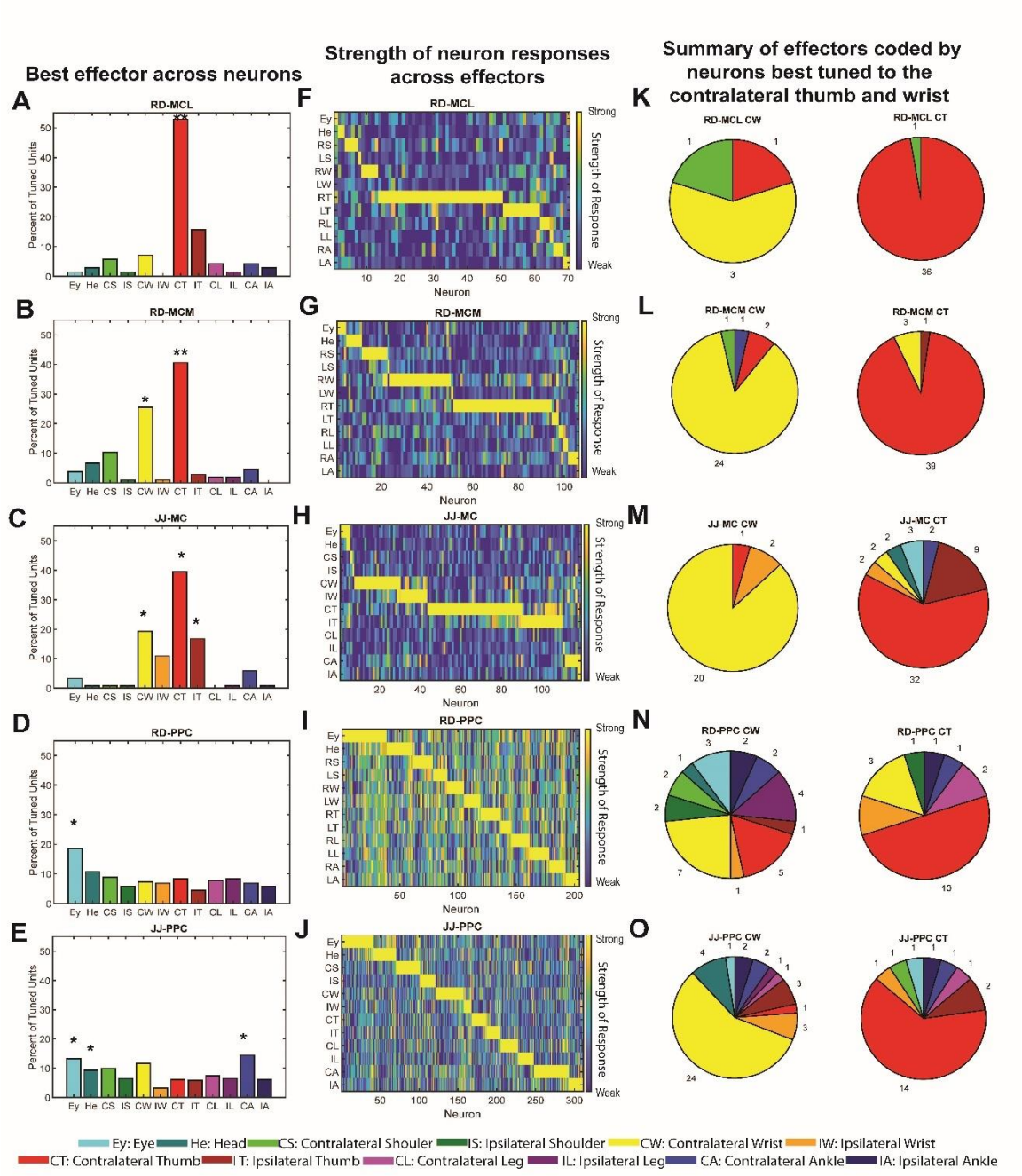

Figure 2.2 Single neuron responses show distinct patterns of overlapping representations across effectors in MC and PPC

2A-O: The strength of single neuron responses across effectors was found by determining each neuron's best tuned direction and worst tuned direction, and then subtracting the firing rate during movements in the worst from the best for each condition.

A-E: The best effector for each neuron was the effector that evoked the strongest response, or had the greatest difference in firing rates. Conditions are along the x-axis and the y-axis is the percent of neurons. A one was anova was used to test for significant differences between the number of neurons best tuned to each effector. Two stars indicate that there were significantly more neurons best tuned to that effector than all other effectors. One star indicates that there were significantly more neurons best tuned to that effector than neurons best tuned to specific other effectors listed below. $p<0.05$.A: RD-MCL: CT>all. B: RD-MCM: CT> all, CW> all but CT. C: JJ-MC: CT> EY,HE,CS,IS,IW,CL,IL,CA,IA; CW>EY,HE,CS,IS,CL,IL,IA; IT> EY,HE,CS,IS,CL,IL,IA. D: RD-PPC: EY> all but HE. E: JJ-PPC: EY> IS,IW,IT,CT; H> IW,CT; CA> IS,IW,CT,IT,IL. F-J: The strength of a neuron's response, with neurons sorted by their best effector and then by the number of effectors they coded. The strength of neural responses were normalized to the strongest response from each array. Each column shows a single neuron's response across all 12 effectors. K-O: Breakdown of effectors coded by neurons best tuned to the contralateral wrist (left) and the contralateral thumb (right).

In order to compare the strength of single neuron responses across effectors in each brain area, we ordered each neuron's response across effectors from best to worst. Then, we plotted the distribution of the strength of neuronal responses for the most preferred to least preferred effector. This reveals a trend toward stronger representation across all effectors at the single neuron level in PPC than MC for both subjects (Supplemental Figure 2.7 a & b). To ensure these effects were truly driven by single neurons, we applied a stricter criterion for spike quality to rule out any potential signals from multi-unit activity and found the same pattern of results (Supplemental Figure 2.8 a-e).

As a final means of characterizing the single unit activity during movements of each effector, we compared the directional tuning properties of neurons across the effectors they coded. The first question we asked was whether single neurons used the same spatial code for the different effectors they coded. To compare the directional tuning properties of a neuron across effectors, we found the linear regression coefficients for each neuron, and used those coefficients to determine the angle between the directions coded by each response. An angle of zero implies that the neuron used the same directional tuning across effectors. This comparison was done for the most preferred and second most preferred effector for each neuron (determined using the same criteria used in Figure 2.2a-e). Because of this criteria, very few neurons from RD-MCL and RD-MCM are included, and thus no strong claims can be made about the directional tuning of these neurons (Supplemental Figure 2.9a

& b, n=4 for RD-MCL and n=12 for RD-MCM). In JJ-MC, RD-PPC, and JJ-PPC, we found most neurons are tuned to the same direction across effectors, meaning zero angle of difference (Rayleigh test for uniformity $p<0.05$; circular mean JJ-MC = 0.000° 18.5°, RD-PPC = -0.493° 4.412°, JJ-PPC = 0.000° 4.84°; Supplemental Figure 2.9c-e).

The second question we asked with regards to the directional tuning is whether neurons implemented an intrinsic or extrinsic reference frame to represent direction. Spatial information for a movement can be represented intrinsically, or with respect to the relative location of our body and joints, or extrinsically, with respect to the location in the external world. In certain cases, for example the movements shown in Supplemental Figure 2.10a, movements that are the same direction in an extrinsic reference frame are opposite directions in an intrinsic reference frame. Likewise, movements that are the same in an intrinsic reference frame can be opposite directions in external space (Supplemental Figure 2.10b). Thus, to properly compare direction coding for contralateral and ipsilateral effectors, we must determine the reference frame being used in each brain area. We used a linear regression to find the directional coding for effectors on the contralateral and ipsilateral sides of the body, and used the relationship between the resulting betas to determine the reference frame used by each neuron. In both RD-MCL and RD-MCM there were too few neurons tuned to multiple effectors to determine a trend towards one reference frame or the other ($n<=2$). In JJ-MC, there was a significant negative correlation between the betas for the pairs of contralateral and ipsilateral effectors, meaning an intrinsic reference frame is being implemented (Supplemental Figure 2.10c, Pearson correlation=-0.71, $p<0.001$). In contrast, RD-PPC shows a positive correlation between contralateral and ipsilateral betas, suggesting an overall extrinsic reference frame being coded (Supplemental Figure 2.10d, Pearson correlation, $r=0.94$, $p<0.001$). Finally, in JJ-PPC there was no trend toward a positive or negative relationship, implying a mixture of both intrinsic and extrinsic

reference frames being implemented (Supplemental Figure 2.10e, Pearson correlation ,r=-0.10, p=0.6).

Arbitrary vs specific shared information

How might MC and PPC be using these overlapping effector representations? One possible explanation discussed in motor literature is that this provides a shared architecture through which learned motor skills can be transferred across limbs (Willett et al., 2020; Yu et al., 2014; Zhang et al., 2017). At the level of effector preference, we report clear distinctions between representations in MC and PPC. While these differences in the structure and extent of overlap in effector representation give some intuition, they do not answer the question of how efficiently information can be shared across effectors in either area. We call the extent to which information is shared between effectors the transfer efficiency. If the neural code has high transfer efficiency across effectors, information is shared between two effectors regardless of their location on the body or function in movement. Another possibility is that high transfer efficiency only exists between specific effectors, for example that are more likely to be moved together such as the contralateral wrist and the contralateral thumb, or the contralateral and ipsilateral wrist for bimanual tasks.

To assess how information was shared across effectors in MC and PPC, we trained a partial least squares linear regression model to find a directional coding subspace that was shared for two effectors and not the rest. In other words, we looked for a subspace where the spatial code was approximately the same for two effectors, but distinct from other effectors. This was done for the 66 possible pairings of effectors. To evaluate the transfer efficiency of information between these effector pairs, we found the correlation matrix for actual vs model-predicted position. Pairs with high transfer efficiency will have high r2 values, and the average r2 across pairs gives a sense of the population's overall transfer efficiency. To determine significance, this r2 value was compared to a null distribution of r2 values

that was generated for each pair by shuffling the firing rates for trials with one effector, in order to mimic a population where no information is shared between effectors.

We found that only specific pairs of effectors significantly share directional coding in MC (Figure 2.3b-d). The fewest pairs were found to share information in RD-MCL, where the contralateral thumb shared information with the contralateral shoulder, contralateral ankle, and eyes. The contralateral ankle was also seen to share with the contralateral leg and the eyes. In RD-MCM, the contralateral thumb, contralateral wrist, and contralateral ankle share information with other effectors, and do so significantly with the eyes, head, and other contralateral effectors. In JJ-MC the contralateral wrist, thumb, and ankle shared information with each other, and with their ipsilateral counterparts. The focus of shared spatial information within the hand is somewhat expected based on the pattern of effector overlap observed in single unit tuning and emphasizes the robust nature of the dominance of coding for the contralateral hand. The finding of shared information with the contralateral ankle across arrays is a bit more surprising; however, previous work has shown that certain motor skills like writing can be transferred from the hands to the feet. Perhaps this shared spatial information reflects the functional organization that has also been reported alongside somatotopy in MC. The interpretation of this finding will be expanded on further in the discussion.

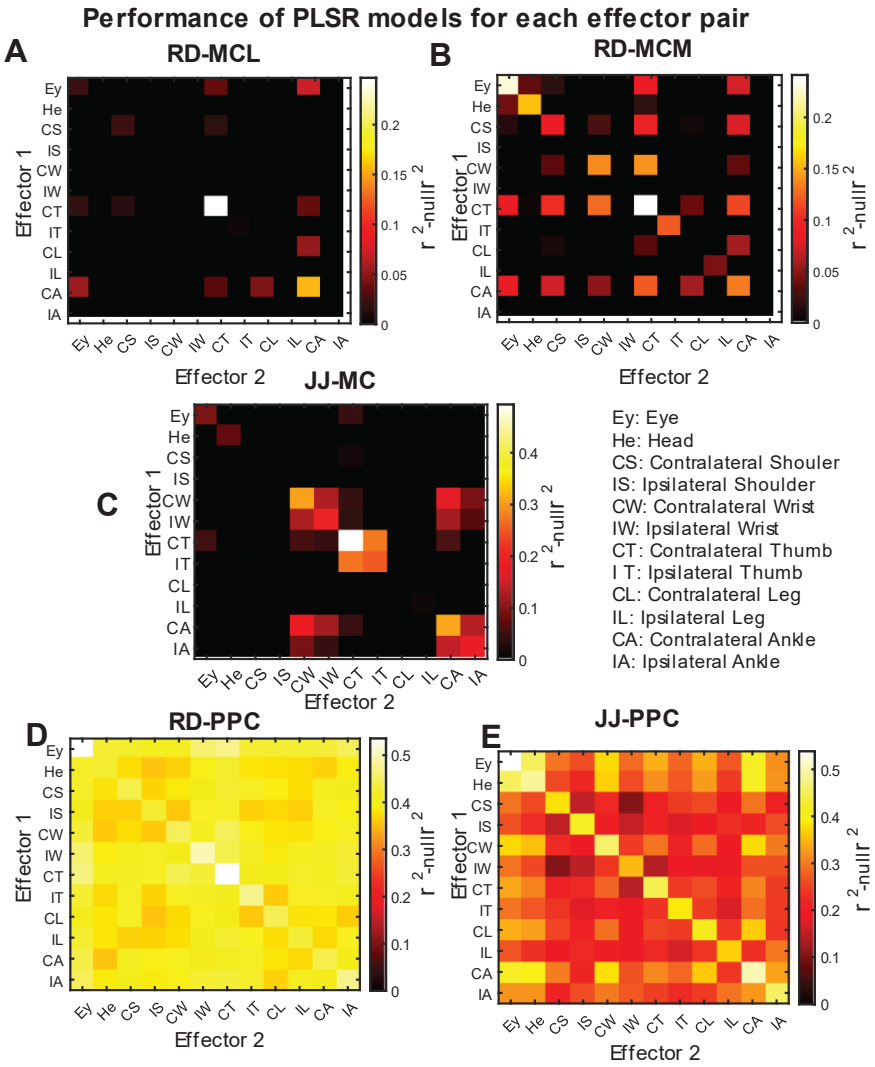

Figure 2.3. Evaluating shared spatial information between pairs of effectors
APLSR model was trained using firing rates from all neurons, and position information for two effe tors, for each possible pairing of effectors. The positions predicted by the model were then correlated with the original input position values to determine whether spatial information had been shared between the two effectors. This was done for a matrix of shuffled firing rates to obtain a null distrib tion to compare these model's performances with for significance. A-E:Performance of models trained for each effector pair. The x- and y- axes are the two effectors used in the pair. The diagonal is made up of a single effector rather than a pair of effectors. A: RD-MCL, B: RD-MCM,C: JJ-MC, D: RD-PPC, E: JJ-PPC.

In RD-PPC and JJ-PPC, shared directional coding is found for every set of effectors tested except for two and one pair respectively (Figure 2.3e-f). All other effector pairs seem to share information equally especially in RD-PPC. Although significant sharing is found for all pairs in JJ-PPC as well, more variation is noticeable across pairs. This could be a result of the mixed intrinsic and extrinsic

reference frames used, which were not fully accounted for in this analysis in part because even some individual neurons are not exclusively one or the other. In RD-SMG there are no effector pairs that share information (Supplemental Figure 2.11). The previous analysis (Supplemental Figure 2.4c) revealed that compared to RD-PPC and JJ-PPC, RD-SMG has fewer neurons tuned to the task (<40 across six sessions), which may contribute to the overall weaker sharing of information.

Coding for direction during simultaneous movements of two effectors is distinct from that during individual movements

One question that arises from the overlapping representations of effectors seen is how these representations are combined during simultaneous movements of two effectors at once. To answer this, a new task was used to show two different target cues for two different effectors (Supplemental Figure 2.1b). The subjects made movements of two different individual effectors as well as simultaneous movements of these effectors in either the same or opposition directions. In both subjects, the contralateral and ipsilateral thumbs were tested. In JJ, the contralateral thumb and contralateral leg were tested as well. It has been proposed that a characteristic of higher cognitive areas like PPC is that these combinations are compositional in nature, and can be constructed from a linear or nonlinear mixture of responses to each individual component of the combination. In contrast, most work in simultaneous movements in MC suggests that the responses to any nonpreferred effector are suppressed if the nonpreferred effector is moved with a preferred effector. To evaluate the relationship between simultaneous and individual movements, a linear model was trained on the single effector trials, and then tested on trials with simultaneous movements. This reveals whether simultaneous movements can be explained as a linear combination of individual movements. We also tested decoders trained on each condition within their trained conditions.

In RD-MCM, a linear decoder trained on individual movements is better able to predict movements of the contralateral thumb than the ipsilateral thumb (permutation test, $p < 0.05$ Figure 2.4a & b). In JJ-MC movements of the linear decoder trained and tested on the contralateral thumb shows better ability to predict direction than movements of the contralateral leg (permutation test $p<0.05$, Figure 2.4c & Supplemental Figure 2.12a). In all MC arrays, models trained on contralateral thumb movements are able to explain simultaneous congruent movements just as well as the model trained on congruent simultaneous movements (permutation test; $p>0.05$; Figure 2.4 a-c, Supplemental Figure 2.12a). Further, the cross decode performance of the model trained on contralateral thumb movements and tested on congruent movements is significantly better than that of the model trained on ipsilateral thumb movements and tested on congruent movements (permutation test, $p<0.05$). Notably, all models tested on incongruent simultaneous movements performed worse than those tested on individual and congruent movements (permutation test $p<0.05$). Additionally, unlike during individual movements, where individual movements could be decoded across effectors, there is little or no decoded representation of the ipsilateral thumb, or ipsilateral leg direction during simultaneous movements. This suggests that during simultaneous movements, the representation of the preferred effector, in this case the contralateral thumb, suppresses representations of other effectors.

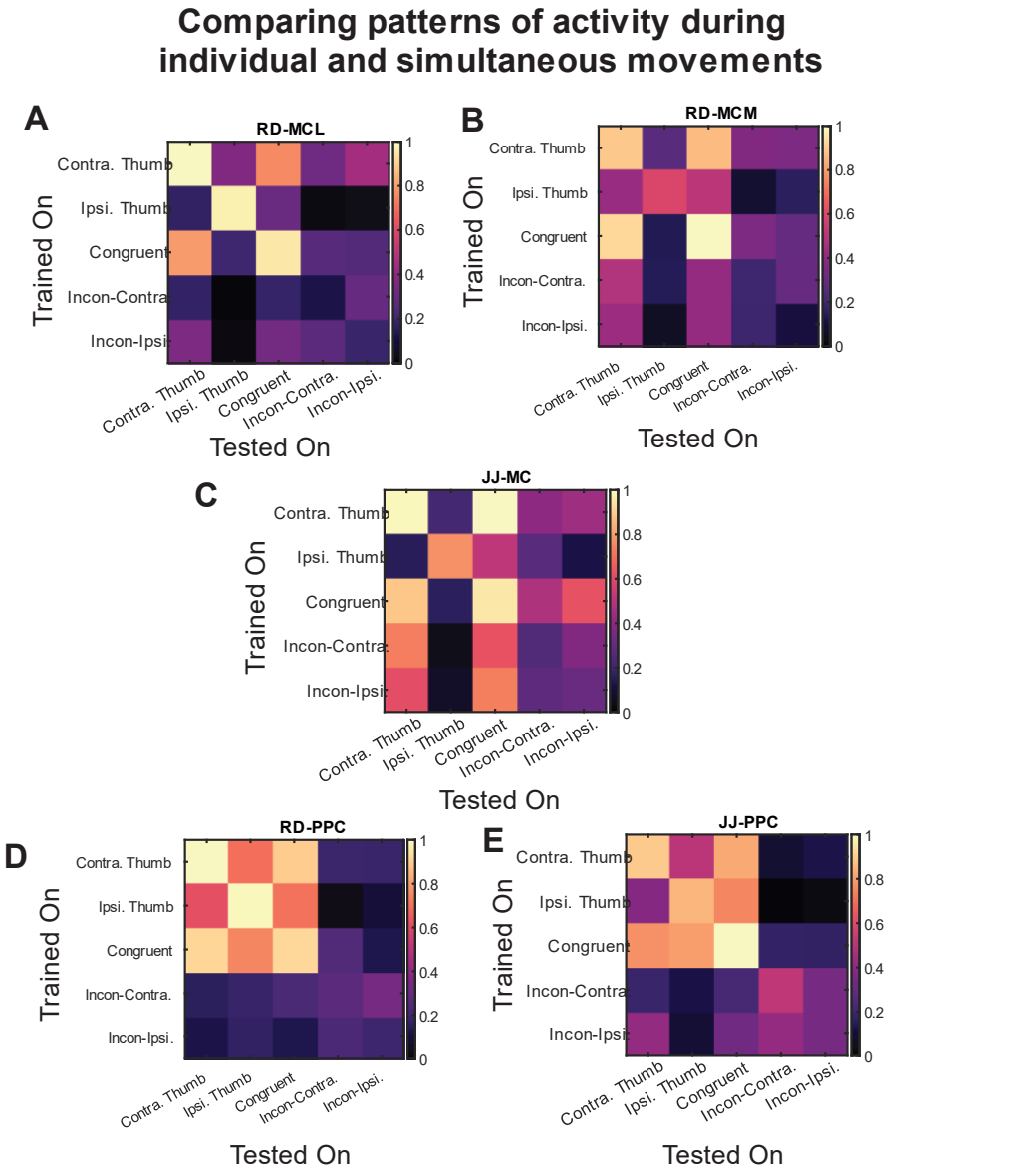

Figure 2.4 Comparing individual and simultaneous movements
A-E: A linear regression model was trained to predict direction from neural activity during each condition, with two models being trained for the incongruent condition (Intra-Contra and Intra-Ipsi, one for each effector's movement direction). These models were tested both within the condition they were trained on as well as across the remaining conditions. Model performance is described by the correlation between actual and predicted direction information. These r2 values were normalized to the maximum value for each array. The y-axis shows the condition each model was trained on and the x-axis shows the condition each model was tested on. The diagonal shows each model's performance within trained conditions. A RD-MCL; B RD-MCM; C JJ-MC; D RD-PPC; E JJ-PPC.

In RD-PPC and JJ-PPC, linear models trained and tested on individual movements performed similarly across all effectors (Figure 2.4d-e, Supplemental Figure 2.12b). In the case of RD-PPC, no linear model tested on incongruent movements was able to predict direction as well as models trained and tested on individual and congruent movements (permutation test $p<0.05$; Figure 2.4d). Additionally, there was no difference in cross-decode performance of models trained on individual movements and tested on incongruent movements and the models trained and tested on incongruent movements (permutation test; $p<0.05$). In JJ-PPC, again the models trained and tested on individual and congruent movements were better able to predict direction within their conditions than those trained and tested on incongruent movements (permutation test $p<0.05$; f Figure 2.4e , Supplemental Figure 2.12b). Similarly in RD-SMG although individual and congruent movements could be decoded by linear models, performance for decoding direction during incongruent movements was much weaker. However, interestingly, the model trained on incongruent movements in the direction of the contralateral thumb was able to predict individual contralateral thumb movements nearly as well as the contralateral thumb-trained model, which was not the case for the model trained on congruent movements (Supplemental Figure 2.13).

2.3 Discussion

Hand knob of MC shows strong preferential tuning for contralateral hand movements

Traditionally, the organization of primary sensorimotor areas has emphasized the anatomical separation of effector representations. However, the extent to which these representations overlap has come into question in numerous studies over the past two decades (Gordon et al., 2023; Jensen et al., 2023; Meier et al., 2008a; Willett et al., 2020). In the present study we find tuning to effectors across the body in the hand knob of motor cortex, however the population pattern of results does not contradict an overall somatotopic organization across MC. There is a clear dominant effector, the

contralateral thumb, with the next preferred effector being the contralateral wrist, supports a gradual transition between coding for neighboring parts of the body.

At the single neuron level, we found overlap between coding for three main sets of effectors. Two of these sets are the contralateral/ipsilateral thumb and the contralateral/ipsilateral wrist. Previous work in both humans and nonhuman primates has also found coding for both sides of the body in a single hemisphere, although with some inconsistencies as to whether ipsilateral movements are encoded in the same neural populations as contralateral movements (Alkadhi et al., 2002; Ames & Churchland, 2019; Heming et al., 2019; Steinberg et al., 2002). The final effectors for which we consistently saw overlap are the contralateral thumb and contralateral wrist. This overlapping representation of the thumb and wrist again supports the gradual transition between effectors proposed for the somatotopic organization of motor cortex.

During simultaneous movements, the representation of the non-preferred effector appears to be largely suppressed. This argues against interpreting the representation of non-preferred effectors during individual movements as the same in nature as those for the preferred effector of an area within MC, and could indicate that this non-preferred representation does not contribute to actual motor output. Additionally, we observe different coding of direction during individual movements and movements in opposing directions. Most literature in both NHPs and humans has found that although coding for both a contralateral and ipsilateral effector may be present in one hemisphere of motor cortex, this representation changes between simultaneous and individual movements (Donchin et al., 1998; Steinberg et al., 2002; Willett et al., 2020).

Why would an area use either an effector-specific or overlapping effector representations in the first place? For example, in the primary somatosensory cortex (S1), somatotopic organization is logical as closer locations on the body are more likely to have correlated sensory input. This is not as exclusively

the case for movement, where multiple parts of the body are regularly moved in coordination. Thus a strictly somatotopic organization is perhaps less intuitive than one that also incorporates some functional or ethological organization as well. In addition, it has been proposed that in more dexterous NHPs and in humans, there could be two primary motor cortices with differing organizations to accommodate a more complex motor repertoire (Geyer et al., 1996). This would imply potential for different patterns of effector specificity within even neighboring areas of motor cortex. This result is further supported by a recent fMRI study which found patches of more effector specialized areas interleaved with less specialized areas in motor cortex (Gordon et al., 2023).

In this way, our implant location is likely to impact the degree of effector specificity seen. And to some extent we see that this is the case between our three implant locations in our two subjects. The two arrays in RD have fewer active channels than the one in JJ, and also showed less of a response across effectors that are not the contralateral thumb than seen in JJ. The arrays in RD are placed slightly medially and laterally relative to each other, and the overlap in effector representation seen is in line with what would be expected from a homunculus-like organization. In the more medial array, the next strongest represented effector after the contralateral thumb is the contralateral wrist. In contrast, in the more lateral array the second strongest coded effector is the ipsilateral thumb. As a further note on specificity in effector representations, we are limited to the surface of the cortex. Deep in the sulcus, there may be more anatomically specific responses, although a recent study that recorded from human central sulcus with sEEG also found overlap in effector representations (Jensen et al., 2023). In addition, as the implant site becomes more anterior, it becomes closer to premotor cortex where there would be more overlapping representation (Willett et al., 2020). The different levels of overlapping representation in two patients seen in Willet et al., 2020 further emphasizes the importance of implant location and level of effector preference.

PPC codes for effectors across the body without emphasis

Much like for MC, early work in PPC found generally that neurons within the same anatomical areas also coded for the same effector. This result was largely established in nonhuman primates and focused on distinguishing between eye and arm movements (Andersen et al., 2007). Functional MRI work in humans has shown much more complex patterns of effector representations across PPC. For example, individuals born without arms show extensive coding for the hand and toes in overlapping areas in PPC (Striem-Amit et al., 2018). This was first proposed to be reorganization of cortical circuits that would otherwise be used for hand movements in motor intact individuals. However, this overlap is seen in PPC for fully intact subjects as well (Heed et al., 2016). Additionally, damage to PPC can cause optic ataxia, which has been shown to cause similar deficits in both hand and foot movements (Evans et al., 2013).

These findings have led to a functional organization to be proposed, where the same code is used across effectors to achieve a particular movement. Although we do not find an effector specific organization, this generic organization does not fit our results either as at the single neuron level, there is not one single functional code being implemented across all effectors. This discrepancy is likely due to the resolution of fMRI compared with our single unit recordings, as the population code would likely be impossible to differentiate at the fMRI level.

Previous single neuron recordings in human PPC from our lab found the contralateral and ipsilateral hand and shoulder encoded in the same, small patch of cortex. The present finding extends this result to the entire body, although we found less structure based on the side of the body in the present study. In this study, we also extended the task to simultaneous movements. Our inability to explain simultaneous movements as a linear combination of individual effector movements would be a feature of the partially-mixed selectivity structure found in our previous study, and allow for more flexible computation across more limb combinations than linear combination would allow (Rigotti et

al., 2013; Zhang et al., 2017). The role of overlapping effector representations in computational efficiency will be expanded on in the next section.

Implant location within PPC likely impacts the anatomical separation of effectors. Evidence from lesion studies show damage to different areas of PPC can cause different motor deficits, for example damage to anterior bank of IPS causes deficits in grasping, while more medial lesions cause optic ataxia (Andersen et al., 2014; Grefkes & Fink, 2005). Our recordings are generally speaking from SPL which has been implicated in both visually guided movements and attention. Notably, the use of distinct neural populations for different effectors argues against the interpretation of a simple effector-independent attentional signal. Most work emphasizing effector specificity in NHPs came from within the IPS in NHPs, while our recordings are from the cortical surface. Thus, future recording from within human IPS may be needed to make true comparison to effector specific areas found in NHPs.

Coding for full body movements supports different structures of shared information in MC and PPC

What is the functional purpose of the overlapping effector representations we see in each area? In motor literature, it has been suggested that this could facilitate the transfer of motor skills from one limb to another (Willett et al., 2020; Zhang et al., 2017). Transfer of motor skills can occur both between limbs in motor intact individuals. Not only are skills transferable, but often, an individual's movement characteristics are preserved from one body part of the next (Liu et al., 2022). An example of this is in handwriting, where it has been found that writing produced by the digits, wrist, arm, and foot all share common characteristics (Wing, 2000). One fMRI study comparing finger and foot movements during name signing and zig-zag motions found increased activation of SPL regardless of effector or condition (Rijntjes et al., 1999). Further, both amputees and dysplasic individuals show

great dexterity with the feet when used in place of the hands (Yu et al., 2014). This suggests that at least some motor brain areas could contain a shared substrate for multiple effectors. Our data supports that in some areas, these shared substrates can occur between effectors across the full body within small neural populations, as in PPC. In other regions like MC, however, these shared substrates seem to only exist for particular effectors.

As mentioned in the previous section, another potential role for the coding structure, in particular in PPC, is computational efficiency. PPC has been shown to implement a coding strategy called partially mixed selectivity, where some variables are coded randomly (or nonlinearly) with respect to each other across the population, while other variables are coded with some structure (Fusi et al., 2016; Jeffrey Johnston et al., 2020; Rigotti et al., 2013; Zhang et al., 2017). For example, in our results we find that single neurons code for random combinations of effectors; however, a single neuron tends to use the same spatial/direction code across the effectors it encodes. Mixed selectivity in other cortical areas like prefrontal cortex has been suggested to provide a more efficient way of representing more complex and/or higher cognitive information, which would suggest PPC having a higher-level representation of motor control (Dang et al., 2022; Rigotti et al., 2013). This notion is further supported by results from fMRI studies that have found similar activity in PPC during overt movements to that during observed and imagined movements, but not as much so in MC (Abdollahi et al., 2013; Jastorff et al., 2010; Lotze et al., 1999; Miller et al., 2010; C. hyun Park et al., 2015; Rastogi et al., 2020; Vargas-Irwin et al., 2018). Given that PPC is an area with great variety in the types of information it represents from motor control to semantics, there is still much to be explored when it comes to understanding its functions (T. Aflalo et al., 2020; T. Aflalo, Zhang, et al., 2022; Andersen et al., 2019).

Limitations and Concluding Remarks

This study leaves the question of whether these results would hold in motor intact individuals, however it seems likely based on recent fMRI work. Additionally, recent results from a participant with less mobility than the subjects in the current study show the relationship between neural responses are linked to the biomechanical nature of movements (Guan et al., 2022). There is also some question of whether during each individual movement, other muscles weren't ultimately also being activated. Given that the representation of nonpreferred effectors was suppressed during simultaneous movement, it is also important to follow up with more complex, coordinated movements. Finally, although much of our results align across the two subjects there were slight differences that indicate the importance of replicating this type of experiment in other subjects.

This study presents the first single neuron evidence for encoding of effectors across the body in human posterior parietal cortex. In addition, we recorded from motor cortex simultaneously, allowing us to compare the encoding of movement variables in distinct neural populations. The surprising nature of these results contributes to the growing body of work that suggest that designing simplified and highly controlled experiments to probe predefined functions determined by existing cortical maps may limit our understanding of the more complex coding properties of different areas of cortex (Musall et al., 2019; Stringer et al., 2019). These results also have implications for evaluating the use of different brain areas in the control of therapeutic devices with brain-machine interfaces for those with impaired movement. In MC, strong representation of single effectors supports its usefulness in biomimetic control. In PPC, equal representation across effectors highlight its potential to be used flexibly across several applications.

2.4 Methods

Study participants

The present data was collected from two participants enrolled in a BMI clinical study (ClinicalTrials.gov Identifier: NCT01958086). The institutional review boards of California Institute of Technology, Casa Colina Hospital and Centers for Healthcare, and University of California, Los Angeles approved study procedures including informed consent, implant surgery, and experiment design. Participant RD is a right-handed male (age) with a C3-C4 level spinal cord injury that occurred approximately ten(check) years before his enrollment in the study. RD is able to move his eyes, head, and shoulders (can move shoulder but cannot stabilize arm). In addition, RD shows weak residual movements (twitches) of the wrist and thumbs. Participant JJ is a right-handed male (age), with a C4-C5 level spinal cord injury that occurred approximately three years before his enrollment in the study. JJ is able to move his eyes, head, and shoulders like RD.

Experimental Procedures

Two adaptations of a traditional center out task were used. Both tasks were displayed on a screen in front of the participant. participants were instructed to attempt movements as though they were motor-intact. At the start of the trail, participants were in a neutral position with their eyes fixed in the center of the screen. In the first task, the participants were instructed to attempt movements of twelve different effectors (head, eyes, right/left shoulders, wrist, thumbs, legs, and ankles) in five different directions, 72 degrees apart, indicated by one of five targets on the screen changing color from gray to red as a “go” cue (Supplemental Figure 2.1.a). The participants were asked to make the instructed movement and then relax. Fixation was kept at the center except during trials for the eyes. Between each trial was an inter-trial-interval during which time the participant was at rest. Each inter-trial-interval was 1.5s and each go phase was 2s. The participants moved one effector to each of the five

targets before the instructed effector changed to the next. A total of seven sessions were collected for JJ and six for RD. Three runs of the task with two repetitions for each movement were collected for each session.

The second adaptation to center out incorporated simultaneous movements of a pair effectors (Supplemental Figure 2.1.b). In participant RD the contralateral thumb and ipsilateral thumb were tested. In participant JJ, movement pairs were the contralateral thumb and contralateral leg as well as the contralateral thumb and ipsilateral thumb. There were four conditions, or movement types; one where the participant attempted individual movements of the contralateral thumb, one where the participant made individual movements of the other effector (e.g. ipsilateral thumb), one where the participant moved both effectors in the same direction simultaneously, and a final condition where the effectors were moved in opposing directions simultaneously. Movements were made to six targets 60 degrees apart indicated on the screen. Trials were split into three runs and for each run of the task the participants went through each of the six movements for a condition before moving onto the next condition. The participant was cued for which movement direction and which effector(s) using red and/or blue markers over the target(s). An inter-trial-interval of 1s interleaved each go phase of 2s. Six sessions for each effector pair tested in JJ and six sessions for the pairing tested in RD were collected. Each data session for each effector pair consisted of three runs of the task with three repetitions of each movement per run.

Implant Locations

Participant RD was implanted with four 64-channel NeuroPort Utah electrode arrays in his left hemisphere in July 2023 (Figure 2.1a). Two arrays were placed near the hand knob of left precentral gyrus, with one slightly more lateral and the other slightly more medial (denoted RD-MCL and RD-MCM respectively). A third array was placed in the superior parietal lobule (RD-PPC). Finally, a

fourth array was placed within the supramarginal gyrus (RD-SMG). Data from participant RD was collected ranging from three to six months after implant surgery. Participant JJ was implanted with two 96-channel NeuroPort Utah electrode arrays in his left hemisphere in December 2018 (Figure 2.1b). One array was placed near the hand knob of left precentral gyrus, and is referred to as motor cortex or "JJ-MC". The second array was implanted in the left superior parietal lobule and is denoted "JJ-PPC". Data from JJ was largely collected 20-22 months after surgery (along with one session 13 months and a final session 27 months post implant). A presurgical functional MRI during which each participant performed a grasping imagery task showed substantial bold response in regions surrounding each of the implant locations.

Neural signal recording and preprocessing

Microelectrode arrays in each participant were recorded from simultaneously. Neural signals recorded from the electrodes were amplified, bandpass filtered (0.3 Hz–7.5 kHz) and digitized (30 kHz, 16 bits/sample) (NeuroPort Neural Signal Processors, Blackrock Microsystems Inc.). To detect action potentials, the signal was then high-pass filtered at 250 Hz and thresholded at -3.5 times the root-mean square voltage (for each electrode). We used the k-medoids clustering method along with the gap criteria in order to identify single neurons and the total number of waveforms respectively (Tibshirani et al., 2001). This was done for the first four principal components, (n was selected to account for 95% of waveform variance).

For analysis of each behavioral epoch during the 12-effector task, we calculated firing rates from neural activity over a 500ms window of neural activity. The movement execution ('Go' or 'move') analysis window was defined as the 500 ms window starting 250 ms after the Go cue. Similarly, the 500 ms inter-trial interval window used in the crossnobis analysis began 250 ms after the end of the

go phase. For the simultaneous movement task the cross decode window used was 1 s and began 250 ms after the go cue.

Neurons with an average firing rate of less than 1 Hz across the entire task were excluded from the analysis as noise. Additionally, all analysis was repeated on well-isolated neurons to avoid influences from multi-unit clustering (Supplementary Figure 2.8). We classified neurons that corresponded to the lowest third of L-ratio values as well-isolated (Schmitzer-Torbert et al., 2005).

Crossnobis analysis for population and single unit firing rates

The cross-validated mahalanobis distance was used to compare the population level neural activity during movements of each effector and a baseline (no movement). Leave-one-out cross validation was used. A permutation test was used to determine whether there was a significant difference between the distances of firing rates from baseline during movements of each effector.

Event Related Averages

Firing rates for each neuron were grouped by condition and then the mean and standard error of the mean of these responses were found for 100ms bins across a 2.5s window.

Strength of single unit responses across effectors

In order to determine the strength of an individual neuron's response to different effectors, first we determined a single neuron's cross validated best and worst tuned direction by finding maximum and minimum firing rates across trials. The response for each effector was then evaluated by subtracting the neuron's firing rate during its best tuned direction from the neurons firing rate during its worst tuned direction during movements of each effector. To evaluate whether the response to an effector was significant, the same measure was performed with shuffled firing rates in order to find a null

distribution for that neuron to compare the strength of response for each effector (>95 percentile). The best effector for each neuron was then determined by finding the largest difference in firing rates between best and worst direction. Main figure results were also normalized and neural responses were sorted first by best effector (eyes to ankles) and then the number of effectors to which that neuron was tuned (least to most).

Comparing spatial tuning of single neurons across effectors

The spatial tuning of each neuron was determined independently for the most preferred and second most preferred effector for each significantly tuned neuron (most preferred, second most preferred, and test for significance described in the analysis for Figure 2.2). This was done by performing a linear regression using neural firing rates as predictive variables and x and y values for the target location on the screen as response variables. The coefficients from this regression give the directional vector coded by each neuron. The angle between these resulting vectors was calculated to compare the spatial tuning between a neuron's most preferred and second most preferred effectors. Finally, the matlab toolbox CircStat was used to calculate the circular mean and confidence intervals for each distribution, and also to perform the Rayleigh test for uniformity.

Determining body vs world-centered coordinated

To determine whether neurons were encoding space in a body-centered, or intrinsic reference frame, or a world-centered, or extrinsic reference frame, linear regression was used to find the direction vector coded by each neuron for pairs of contralateral and ipsilateral effectors (described in section above). Then the beta values from these regressions were correlated for each pair of effectors. A positive correlation indicated extrinsic coding, a negative correlation indicated intrinsic and no correlation implies some combination of the two. We found a significant negative correlation in JJ-MC that implies intrinsic coding of direction (Supplemental Figure 2.10). Thus, in any of the analyses

where we want to compare between directional coding of the contralateral and ipsilateral sides of the body, we must adjust the position information to be the same in intrinsic rather than extrinsic coordinates. This can be achieved by switching the position information for movements to the left and right targets. This was only done for JJ, because no such intrinsic relationship was found in RD.

Finding shared subspaces between effectors within the population code

We evaluated the structure of the population using a cross-validated partial least squares regression model to find shared directional subspaces between pairs of two effectors, for each possible combination of effectors. A model for each effector pair was trained using neural firing rates across all units as predictor variables and the target position information for all trials for the two effectors as the response variable. The model output was the predicted position information. The performance of this model was evaluated by taking the bootstrapped correlation between the input labels and those predicted by the model. In order to determine whether the r2 values were driven by shared information or a single pair in the effector, a null r2 distribution was generated. The null r2 distribution was found using the same general steps, but with randomly shuffled firing rates. The threshold for significance for shared information was the 99th percentile of that null distribution. Both models were k-fold cross validated over six folds.

Explaining simultaneous movements with individual movement components

A linear regression model was trained using firing rates from each condition of the task as predictive variables and using both x and y position information as response variables. Position information was given by the target location on the screen. For congruent simultaneous movements, there was a single target location and thus a single model was trained using that location. In the case of incongruent movements, there were two target locations, and thus two models were trained, one for each effector's direction of movement. Then the model was tested on its ability to predict position information both

within the trained condition, and across all other conditions. Model performance was determined by the correlation between actual and predicted position information (r2). This model was cross validated using k-fold cross validation with 5 folds. The r2 values for x and y values were averaged as a single performance measure and then normalized to the max r2 value.

Author contributions

K.K., T.A., and R.A.A. designed the study. K.K. and T.A. developed the experimental tasks. K.K., T.A., and J.G. analyzed the results. K.K., T.A., J.G., and R.A.A. interpreted the results. K.P. coordinated regulatory requirements of clinical trials. N.P. and A.B. performed the surgery to implant the recording arrays.

Supplemental Figures

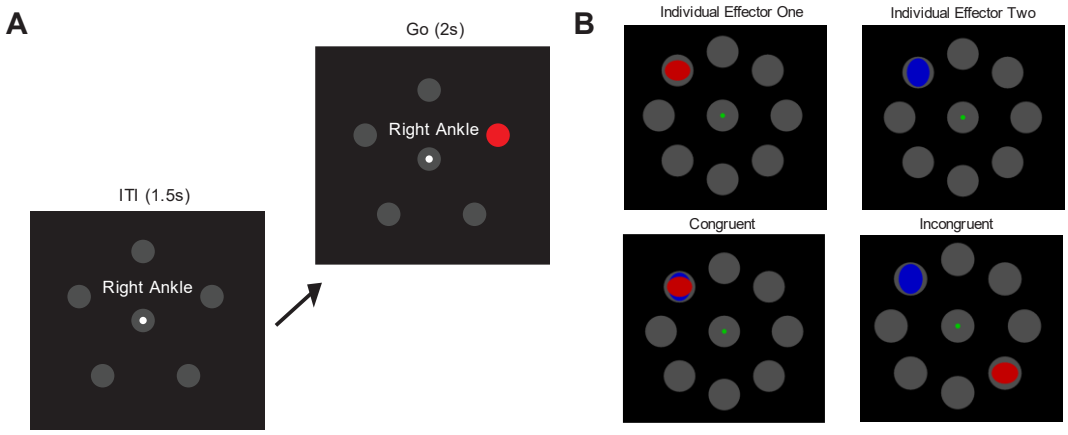

Supplemental Figure 2.1
A: Example frames from the twelve effector center-out task. In this task, participants moved one of twelve possible body parts in five directions (shown by the gray targets) before moving on to the next effector. The effector being moved was instructed by text on a screen in front of the participant, and motor initiation was cued when one of the five outer targets changed from gray to red. Movement execution phases were 2s and followed by 1.5s of rest during an inter-trial-interval. B: Example frames from the simultaneous movement task. In this task, participants moved either one or both of two effectors in six possible directions. Individual movements of an effector were cued by a red or blue circle over the target in the instructed movement direction. Simultaneous movements in the same direction, or congruent movements, were cued with both red and blue circles appearing over the same target. Simultaneous movements in opposing directions, or incongruent movements, were cued with red and blue circles appearing on targets directly opposite each other. Movement execution phases were 2s and followed by 1.5s of rest during an inter-trial-interval.

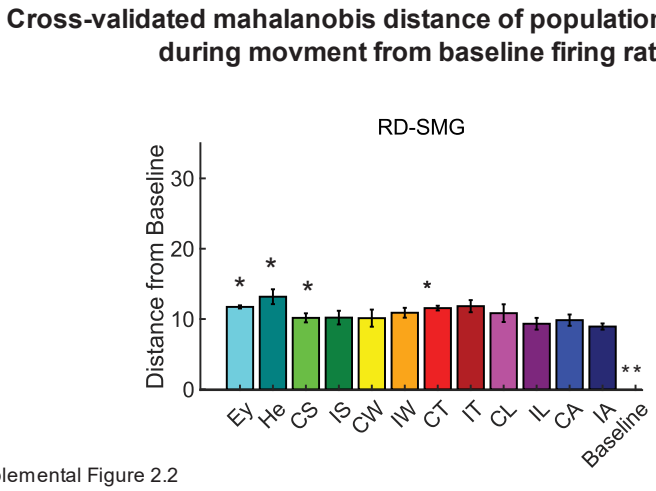

Supplemental Figure 2.2
Cross validated mahalanobis distance between population firing rates during movement and rest in RD-SMG. The responses during movements of the head were significantly stronger than movements of the ipsilateral shoulder, both wrists, the contralateral thumb, both legs, and both ankles. Additionally, the responses during ipsilateral leg and ankle movements were weaker than the eyes, head, contralateral shoulder and contralateral thumb.

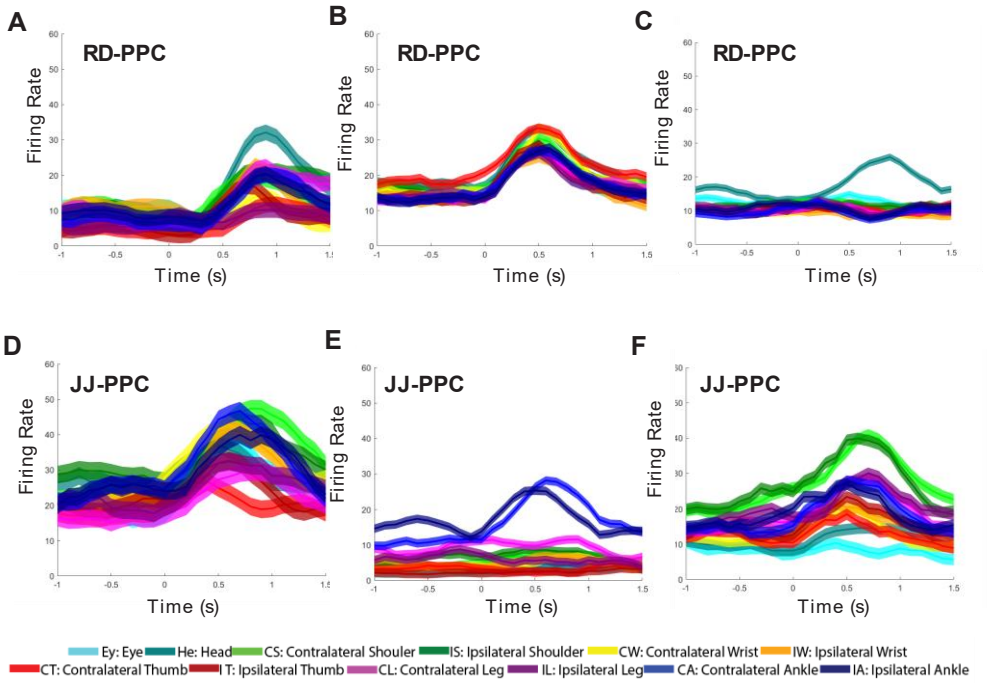

Supplemental Figure 2.3
Event- Related Averages for more example neurons. A-C examples from RD-PPC. D-F examples from JJ-PPC.

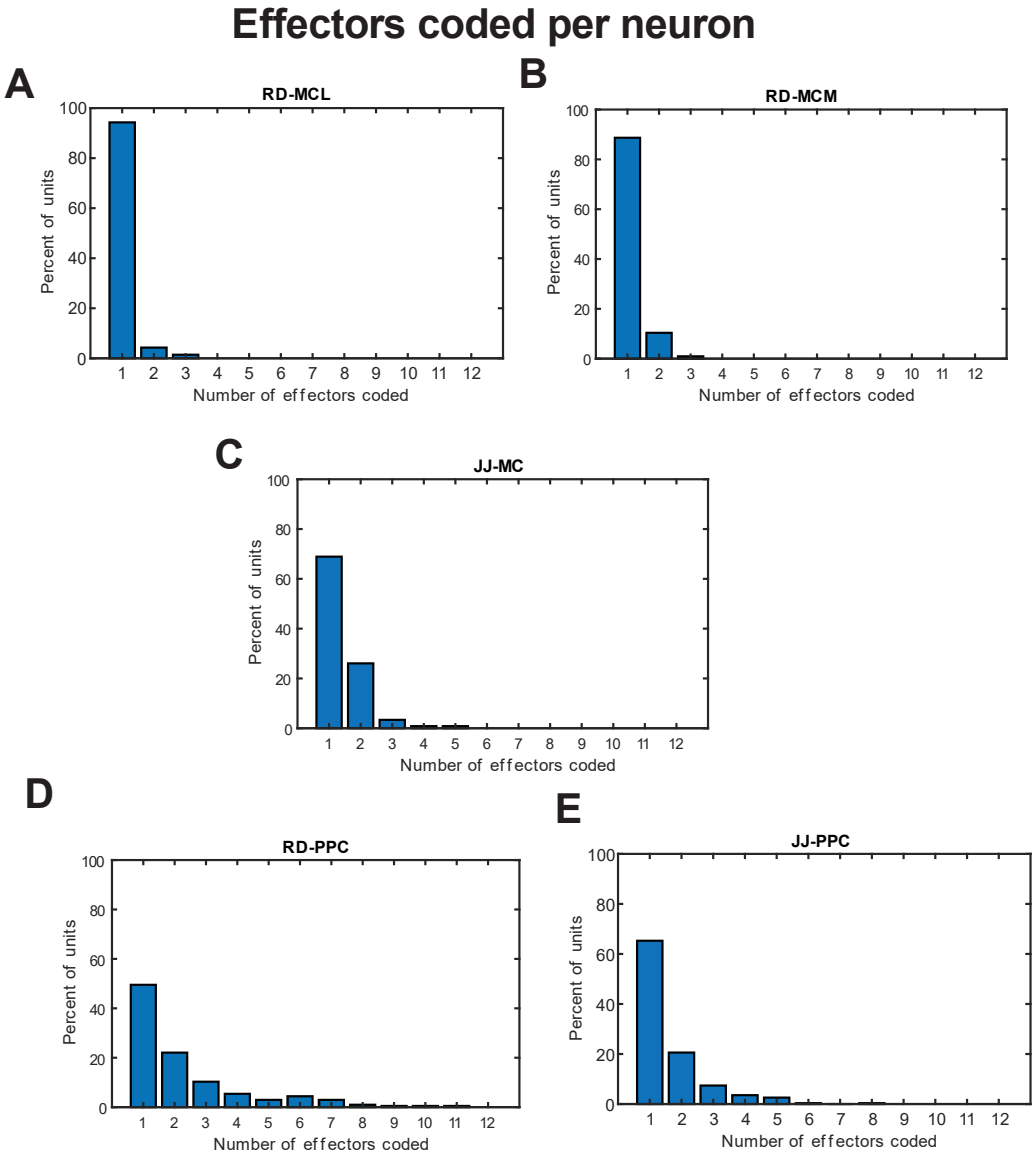

Supplemental Figure 2.4
The number of effectors coded by each neuron was found by determining the number of effectors that evoked a significantly strong response from that neuron (as computed for figure 2). A: RD-MCL, B: RD-MCM, C: JJ-MC, D: RD-PPC,E: JJ-PPC.

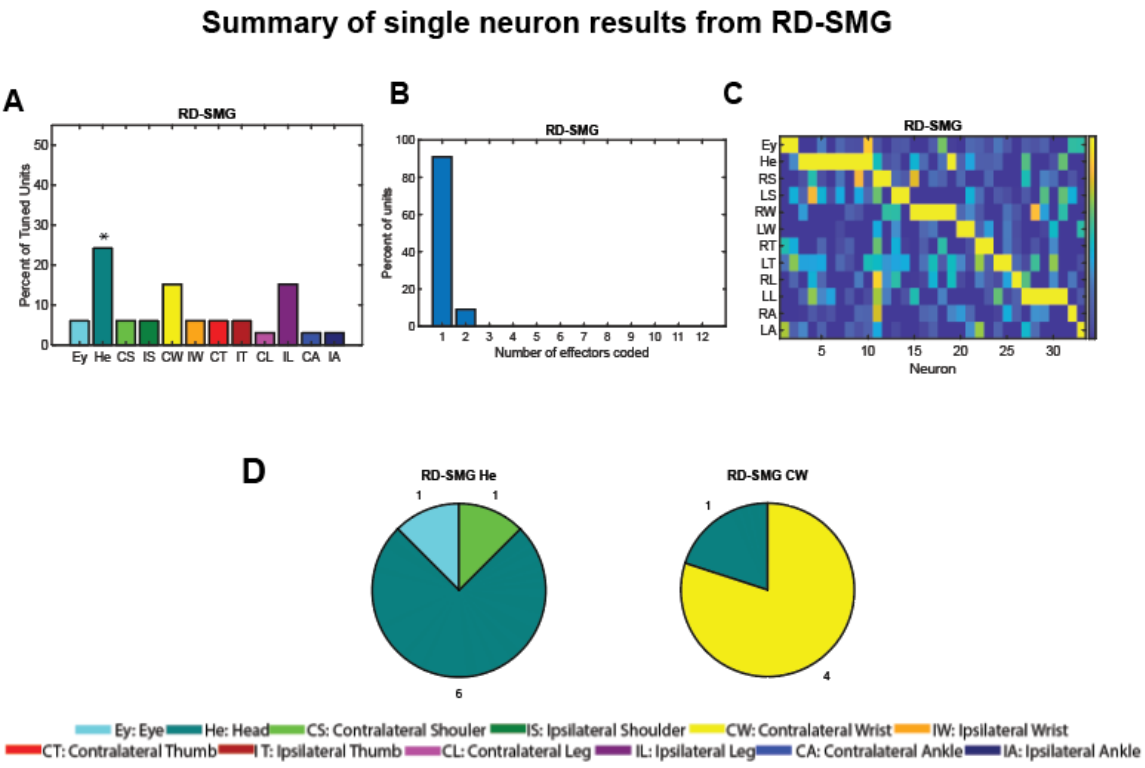

Supplemental Figure 2.5
Single neuron responses across effectors in RD-SMG. A. The single neuron effector preferences in RD-SMG are spread evenly across effectors with the exception of HE being more commonly preferred than EY, CT, IT, IL, CA, and IA. B. The percent of population coding for one, two, three, etc. effectors. C. Strength of single neuron responses in RD-SMG across effectors. D. Summary of effectors coded by the two neurons in RD-SMG that were tuned to more than one effector.

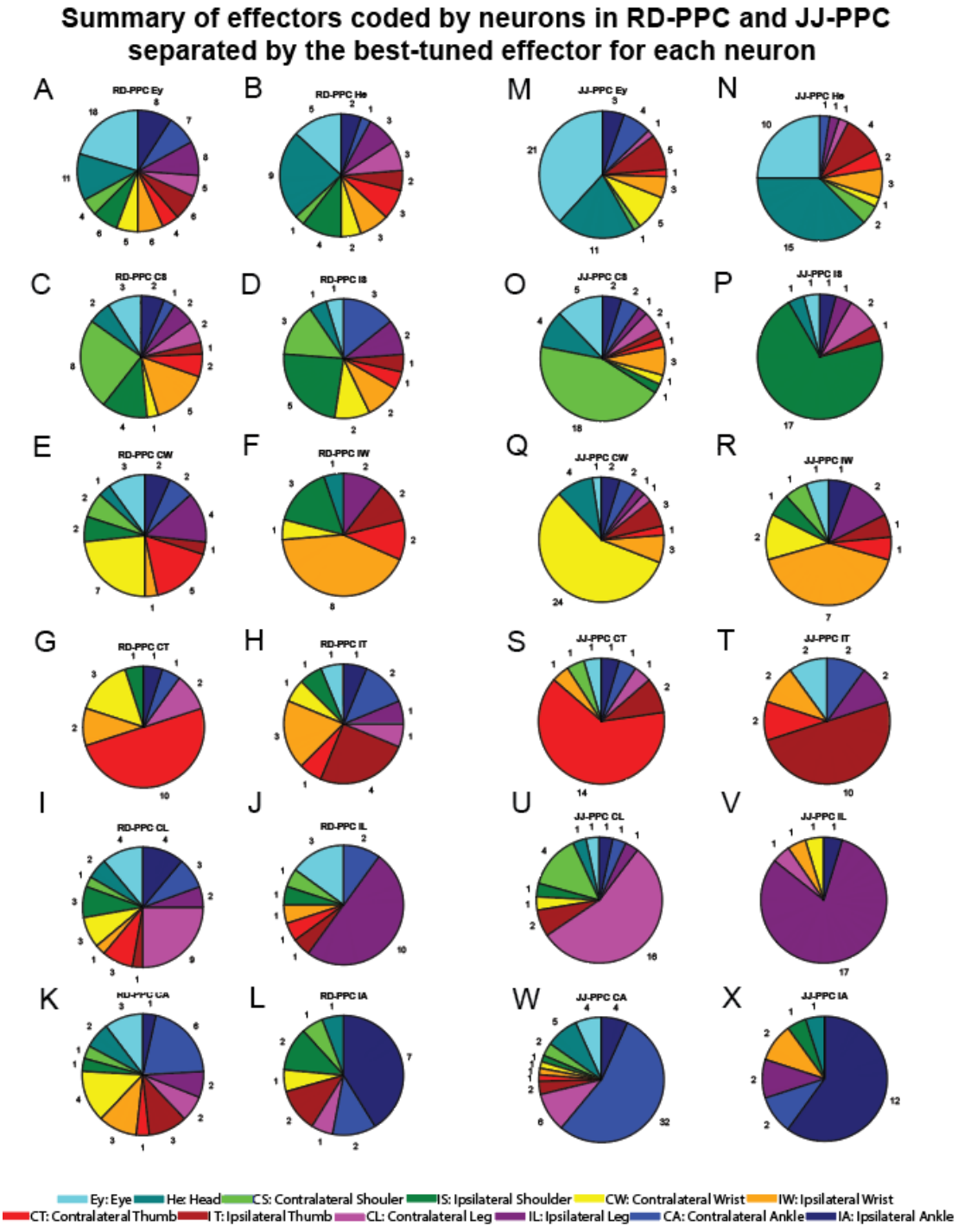

Suplemental Figure 2.6. Breakdown of single neuron tuning preferences for all effectors.

Neurons are sorted into groups based on the effector they most preferred. The different effectors coded by neurons with each effector preference are summarized in eaech pie chart. A-L: RD-PPC, K-X: JJ-PPC.

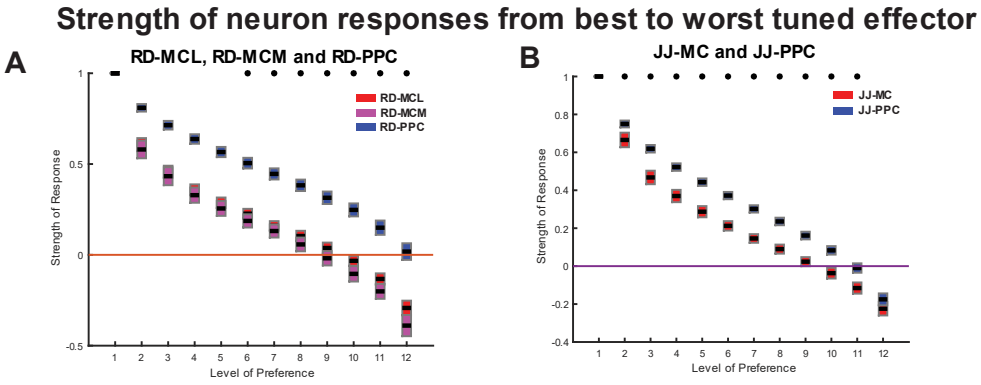

Supplemental Figure 2.7

A & B The strength of each neuron's response across all twelve effectors was sorted from strongest to weakest response. Then the distribution of responses across the best effector, second best effector, and so on, was plotted for each array (corresponding to a level of preference of 1 and 2, respectively, and so on until 12 for the least preferred effector). A: Distribution of responses from RD-MCL (red), RD-MCM (magenta), nd RD-PPC (blue). Stars indicate differences between RD-MCL and RD-PPC as well as RD-MCM and RD-PPC. B: Distribution of responses from JJ-MCL (red) and JJ-PPC (blue). Stars indicate differences between JJMC and JJ-PPC.

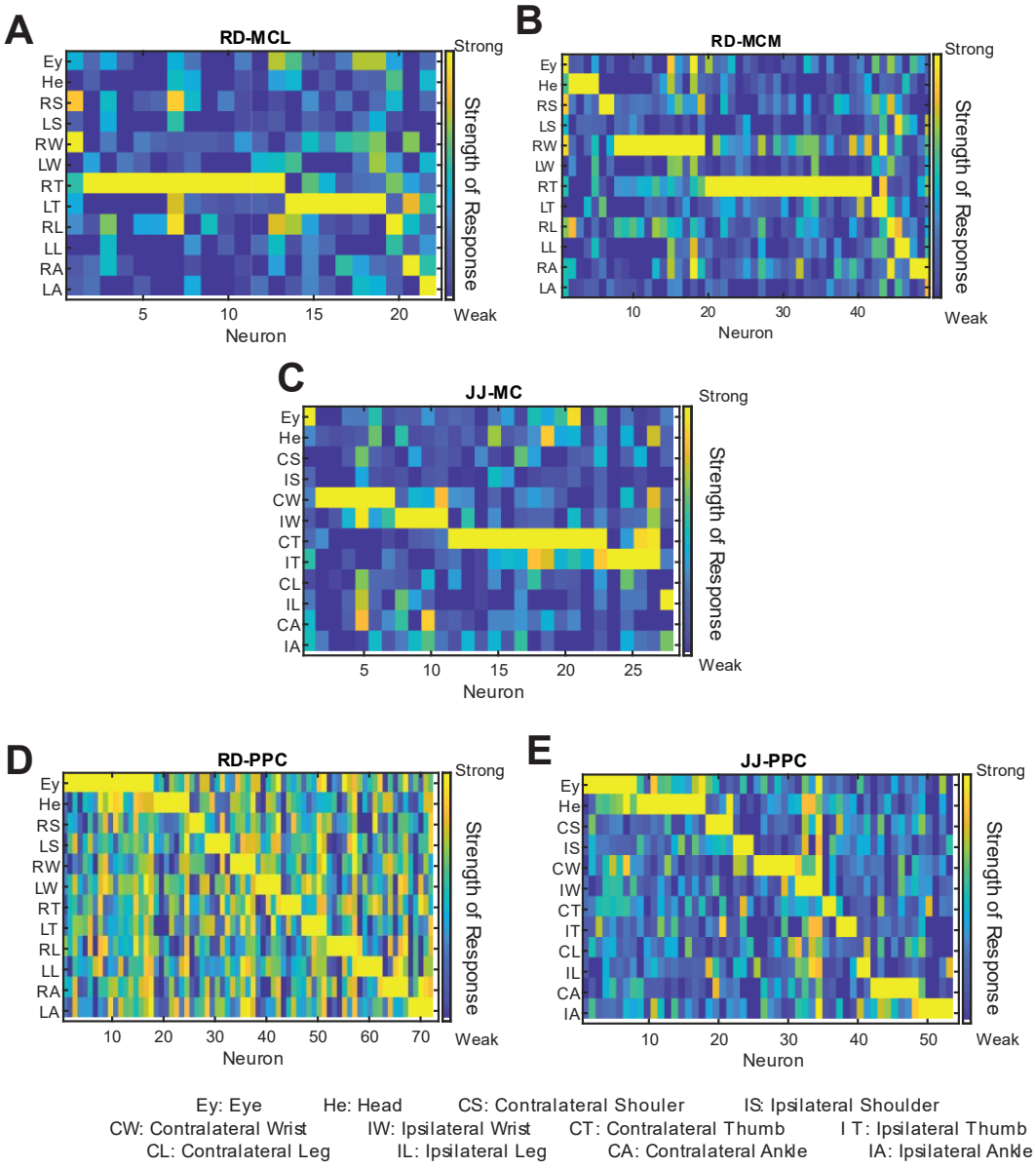

Supplemental Figure 2.8 Responses from well isolated units
A-E: The same strength of response used in figure 2F-J was found for neurons that met a more rigorous criteria in spike quality. A: RD-MCL, B: RD-MCM, C: JJ-MC, D: RD-PPC,E: JJ-PPC.

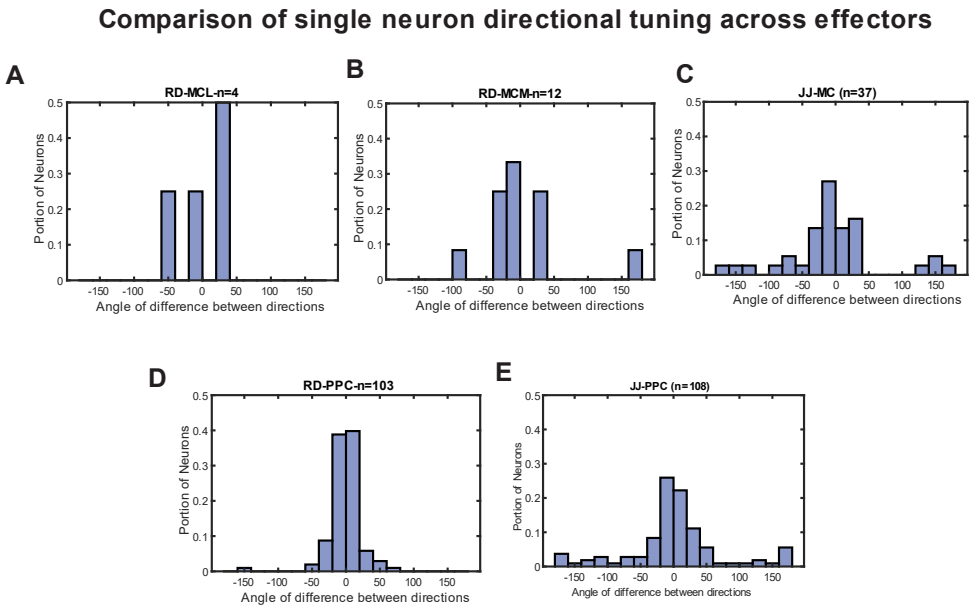

Supplemental Figure 2.9
A-E The angle betw een the direction vectors coded for the most preferred and second most preferred effector of single neurons. A. RD-MCL circular mean (cm) = 0.344° +/- confidence intervals (ci) = 48.129°. Rayleigh test for uniformity p <0.05 B RD-MCM cm = -11.05°, ci = 31.341°. Rayleigh test for uniformity p <0.05. C.JJ-MC cm = 0.000°, ci=18.5°. Rayleigh test for uniformity p<0.05. D RD-PPC cm = -0.493°, ci = 4.412°. Rayleigh test for uniformity p <0.05. E JJ-PPC cm = 0.000°, ci = 4.84°. Rayleigh test for uniformity p <0.05.

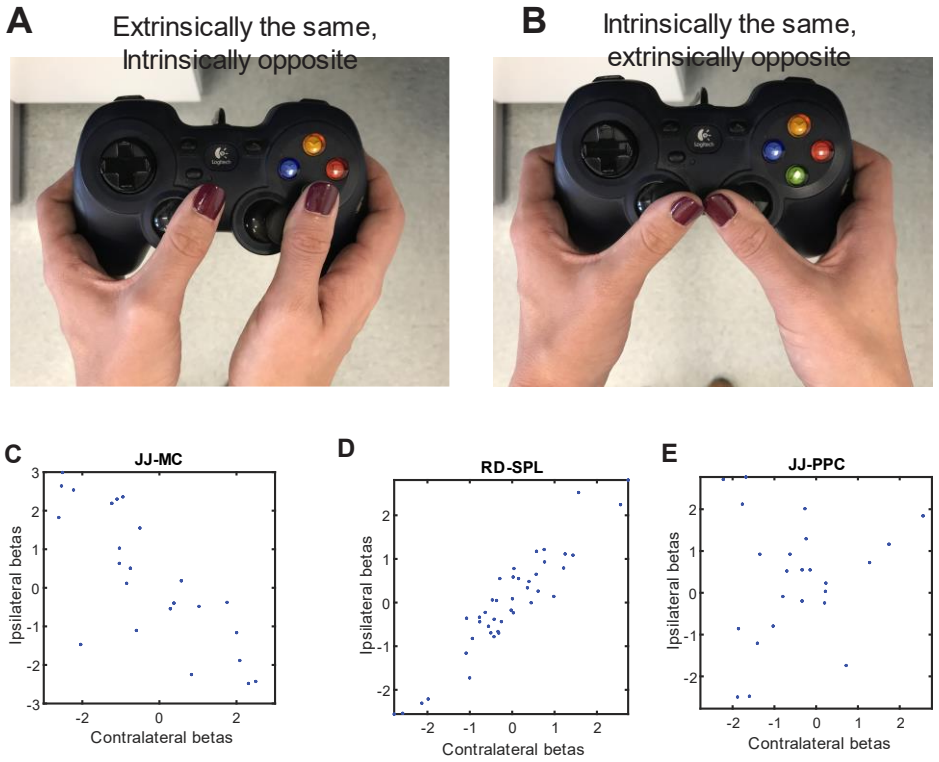

Supplemental Figure 2.10.
A An example of thumb movements that are both extrinsically in the same direction, to the right, but they require movements in opposite direction relative to the joint of the thumb, or intrinsically in opposite directions. B An example of movements that are in extrinsically opposite directions (ipsilateral thumb to the right, contralateral thumb to the left), they require movement in the same direction relative to the thumb joint, and are intrinsically the same. C - E The resulting betas for linear regressions for contralateral and ipsilateral pairs of effectors. C JJ-MC r2 = -0.75, p < 0.001 D RD-PPC r2= 0.94, p <0.001 E JJ-PPC shows no correlation.

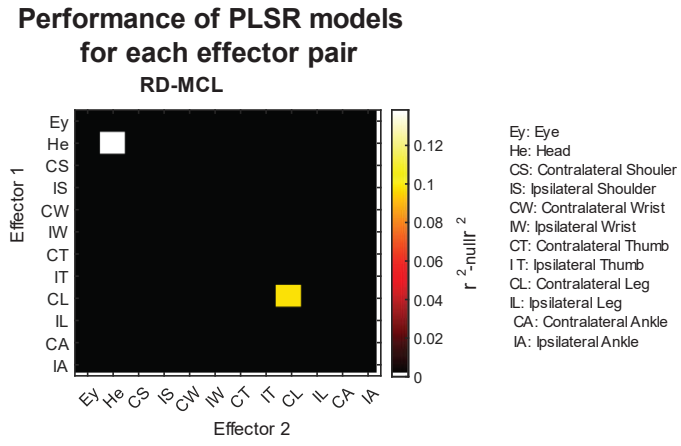

Supplemental Figure 2.11
Shared directional subspaces in RD-SMG. No pairs shair information, and even within effectors spatial tuning is weak.

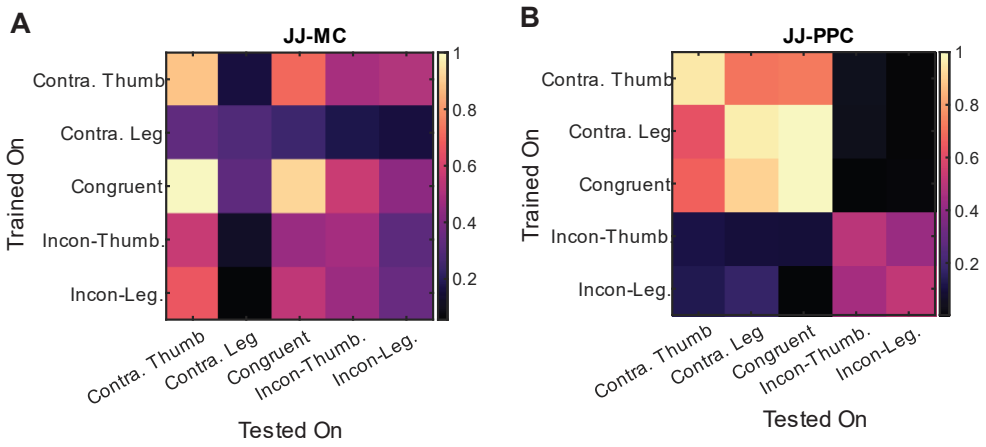

Supplemental Figure 2.12 Comparing individual and simultaneous movements of the thumb and leg A-B Performance of linear models trained for individual and simultaneous movements of the contralateral thumb and leg. A. JJ-MC B JJ-PPC

Chapter 3

CONTEXT-DEPENDENT COORDINATE FRAMES IN HUMAN POSTERIOR PARIETAL CORTEX

Summary

Our ability to interact with objects around us is easy to take for granted, but requires complex neural transformations to convert spatial information from the input of retinal coordinates into the proper motor output. When reaching out to grasp an item, the object position transitions from being coded relative to the position of the eyes to being coded relative to the position of the hand. Traditionally it has been thought that this process, like other parts of motor control, is organized with anatomically separate areas in the cortex coding for different effectors. We recorded from 96 intracortical electrodes implanted in the left hemisphere of the posterior parietal cortex (PPC) in two subjects and in the left hand knob of the motor cortex (MC) of one subject. We used two versions of the same task to test movements of different effectors. First, the subject positioned their eyes and right hand at varying locations on a monitor. Then a target was shown, followed by a delay period during which the subject maintained gaze and hand position. Finally, after a go cue, the subject performed either an imagined reach (IR) or a saccade to the target depending on the version of the task. We found that in the early phases of both versions of the task when the relevant information is the hand and eye position, the neural population in PPC encoded a vector from the hand to the eye. When the target became visible, the coding seen in PPC began to differ between the two tasks. In the IR task, the population began to code a vector from the hand to the target in addition to the vector from the hand to the eyes, while in the saccade version of the task, it began to also code a vector from the eyes to the target. Finally, during movement execution, PPC encoded the vector from the hand to the target if an IR was being performed, and a vector from the eyes to the target if the subject made a saccade.

This population result was also seen at the single unit level, where some individual units showed changes in vector coding through the task. In MC, there was no vector coded during the initial phases of the task without movement. During the go phase, a hand-target vector was coded for the IR task, but no vector is coded for saccades. The results from MC are in line with what is expected from an effector-organized network, but the flexibility of the vector coding seen in PPC is surprising. As we have been able to study PPC in humans more thoroughly, a higher cognitive movement code has emerged. The exact purpose of this switching of representation is not immediately clear, but is a promising area for future research.

3.1 Introduction

Our ability to coordinate between visual inputs and motor outputs is an essential part of our interactions with the world around us. For proper hand-eye coordination for example, our neural coding of spatial information must be with respect to our hand in order to accurately interact with a visual target, but the initial spatial information will have been received at the retina, and thus be coded with respect to the eyes (Andersen et al., 1993). This means a transformation in the relative spatial coding, or the coordinate frame, that is used by visual input versus motor output neural populations.

When considering the brain areas that may be most important to this transformation, we can assume that the visual cortex (V1) and motor cortex (M1) as input and output coordinate frames respectively, but where is this transition occurring? Between V1 and M1 is posterior parietal cortex (PPC) (which also receives inputs from S1) making it in prime anatomical position for a role in this process (Andersen et al., 1985, 1997; Buneo & Andersen, 2006). This has led to PPC being a target area of non-human primate research, which has given us great insight into the cortical organization of coordinate frames. Initial investigations found singular coordinate frames being implemented by PPC populations, such as coding in gaze-centered coordinates in the lateral intraparietal area (LIP) and

parietal reach region (PRR) (Andersen et al., 2007; Andersen & Buneo, 2002; Batista et al., 1999; Bremner & Andersen, 2012; Buneo et al., 2002; Cohen & Andersen, 2002; Snyder et al., 1998). Recordings in area 5d, however, revealed a dynamic coordinate frame that was context dependent and shifted the relative coding of hand position between movement planning and execution (Bremner & Andersen, 2014). Ultimately flexible coordinate frames have now been observed in several areas of NHP PPC including within the intraparietal sulcus (Caminiti et al., 2015; S. W. C. Chang & Snyder, 2010; Chen et al., 2018; Mcfadyen et al., 2022; McGuire & Sabes, 2011; Mullette-Gillman et al., 2005, 2009; Taghizadeh et al., 2024).

Functional MRI in humans has suggested there may be a similarly flexible population level coordinate frame in area 5 of PPC, but this has yet to be studied in single neurons of human PPC (Bernier & Grafton, 2010; Chen et al., 2018; Leoné et al., 2015). Not only is this of interest for comparing findings from NHPs to humans, but also for evaluating neural signals in PPC in the context of control of neural prosthetics. In many instances, results seen in human PPC have demonstrated higher complexity than those in NHPs (Bruner et al., 2023; Heed et al., 2016; Kastner et al., 2017; Zhang et al., 2017). Thus, we sought to examine coordinate frame coding in two participants with intracortical utah arrays in PPC, implanted as part of an ongoing BMI clinical trial.

We studied the coordinate frames coded by these populations with two different contextual manipulations. In the first, we implemented a similar delayed reaching paradigm used to show context dependent coordinate frame coding in area 5d of NHPs, in order to compare our findings. We report a similar population level shift in coordinate frame coding of hand position relative to gaze position to coding hand position relative to target position. This is driven both by independent populations of neurons active across different phases of the task, as well as by a shared population of single neurons switching between these relative position codes.

There has been a recent emphasis on an overlapping representation of different parts of the body in human PPC, both in single neuron recordings as well as neuroimaging studies (Heed et al., 2016; Striem-Amit et al., 2018; Zhang et al., 2017). This is in contrast to a previous emphasis on separation of representation of at least certain effectors, such as the hands and eyes, into distinct anatomical locations of cortex (Andersen et al., 2007). Thus, to determine if the flexibility in coordinate frames extends to the context of movements of different parts of the body, we had the subjects perform a delayed saccade paradigm that was identical to the delayed reaching task except in that the movement executed was a saccade. In this case, we found that the population in PPC shifts from coding the hand position relative to the gaze position to coding the gaze position relative to the target position. Unlike the shifting population coordinate frame seen in the reach version of the task which was driven by both distinct and shared neurons, the population vector observed during the saccades version of the task was almost entirely driven by distinct neurons with a few exceptions. These results help provide further context to recent findings of overlapping representations of movement of different parts of the body in PPC and show that this is likely supported by the populations ability to flexibly implement a coordinate frame for each effector.

Results

We recorded from single neurons intracortically in human posterior parietal cortex in two participants implanted with Utah arrays. Subject JJ has a C4/C5 spinal cord injury and has one 96 channel array in hand knob of motor cortex (JJ-MC) and one 96 channel array in the superior parietal lobule of PPC (JJ-PPC) (Figure 3.1A). Subject NS has a C3/C4 spinal cord injury and one 96 channel in PPC at the junction of the post central gyrus and intra parietal sulcus (NS-PPC) (Figure 3.1B). All implants in both subjects are located in the left hemisphere. A functional MRI was used to help guide implant location, during which the participants performed a grasping motor imagery task (Guan et al., 2022).

In order to determine what coordinate frames were encoded by populations of neurons in human PPC, we first used a delayed imagined reaching paradigm (Figure 3.1C). During this task, the subject was instructed to fixate their gaze at a circle on a monitor in front of them, and at the same time imagine holding their hand in line with a hand icon on the same monitor. A target appeared on the screen above their held gaze and hand positions. After a 1.5s delay, a go cue was given and the subject imagined reaching to the target while maintaining their gaze position. After 6 s the trial ended and after an inter-trial-interval, the next hand and gaze start positions were shown. A combination of four possible hand, gaze, and target positions were used each trial.

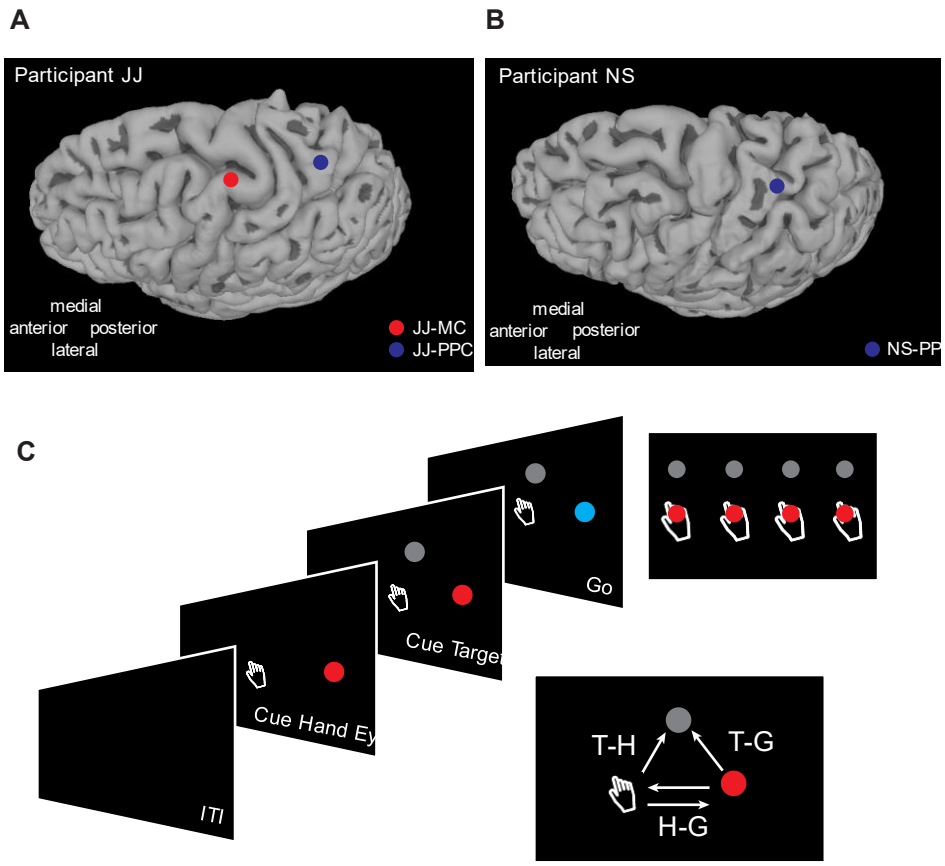

Figure 3.1. Implant locations and behavioral task
A: JJ Implant locations, JJ-MC (red), and JJ-PPC (blue). B: NS Implant locations, NS-PPC (blue). C: Delayed reach/saccade task with four combinations of hand, gaze, and target position (positions shown in top right). The geometry for vectors between each position are shown in the bottom right

First we assessed the directional tuning properties of the neural populations in PPC during this task. Recorded data was spike sorted and then an n-way anova was used to determine whether individual neurons were tuned to the position of the hand relative to the position of gaze, or hand relative to target. Then we plotted the percent of significantly tuned neurons across time from the initial set up phase through movement execution (Figure 3.2a and b; results for individual participants in Supplemental Figure 3.1). After adjusting for multiple comparisons, we found that 20% of neurons

are tuned to the hand position relative to gaze position during the initial cue phase. During imagined reaches, 25% of neurons are tuned to the hand position relative to the target position. To begin to understand the tuning preferences of individual neurons, we then found the event related averages for every combination of hand, gaze, and target position (64 combinations total). An example neuron is shown for which firing rate appears to vary with both gaze and hand position (Figure 3.2c).

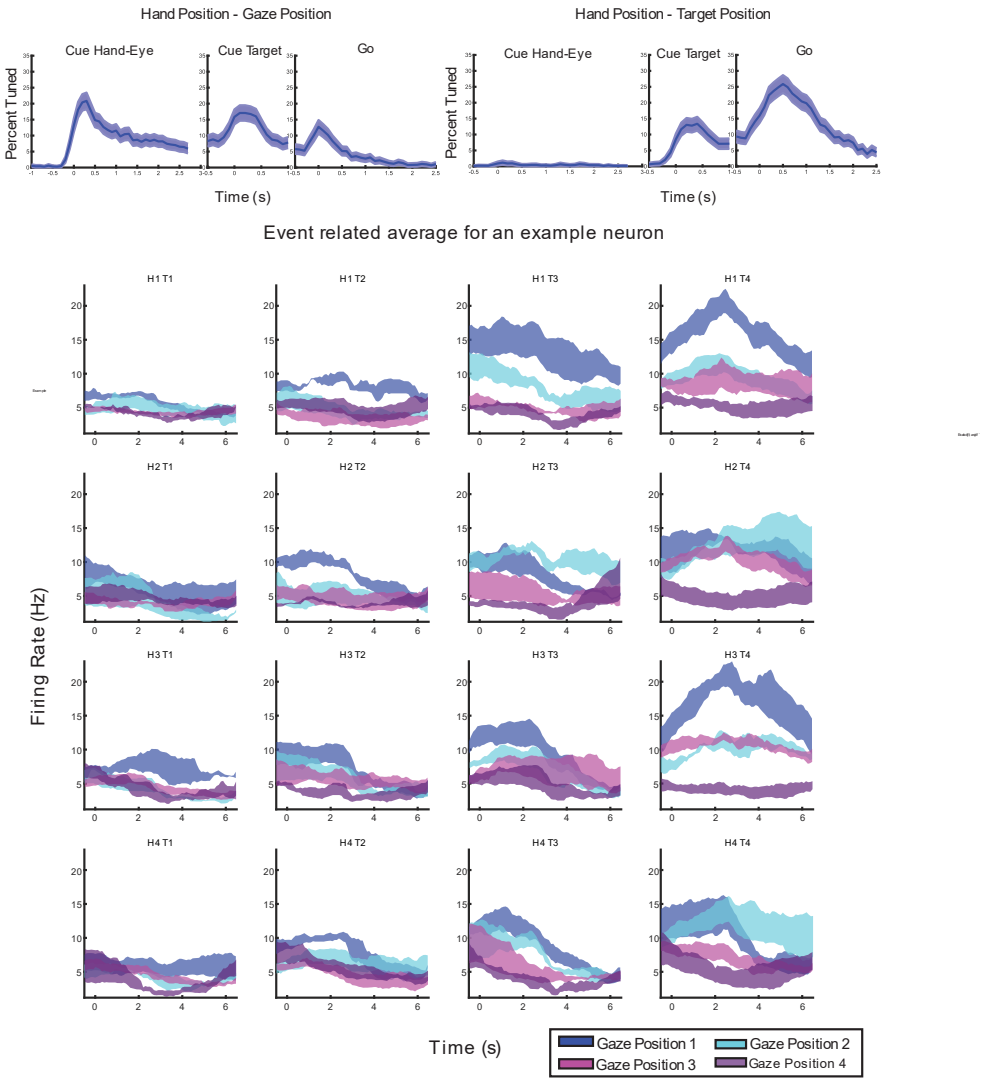

Figure 3.2. Neurons in PPC are linearly tuned to relative position information
A: Percent of neurons tuned to hand position realtive to gaze position throughout the task (anova with multiple comparisons). B. Percent of neurons tuned to hand position relative to target position throughout the task. C. Event related averages for an example neuron for every combination of hand, gaze, and target position.

Population in PPC shifts from coding a hand-gaze to hand-target vector during imagined reaches

In order to evaluate which of these position variables influenced neural firing rates, we used the analysis described in (Bremner & Andersen, 2014). For this analysis, first neural firing rates are organized into three four by four-by-four matrices, where in each matrix two of the three position variables were varied while one was maintained (Figure 3.3). For example, the leftmost matrix shown in Figure 3.3 shows the firing rates of a neuron while hand and gaze position are varied, but target position is constant. Next, the gradient of each matrix was computed in order to determine the position variables that drove changes in that neurons firing rate. The resultant angle and length of the gradient gives a 2-dimensional vector that indicates the relative coding of position for that neuron. For example, the example neuron in Figure 3.3 is an idealized hand-gaze coding neuron. In this case, gradient descent of the hand-gaze matrix results in an angle of 0 degrees, which corresponds to that neuron's firing rate being driven by changes in hand but not gaze position. Similarly, the resultant angle for the gradient of the gaze-target matrix is 0 because changes in target but not gaze position drive changes in firing rate. However, when hand and target position are varied, the resultant angle of -90 degrees shows that both variables drive that neuron's firing rate. Taken together, these resultant angles demonstrate an ideal response for a neuron coding a hand-target vector (i.e. hand and target position relative to each other, gradient result for neuron shown in Figure 3.2c shown in Supplemental Figure 3.2).

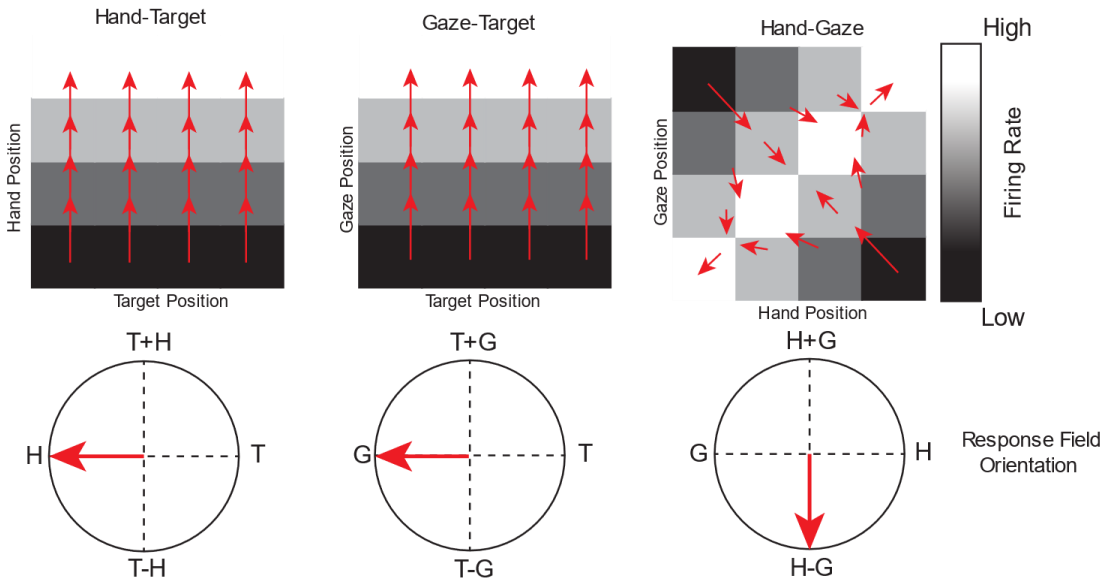

Figure 3.3 Response of an ideal hand-gaze centered neuron.
This shows the response field orientations for an idealized neuron that represents hand and gaze position relative to each other. These response fields are found for each variable pair by performing a gradient analysis on the firing rate matrices shown in the top row (right: hand-target, middle gaze-target, left: hand-gaze). The resultant from the gradient analysis shown in red can be used to derive the response fields shown in the bottom row.

Are coordinate frames in PPC context dependent? In order to evaluate the temporal dynamics of the vectors coded by the population, we performed the gradient analysis described above for each neuron for binned time windows across the entirety of the task. The resultant vector coded by the population was then found by summing the resultants of individual neurons and then dividing by the number of neurons. We found that at the beginning of the task, the population codes the hand position relative to the gaze position, or a hand-gaze vector (Figure 3.4a, Supplemental Figure 3.2 shows individual participant results). When the target appears, a population code for the hand relative to the target position, or a hand-target vector, begins to emerge. The response for the hand-target vector increases after the go-cue and then decreases after movement completion.

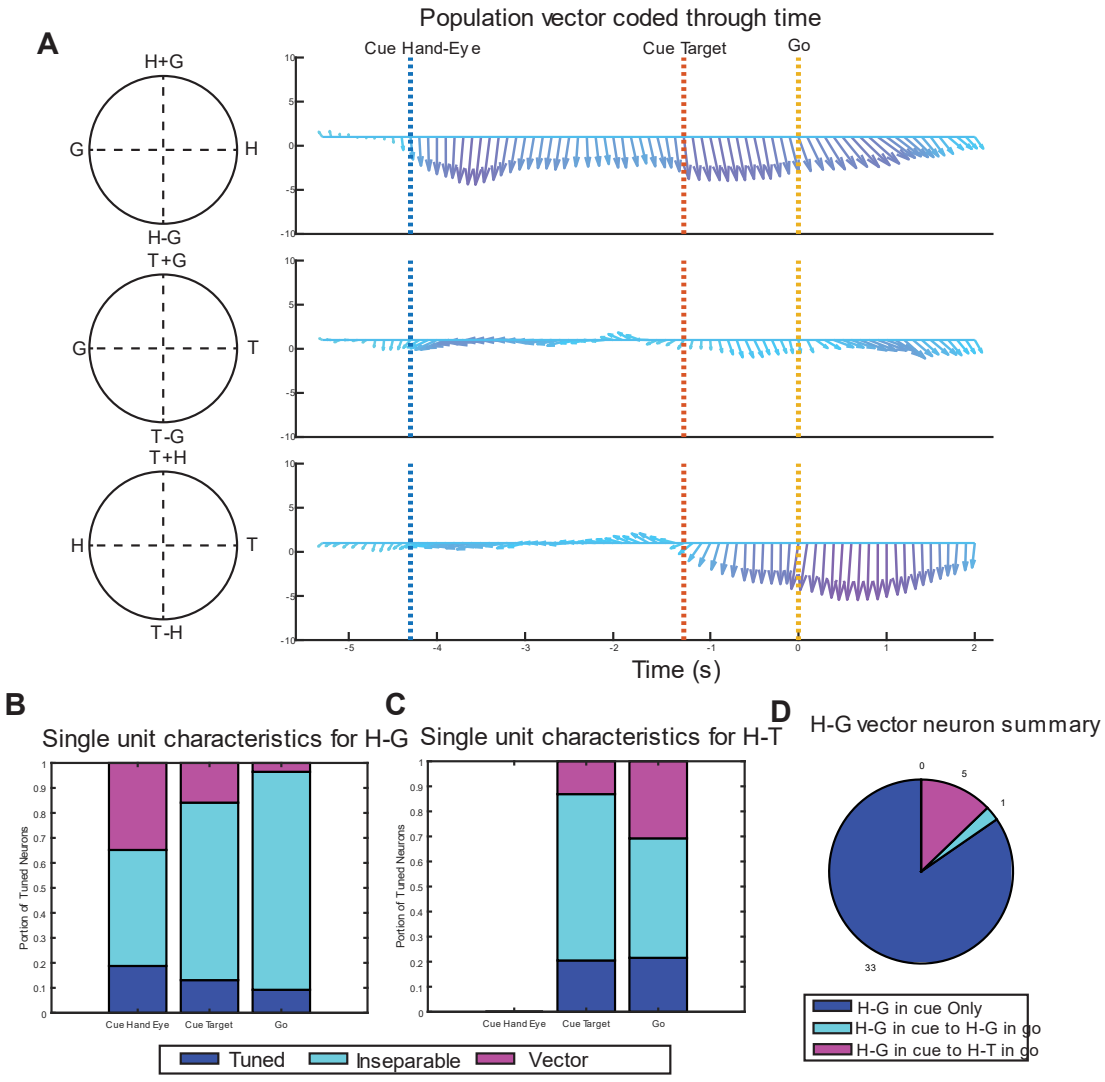

Figure 3.4. Relative coding for hand position in PPC changes from hand-gaze to hand-target with task context.
A: Population vector through time for JJ-PPC and NS-PPC during the delayed reaching task. Gradient analysis was performed on 100ms time bins across the duration of the task. Gradient results for each variable pair were averaged across all neurons to find the population vector magnitude and angle, shown by the length and direction of each arrow (top: hand-gaze, middle: gaze-target, bottom: hand-target) B. Gradient analysis was done for each neuron for a 1s window from each phase (cue hand eye, cue target, go). Each bar corresponds to the vector coding characteristics of neurons significantly tuned to the hand-gaze variable pair during each phase. Neurons that were tuned but did not meet other criteria for vector coding are shown in blue, neurons that were tuned and inseparable for the hand-gaze pair are shown in light blue, and neurons that met these criteria along with the angle criteria for hand-gaze vector coding are shown in pink. C: Same summary shown in B, but for the hand-target variable pair (note: target not shown before cue target phase). D. Summary of neurons that coded hand-gaze vectors during the cue hand eye phase. Neuron that only coded a hand-gaze vector during the cue phase are shown in blue, neurons that

coded a hand-gaze vector during both the cue and go phase are shown in light blue, and neurons that switched from coding a hand-gaze vector during the cue to a hand-target vector during the go phase are shown in pink.

To evaluate whether this shift in population vector was driven by distinct or shared single neurons, we classified neurons based on their vector coded for each phase. In order to be considered as a vector coding neuron for a certain variable pair, that neuron had to be significantly tuned to the variable pair, show inseparability for that variable pair, and have the appropriate resultant angles from each variable pair matrix. In this case, for each neuron the gradient descent was done over a one second time window corresponding to each phase of the task (cue hand-eye, cue target, go, Supplemental Figure 3.4). In the cue hand-eye phase, 112 neurons were significantly tuned to the H-G variable pair in PPC (Figure 3.4b). Of these, 91 were inseparable for the H-G pair (or 81% of significant units). The mean response field for the HG pair for these 91 neurons was -93.2° ($\pm$9.4° 95% CI) and response fields were unimodally distributed ($p<0.05$; Rayleigh test) and nonuniform ($p<0.05$; Omnibus test). Finally, just under half of the inseparable and significant neurons met the criteria for the resultant angles criteria to be classified as H-G vector coding (39 neurons). During movement execution, or the go phase, there were 128 neurons that were significantly tuned to the H-G pair and inseparable for that pair; however, the mean response field was found to be -41.8° ($\pm$10.4° 95% CI; unimodal ($p<0.05$ Rayleigh test) and nonuniform ($p<0.05$; omnibus)), and only five of these neurons met the remaining criteria for H-G vector coding. In the case of H-T vector coding, there is no target information during the initial phase, and thus no coding for such a vector (Figure 3.3c). In the go phase, 195 neurons were significantly tuned to the H-T variable pair, and of these, 153 were inseparable (78%). The mean response field for these neurons in the H-T variable pair was -87°$\pm$6.3° 95% CI) and responses were unimodal ($p<0.05$; Rayleigh test) and non-uniformly distributed ($p<0.05$; Omnibus test). Finally, 60 of these neurons also met the resultant angle criteria and were classified as H-T vector coding (see Supplemental Figure 3.5 for event related average and response field for an example H-T neuron).

Next we tracked which neurons that were active during reaches were also active during the initial phases with no movement. We found that of the small portion of neurons that coded a H-G vector during reach, two of these were only active during the go phase (Figure 3.4d). Additionally, there were a small portion of neurons that coded a G-T vector during reaches. Finally, we found a small portion of neurons that switched from coding a H-G vector during the go phase to coding a H-T vector during the go phase (n=5). Ultimately, it seems that the differences in vector coding seen in the population response at different stages of the task is largely driven by different populations of neurons being active during each phase. Nonetheless, the neurons that do switch their vector coding throughout the task bring up questions that we will address in the final section of results by modeling different population structures.

Finally, we sought to further categorize each neuron as hand-gaze, hand-centered, or gaze-centered by implementing the criteria used in Bremner 2012(Bremner & Andersen, 2012). This showed that of 39 neurons that coded a H-G vector during the cue phase, 14 were fully hand-gaze. Of the 60 neurons that coded a H-T vector during reaches, four neurons met the full criteria to be considered hand-centered. See Table 3.1 for a complete summary of criteria met by single neurons.

Population in PPC shifts from coding a hand-gaze to gaze-target vector during saccades

The results above indicate flexibility in the coordinate frames that can be encoded by small patches in human PPC. In recent literature, there has been increasing evidence for overlapping effector representations even in small areas of PPC (Heed et al., 2016; Striem-Amit et al., 2018; Zhang et al., 2017). This is in contrast with early findings that emphasized separation of hand and eye movements into different cortical areas of PPC. We sought to test whether the flexibility in coordinate frames we observed also extended to coordinate frames for movements of the eyes rather than the hands. To this end, we had the subject perform a delayed saccade task which was identical in the first phases to the

delayed reaching task, but different in the movement performed in the final phase of the task. In this case, the subjects saccaded to the target while maintaining their imagined hand position.

Once again the directional tuning of the population was evaluated before determining the coordinate frame used. In PPC around 16% of recorded neurons were tuned to hand position relative to gaze position during the cue phase, and 10% were tuned to target position relative to gaze position during saccades (Supplemental Figure 3.6). The event related average of an example neuron that is modulated by both gaze and target position can be found in Supplemental Figure 3.7.

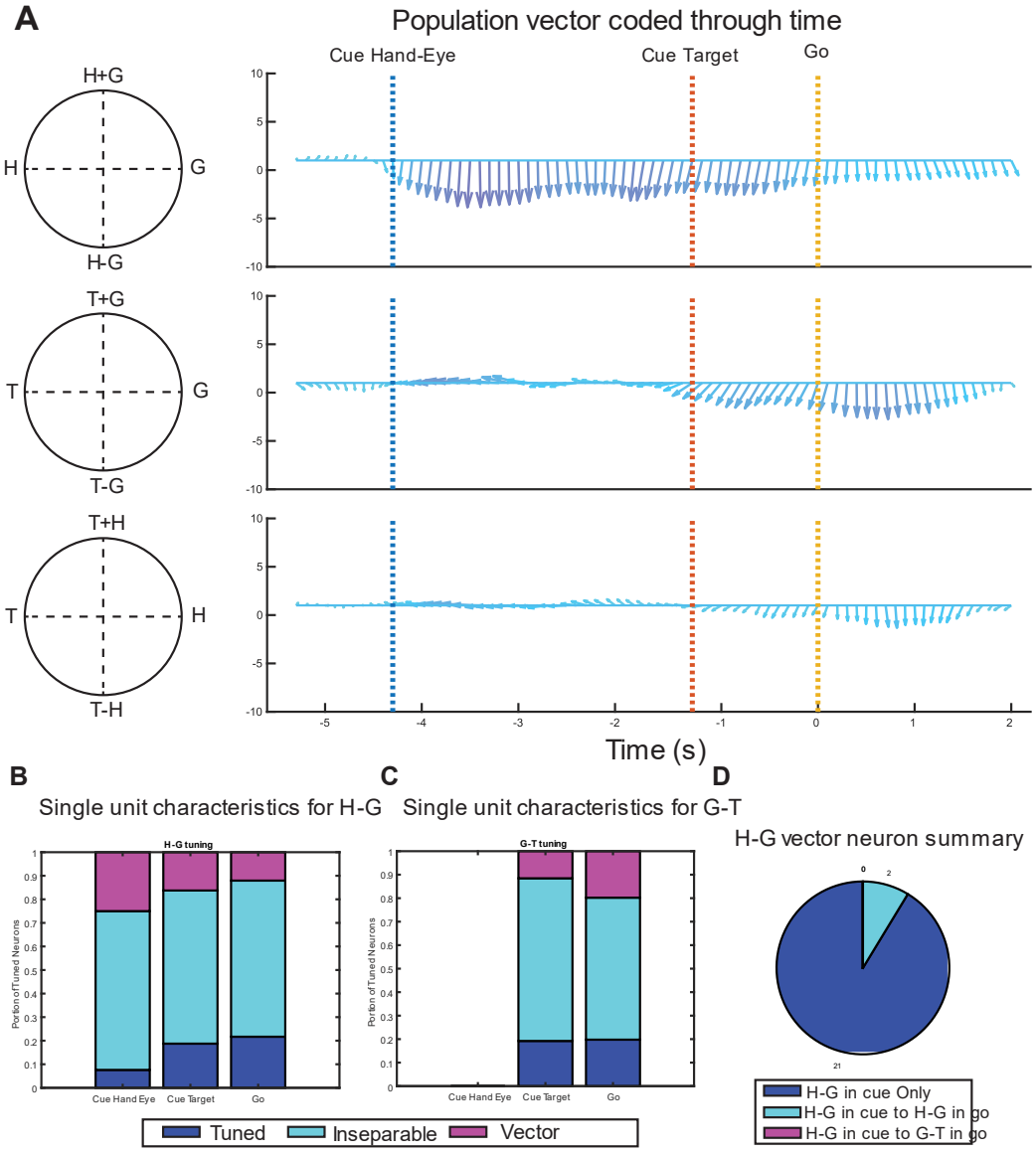

Figure 3.5. Gaze position coded relative to target position during saccades in PPC
A: Population vector through time for JJ-PPC and NS-PPC during the delayed saccade task (top: hand-gaze, middle: gaze-target, bottom: hand-target) B. Summary of single neuron gradient results from each phase (cue hand eye, cue target, go). Each bar corresponds to the vector coding characteristics of neurons significantly tuning to the hand-gaze variable pair during each phase. Neurons that were tuned but did not meet other criteria for vector coding are shown in blue, neurons that were tuned and inseparable for the hand-gaze pair are shown in light blue, and neurons that met these criteria along with the angle criteria for hand-gaze vector coding are shown in pink. C: Summary for the gaze-target variable pair (note: target not shown before cue target phase). D. Summary of neurons that coded hand-gaze vectors during the cue hand eye phase. Neurons that only coded a hand-gaze vector during the cue phase are shown in blue, and neurons that coded a hand-gaze vector during both the cue and go phase are shown in light blue.

Using the same analysis from Figure 3.4, we found the vector coded by the population through time (Figure 3.5a, supplemental Figure 3.8 for individual participant results). Much like in the reach version of the task, the population coded a hand-gaze vector during the first phase. Then, when the target appeared, the population began to code a vector from gaze to target position that continued through the subject's saccading. Although this shift in vector coding was similar between both the reach and saccade version of the task at the population level, the single neuron responses showed some distinctions.

In PPC, 92 neurons were significantly tuned to the H-G variable pair during the cue phase (Figure 3.5b). The majority of these were inseparable (n=85), and these neurons were found to have a mean response field of -93° (±19.2° 95% CI) and were unimodally ($p<0.05$; Rayleigh test) and non-uniformly distributed ($p<0.05$; Omnibus test). Of these 85 neurons, 23 met the resultant angle criteria for H-G vector coding (see Supplemental Figure 3.9 for plot of all resultant angles from tuned neurons). During saccades, 83 neurons were significantly tuned to the H-G pair, and while again a majority were inseparable (n = 65), only 8 of these met the full criteria for coding an H-G vector. In this case, looking at G-T rather than H-T vector coding during saccades, we found 81 neurons significantly tuned to the G-T variable pair (Figure 3.5c). Of these, 64 were inseparable. Response fields were unimodal ($p<0.05$, Rayleigh test) and nonuniform ($p<0.05$, Omnibus test) with a mean response field of -87.6° (±13.1° 95% CI). In total, 18 met the resultant angle criteria to be considered G-T vector coding neurons. The response field for an example G-T neuron is shown in Supplemental Figure 3.7.

In this case when we examine the vector coding neurons during the saccade phase, we found only one neuron between both participants that sustains activity through the entirety of the task (Figure 3.5d). This means that in contrast to the reach version of the task, no neurons switched their vector

coding between phases. A total of five neurons coded a H-T vector during saccades. When further categorizing neurons as hand-gaze, gaze-target, or hand-target, we found three neurons that are fully hand-gaze during the cue phase. During the go phase, three neurons were categorized as fully gaze-centered, and one neuron was hand-gaze (see Table 3.2 for complete summary).

MC codes a hand-target vector during imagined reaches

In participant JJ we also recorded from the hand knob of motor cortex simultaneously alongside PPC. Because our participants are tetraplegic and cannot produce overt reaches, the activity in this region can offer valuable insight into the behavior of the participant during the reaches version of the task. Most work in human hand knob show a majority of single neurons in this area respond to hand movements, with few studies reporting any coding for eye movements in this are. Thus, in JJ-MC, there should be extensive activity relating to hand position during reaches and limited if any activity relating to eye position during saccades.

First examining general directional tuning of neurons in JJ-MC with an anova, we saw that during the reach version of the task, almost all significant responses are during movement execution (<2% tuned before Go cue; Supplemental Figure 3.10). During imagined reaches, around 17% of neurons were tuned to the relative positions of hand and target. Less than 1% of neurons were tuned to any position variables (including relative position) during the saccade version of the task. The presence of tuning to hand position during reaches and not saccades provides some assurance that the participants were executing the two distinct actions.

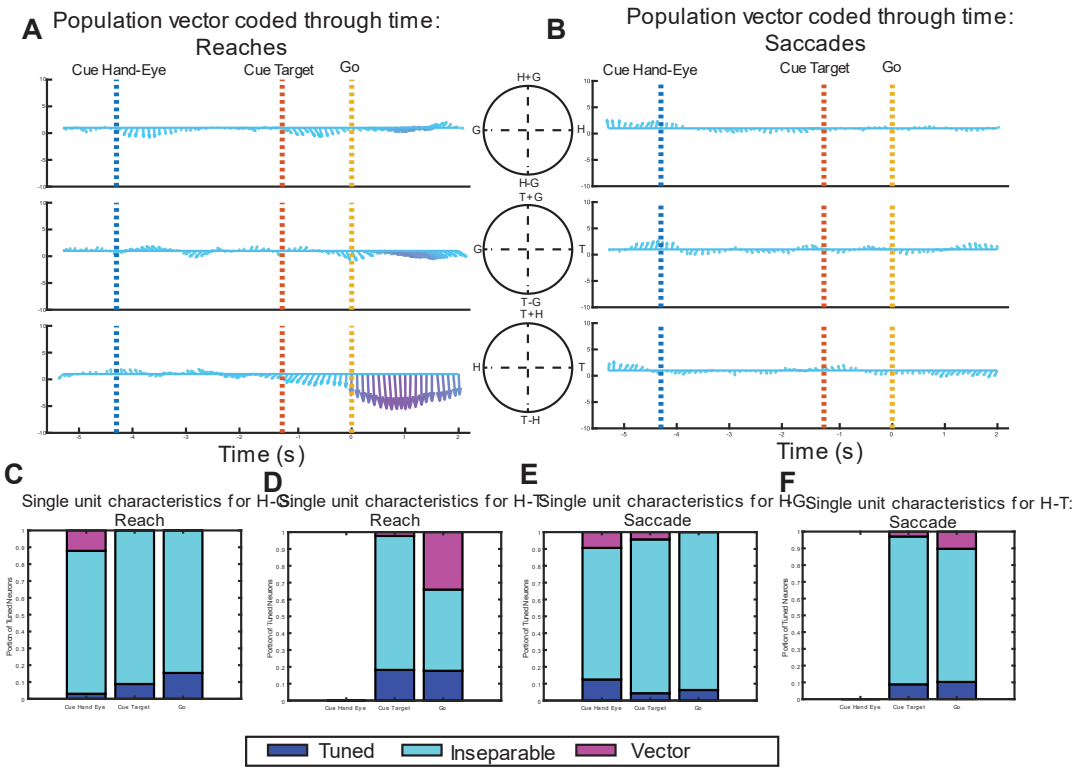

Figure 3.6. Coding for a reach vector during imagined reaches but not saccades in MC
A: Population vector through time for JJ-MC during the delayed reaching task (top: hand-gaze, middle: gaze-target, bottom: hand-target) B. Population vector through time for JJ-MC during the delayed saccading task. C: Summary of vector coding characteristics for neurons tuned to the H-G variable pair during the imagined reach task. First column shows proportion of neurons that were tuned (dark blue), tuned and inseparable (light blue), and fully vector coding (pink) in the first phase of the task. Middle and right column show results during Cue Target and Go phase respectively. D. Summary of vector coding characteristics for neurons tuned to the H-T variable pair during imagined reaches. E. Characteristics summary for neurons tuned to H-G pair during saccade task. F: Summary for neurons tuned to the G-T variable pair during saccades.

Next, looking at the population level response, we found only very weak coding in either the reach or saccade version of the task during the initial phases of the task (Figure 3.6a and b). When imagined reaches are being executed, the population codes the position of the hand relative to the position of the target. During saccades, there is weak (if any) coding for a vector from gaze position to target.

The lack of vector coding outside of imagined reaches is also apparent in examining the single neuron responses, as during the cue phase, a total of only 7 neurons coded for a hand-gaze vector between

both the reach and saccade version of the task (reach n=3; saccade n=4; Figure 3.6c and e). During reaches, 29 neurons coded a hand-target vector which is in stark contrast to the 4 neurons that coded a gaze-target vector during saccades (Figure 3.6d and f). Importantly, during saccades there were no neurons coding for a hand-target vector, further indicating the participant was correctly performing each task. Of these neurons, one neuron met the complete criteria to be considered having a hand-gaze reference frame, and one met the criteria to be hand-centered.

3.3 Discussion

We report the first single unit evidence of context dependent gaze- and hand-centered cording for direction in small patches in area 5 of human PPC. We show different coordinate frames in the fixation and movement phases are coded by distinct subpopulations that share a subset of individual neurons that switch their coding across the task. This results in the mixing of effector agnostic spatial information with effector specified spatial information.

In previous studies examining preparatory activity for reaches, a combination of body- and gaze-centered coding has been observed in single neurons of NHPs in several areas of PPC including area 5 as well as in premotor cortex (PMd) (Caminiti et al., 2015; S. W. C. Chang & Snyder, 2010; Mcfadyen et al., 2022; McGuire & Sabes, 2011). Similarly fMRI work in humans shows both area 5 and PMd represent movement plans in either gaze- or body- centered coordinates depending on whether target location was visually or proprioceptively cued (Bernier & Grafton, 2010; Leoné et al., 2015). Interestingly, this also seems to be true when rather than instructed reaches, the task is a tactile report for location of touch (Avillac et al., 2005; Leoné et al., 2015). Much like in area 5d of NHPs we found that the shift from the population coding a hand-gaze to hand-target vector occurs throughout the task rather than as a change at a single time point (Bremner & Andersen, 2014). This reflects a gradual rather than fully discretized transition in coding of coordinate frames, and may

support other results that indicate a high degree of intermediate gaze and body centered coding in PPC. Our results confirm that this population level flexibility can be seen at the single neuron level as well, although critically is not the result of a uniform shift in coordinate frames across each individual neuron.

A small number of individual neurons actually switched their vector coding between motor planning and motor execution epochs. Different instances of this variability in response for single neurons has now been observed several times in human PPC and highlights a cognitive role outside of traditional motor control (T. Aflalo et al., 2020; Zhang et al., 2017, 2020). Interestingly, only a small portion of neurons switched their vector coding. It has been proposed that even a small number of neurons that implement a nonlinear response scheme to a variable space can allow for a population of neurons to occupy a much higher dimensional response space than purely linear coding allows (Fusi et al., 2016; Rigotti et al., 2013). This is called partially mixed selectivity, and along with its role in supporting the abstraction needed for higher cognition, it is thought to be a computationally efficient way of representing information. Other computational studies of coordinate frames have suggested that intermixing hand and gaze position information may be an example of such an efficiency.

Hand-eye coordination is critical to many of the actions we perform everyday, but we are still learning how and where the neural computations that enable this process occur. PPC has been proposed to be the site in the brain where streams with information for both eye and hand location are integrated in order to compute accurate trajectories to visual targets (Andersen et al., 1993; Bruner et al., 2023; Georgopoulos & Grillner, 1989). Additionally, damage to PPC has been seen to cause deficits in hand eye coordination in both animals and humans (Andersen et al., 2014; Hwang et al., 2014). Previously, results in NHPs have supported a network in PPC in which functional nodes for hand and eye movements were interconnected and freely exchange information and even modulate each other

(Bernier & Grafton, 2010; Pouget & Snyder, 2000). The idea of interconnected functional nodes supports the notion of some emphasis of either hand, arm, or eye movements but also supports the presence of all three within the neural populations. In agreement with this notion, is that areas selective for eye movements like LIP are connected with areas selective for hand movements like PRR (Caminiti et al., 2015). Initially, almost all areas of PPC in NHPs appeared to implement eye-centered coordinates, even those more selective for hand movements than eye movements like PRR and AIP (Batista et al., 1999; Buneo et al., 2002; Cohen & Andersen, 2002). Only area 5d was shown to predominantly implement body-centered coding, although it should be noticed that a mix of each coordinate frame seems to exist within each of these subregions to a certain extent (Beurze et al., 2009; Bremner & Andersen, 2012, 2014; S. W. C. Chang & Snyder, 2010). Generally, it is thought that there is a gradual transition from gaze to hand centered coding as one moves anteriorly in the intraparietal sulcus (Filimon, 2010). The medial regions of the IPS along with SPL seem to show the greatest mixing in both NHP and human studies (Bernier & Grafton, 2010; Leoné et al., 2015).

The organization of coordinate frames in PPC in humans aligns to a certain extent with studies in NHPs, although with some differences. Lesions to SPL and IPS can cause a deficit in visually-guided reaching called optic ataxia (Andersen et al., 2014). This is proposed to be a breakdown in the visuomotor transformation from a gaze centered to hand centered representation of a motor trajectory. One hypothesis is that this is because the gaze and hand position cannot be properly decoupled, supported by the observation that patients with optic ataxia are able to accurately reach objects that are directly in their foveal space. Interestingly, at least one case study also demonstrated that the reaching deficits of optic ataxia also extended to reaches with the feet, and were not limited to the arms (Evans et al., 2013). fMRI work in humans supports more extensive overlap of effectors in PPC than that seen in NHPs, although notably some work has shown separation of hand and eye representations even though hand and foot overlapped. One of the main surprises from this study was

the presence of gaze-centered coding during saccades in an area previously thought to be involved in hand movements but not eye movements.

Although we found gaze-centered coding during saccades, we do not know whether or not this is a signal that will be passed downstream to an eye motor output region like the frontal eye field or whether this is a result of the integration of hand and gaze position. It could also be that this signal is used for coordinating when the eyes and the hand are moved together. When PRR is damaged in NHPs, isolated movements only show deficits for reaches, but both saccades and reaches are impacted if eyes and arm are moved together (Hwang et al., 2014). Our ability to determine the true nature of this organization is limited because in our paradigm, hand and eye movements were performed in isolation and on separate days. In order to truly distinguish between an area where hand and eye movements are fully combined and an area that is receiving inputs from a more "eye movement" region, we would need to have both reaches and saccades simultaneously performed and also single neuron activity during isolated movements.

The mixing of gaze- and body-centered coordinate frames may have other functions outside that of directly controlling eye movements. Mixing of coordinates is even observed as close to movement output at PMd (Bernier & Grafton, 2010; Pesaran et al., 2010). Further, a behavioral study in motor intact individuals found that movement errors could actually be classified as either gaze-centered or body-centered, suggesting there could even be a case for either output (Bosco et al., 2017). This would be advantageous when either visual or proprioceptive information is more accessible, making gaze- or body-centered coordinates more appropriate respectively. fMRI work in humans has demonstrated flexible coordinate frames depending on whether a location cue was visual or proprioceptive (Bernier & Grafton, 2010). Additionally, optic ataxia seems to have a proprioceptive component as well. How two such outputs may occur was proposed in Buneo et al. 2002, and suggested that when the hand's

location in visual space is known, no transformation even needs to occur and it is actually more efficient for goal location to remain encoded in gaze-centered coordinates (Buneo et al., 2002). However, in the absence of visual information, a separate, body-centered proprioceptive transformation must occur.

Although both participants showed hand-target coding during reaches and gaze-target coding during saccades, the strength of these representations differ slightly between the two, with slightly weaker gaze-target coding observed in NS. There are a few possible explanations that relate directly to differences in data collection for the subjects. One is precise implant location. We know from NHP results that different anatomical areas of cortex emphasize different coordinate frames, and we will need further studies to confirm whether this is the case in human cortex as well. Functionally speaking, both implant locations were seen to be highly responsive to grasping imagery during a presurgical fMRI. Anatomically, however, JJ-PPC is located a bit medially and posterior of the junction of the postcentral gyrus and intraparietal sulcus while NS-PPC is almost immediately at the junction. The work that emphasizes effector specificity in NHP PPC is largely focused in the intraparietal sulcus, and NS-PPC is somewhat closer in proximity to these traditionally studied sulcal regions, and specifically to the anterior intraparietal area which has shown a strong preference for hand movements over eye movements (S. W. C. Chang et al., 2008; Grefkes & Fink, 2005). In addition, it has been suggested rather than a fully discretized transformation from gaze to body centered coordinates that perhaps there is a more gradual transition along the dorsal stream with no area necessarily being entirely gaze or entirely body centered (Filimon, 2010). In this case, the closer to the junction of IPS and PC, the more body vs. gaze centered.

Another consideration is that the imagined reach version of the task was collected four years prior to the saccade version of the task for NS. The presence of substantial coding for a hand-gaze vector

during the saccade task implies this may not have had any impact on the strength of the gaze-target vector observed. Nonetheless, we know that overtime signal quality from intracortical arrays can degrade and it is worth mentioning for its possible impact. In participant JJ in contrast, both the saccade and reach version of the task were collected over three years, and started at about the same time.

One limitation in extending our results to NHPs is our use of imagined reaches where previous work examined implemented overt movements. Consequently, while we can validate saccade behavior, we cannot directly validate reach behavior. This makes our recordings from motor cortex particularly valuable, as we can use motor cortex as a sort of proxy to understanding what motor commands are being output. Importantly, we are implanted in the hand knob of motor cortex, an area well established to represent hand movements above all other parts of the body. Thus, our finding of coding for a reach vector during imagined reaches, but essentially no directional coding during saccades, can be used as a sort of behavioral assay validating imagined reaches. This is not to say that there could be no differences between overt and imagined reaches, in particular in MC where it is known that attempted movements evoke much stronger response than imagined and observed movements of the same type (Park et al., 2015; Rastogi et al., 2020). Another limitation of imagined reaches is related to the overall lack of sensorimotor feedback experienced by our participants. An fMRI study in humans found that coordinate frames in PPC changed depending on whether cue context was visual or proprioceptive (Bernier & Grafton, 2010). It could be that in the absence of proprioceptive information, gaze-centered coding is emphasized, and thus more prominent in our results than it would be for motor intact individuals. This seems unlikely however, as the primary somatosensory cortex has been found to still encode a reach vector during imagined reaches where no proprioceptive feedback was given (Jafari et al., 2020).

Future directions and conclusions

One of the limitations of the current study was that the reach and saccade versions of the task were collected on separate days, leaving a complete understanding of the nature of this flexible coding out of reach. In future work, both versions of the task can be collected on the same day interleaved in order to establish whether neurons are shared between the population code for hand-target and gaze-target vectors. In addition, we are limited both in our knowledge of how the neurons we are recording connect to the rest of the network involved in coordinate frame transformations. While this can be examined to some extent at a lower spatial resolution in humans using fMRI and other more common non-invasive techniques, the alignment of our results with work in NHPs emphasizes the importance of continuing to explore this in animal models where more brain areas can be accessed at the same high resolution with electrophysiology.

Further work is also needed to determine whether there are any differences between motor imagery and overt movements, although the findings from motor cortex reported in this paper along with recordings from primary somatosensory cortex in a human tetraplegic patient both support the use of imagined reaches as a behavioral stand in for actual movement (Guan et al., 2022; Jafari et al., 2020). Finally, although we recorded from hundreds of tuned cells, spatially tuned cells only accounted for around 30% of all recorded cells and of the tuned cells, around 30% were vector coding. This leaves many questions open as to how the remaining spatially tuned cells are coding position information as well as what other movement and non-movement variables this area may be tuned to. Modeling work to explain the results seen in NHPs suggests that perhaps single neurons often have an intermediate coding between gaze and body centered, which our current task would not be able to accurately categorize (Pouget & Snyder, 2000).

Overall, these results support the growing body of work that suggests much more intermixing of information in cortical areas than was previously expected. They show for the first time at the single neuron level that rather than one single coordinate frame being implemented by a region of PPC, multiple coordinate frames exist and can be activated based on relevant context. This motivates the need to examine the coordinate frames in other areas of PPC further in order to better understand the function of these overlapping representations and how they are ultimately combined for hand-eye coordination.

3.4 Methods

Study participants

Data was collected from two participants, JJ and NS. JJ has a C4-C5 level spinal cord injury that occurred approximately three years before his enrollment in the study. NS has a C3-C4 spinal cord injury (approximately six years before enrollment). Both participants are right-handed. The procedures in this study were approved by review boards of California Institute of Technology, Casa Colina Hospital and Centers for Healthcare, and University of California, Los Angeles.

Implant Locations

Each participant had two 96-channel NeuroPort Utah electrode arrays implanted in their left hemisphere. In participant JJ, one array was placed in the left superior parietal lobule (JJ-PPC), and the second within the hand knob of left precentral gyrus (JJ-MC). NS had one array implanted in her left hemisphere located at the junction of the post central gyrus and intraparietal sulcus (PC-IP) . For both subjects, a presurgical fMRI was used to identify brain regions active during a grasping imagery task to serve as a functional guide to our target implant location. For JJ data collection began 8 months after surgery and continued for just over three years. Data collection for NS began 12 months after surgery and continued for over five years until the subject's implants were removed.

Neural signal recording and preprocessing

Neural signals were recorded from the implanted microelectrode arrays. These signals were then amplified, bandpass filtered and digitized (0.3 Hz–7.5 kHz, and 30 kHz, 16 bits/sample respectively) (NeuroPort Neural Signal Processors, Blackrock Microsystems Inc.). The signal was then high pass filtered at 250 Hz and thresholded at -3.5 times the root-mean square voltage in order to detect spikes. This was done for each electrode. Single neurons were then identified using the k-medoids clustering method and the total number of waveforms was determined by the gap criteria (Tibshirani et al., 2001). This was done for the first $n \in \{2, 3, 4\}$ principal components (n was selected to account for 95% of waveform variance). Neurons that had an average firing rate of less than 0.25 Hz across an entire task were considered noise and excluded.

For single unit gradients during each phase, behavioral epochs were defined as 1000ms starting 300ms after the onset of the phase. This was defined by the hand and gaze position appearing on screen for the first phase, the target appearing on screen for the second phase, and the go-cue being given for the final phase.

Behavioral Tasks

Two behavioral tasks were used, a delayed reaching task and a delayed saccade task. For both, participants sat in front of an LED monitor that displayed instructed positions for the hand and gaze. A white hand icon and blue fixation point were placed in one of four possible locations all at the same vertical location on the screen. First, the subjects imagined position their hands at the location indicated and fixed their gaze on the fixation point. They maintained this initial set-up position until

a go-cue was given (2s). Before the go-cue was given, a target appeared on the screen at one of four locations above the hand and gaze positions.

1.5s after the target appeared, the go-cue was shown. This is where the two tasks differed. In the reach version of the task, the subject was instructed to imagine reaching to the target with their right arm. During the imagined reach, they were to maintain gaze fixation. Imagined reaches were used because both subjects were not able to overtly reach due to their injuries. During the saccade task, they were instructed to saccade to the target and maintain their initial imagined hand position. In this case, overt movements were used as both subjects are able to move above their necks.

The four hand, gaze, and target positions yield 64 possible layouts. Each position combination was repeated six times across three runs for each session of the two tasks. Four sessions of each task type were collected in each subject for a total of 16 sessions.

Eye Tracking and Fixation-break triggered trial cancellations

Eye tracking data was obtained using a Tobii Eye Tracker 5. During the delayed reach task, any fixation break would trigger a cancellation of that trial and the trial would be repeated again later in the task. This ensured that the subject had the correct gaze position during the task and did not saccade to the target during their reach. For the delayed saccade task fixation breaks before the go cue would trigger the end of a trial, but in this case saccading during the go was not penalized as a canceled trial.

Single unit significance

As a first means of quantifying the population tuning across hand, gaze, and target position, an n-way anova was performed on time windows of 100ms throughout the task. In addition, significant responses for hand relative to gaze, gaze relative to target, and hand relative to target positions are

also considered (relative vector calculated by subtracting one position from the other). P-values were corrected for multiple comparisons before a threshold of 0.05 was used to determine whether a neuron was significantly tuned. The mean percentage of the population that was tuned was plotted with confidence intervals, both calculated from the empirical cdf (MATLAB ecdf).

Gradient analysis for determining population vector coded through time

To determine the degree to which the different position variables (hand, gaze, and target) influence neural firing rates, a gradient analysis was performed (Bremner & Andersen, 2012). This was done to assess three pairs of relative coding: hand relative to gaze (hand-gaze vector), gaze relative to target (gaze-target vector), and hand relative to target (hand-target vector). To assess the impact of two position variables at a time, neural responses were gathered into matrices where two position variables changed and the other was held constant. In other words, we created 4x4 matrices of mean firing rates for all combinations of two position variables, averaging across all trials and the third non-varied position. The gradient was then calculated using MATLAB's gradient function yielding a resultant angle and length that can be used to quantify the modulation by each position variable and its strength respectively. In order to account for symmetrical responses, each angle is doubled in order to prevent instances of perfectly opposing resultants from summing to zero. Additionally, vector magnitudes were normalized. In order to assess the population vector through the different phases of the task, we performed this analysis on sliding windows across the task as in Bremner and Andersen 2014. These resultant angles and vector magnitudes were then summed across all neurons and divided by the total number of neurons to find the average vector coded by the population.

Determining single neuron vector coding

In order to assess the vector coding of single neurons, the gradient analysis described above was done for 1 second windows during each phase of the task. A neuron was considered to be tuned to a variable

pair if the resultant length was significantly greater than that for a randomized matrix. The tuning and resultant angles yielded from the gradient analysis are not sufficient to fully categorize a neuron as vector coding. Prior work has used singular value decomposition (SVD) to determine whether a neuron is vector coding or gain-modulated. SVD can be used to assess the separability of the impact of position in a variable pair on a neuron's firing rate. If a neuron is vector coding for a certain pair of variables, the matrix of weighted sums resulting from the SVD will reveal that multiple values are needed in order to describe that neuron's response to each variable, and thus is inseparable for that variable pair.

In order for a neuron to be classified as a vector coding neuron for a certain variable pair, it had to meet five criteria: 1) significant tuning to that pair, 2) inseparable result from SVD analysis for that pair, and 3-5) the correct resultant angles for each matrix gradient (within a margin of 60 degrees). This is based on criteria used by Bremner and Andersen, 2012 to identify vector coding neurons. This was done for the angles found during the 1 s time bins for each of the three task phases.

Author contributions

T.A., K.K., J.G., M.J., and R.A.A. designed the study. R.A.A., K.K., and T.A. developed the experimental tasks. K.K. and M.J. collected data. K.K. and J.G. analyzed the results. K.K., J.G., and R.A.A. interpreted the results. K.P. coordinated regulatory requirements of clinical trials. N.P. and A.B. performed the surgery to implant the recording arrays.

Participant JJ	Parameter	Significance	Separability	Response field
Hand-gaze (Cue)	HT	Yes(53)	Separable (59)	-180 (237)
8/9 (13)	GT	Yes (81)	Separable (85)	-180 (292)
	HG	Yes (74)	Inseparable (526)	-90 (333)
Hand-gaze (Go)	HT	Yes (130)	Separable (53)	-180 (128)
8/9 (0)	GT	Yes (113)	Separable (43)	-180 (105)
	HG	Yes (99)	Inseparable (537)	-90 (276)
Hand-centered	HT	Yes (130)	Inseparable (514)	-90 (359)
8/9 (3)	GT	Yes (113)	Separable (43)	0 (243)
	HG	Yes (99)	Separable (30)	0 (243)
Gaze-centered	HT	Yes (130)	Separable (53)	0 (123)
8/9 (0)	GT	Yes (113)	Inseparable (527)	-90 (240)
	HG	Yes (99)	Separable (30)	-180 (105)
Participant NS	Parameter	Significance	Separability	Response field
Hand-gaze (Cue)	HT	Yes (28)	Separable (28)	-180 (140)
8/9 (1)	GT	Yes (22)	Separable (19)	-180 (150)
	HG	Yes (38)	Inseparable (363)	-90 (219)
Hand-gaze (Go)	HT	Yes (65)	Separable (33)	-180 (91)
8/9 (0)	GT	Yes (40)	Separable (30)	-180 (72)
	HG	Yes (42)	Inseparable (366)	-90 (160)
Hand-centered	HT	Yes (65)	Inseparable (357)	-90 (221)
8/9 (1)	GT	Yes (40)	Separable (30)	0 (171)
	HG	Yes (42)	Separable (24)	0 (144)
Gaze-centered	HT	Yes (65)	Separable (33)	0 (114)
8/9 (0)	GT	Yes (40)	Inseparable (360)	-90 (141)
	HG	Yes (42)	Separable (24)	-180 (105)

Table 3.1 Summary of single neuron coordinate frame criteria during the imagined reach task
Results shown for each individual participant. Number in parenthesis is number of neurons that met that criterion. Number of neurons that fulfilled at least 8/9 criteria for a coordinate frame are summarized in the left column.

Participant JJ	Parameter	Significance	Separability	Response field
Hand-gaze (Cue)	HT	Yes (49)	Separable (20)	-180 (226)
8/9 (0)	GT	Yes (45)	Separable (52)	-180 (225)
	HG	Yes (50)	Inseparable (460)	-90 (275)
Hand-gaze (Go)	HT	Yes (47)	Separable (34)	-180 (144)
8/9 (0)	GT	Yes (58)	Separable (40)	-180 (126)
	HG	Yes (54)	Inseparable (457)	-90 (211)
Hand-centered	HT	Yes (47)	Inseparable (460)	-90 (244)
8/9 (0)	GT	Yes (58)	Separable (40)	0 (121)
	HG	Yes (54)	Separable (37)	0 (140)
Gaze-centered	HT	Yes (47)	Separable (34)	0 (156)
8/9 (2)	GT	Yes (58)	Inseparable (454)	-90 (259)
	HG	Yes (54)	Separable (37)	-180 (137)
Participant NS	Parameter	Significance	Separability	Response field
Hand-gaze (Cue)	HT	Yes (25)	Separable (27)	-180 (143)
8/9 (0)	GT	Yes (34)	Separable (22)	-180 (139)
	HG	Yes (42)	Inseparable (333)	-90 (195)
Hand-gaze (Go)	HT	Yes (34)	Separable (23)	-180 (91)
8/9 (1)	GT	Yes (32)	Separable (25)	-180 (121)
	HG	Yes (29)	Inseparable (324)	-90 (104)
Hand-centered	HT	Yes (34)	Inseparable (324)	-90 (103)
8/9 (0)	GT	Yes (32)	Separable (25)	0 (86)
	HG	Yes (29)	Separable (23)	0 (103)
Gaze-centered	HT	Yes (34)	Separable (23)	0 (93)
	GT	Yes (32)	Inseparable (322)	-90 (153)
	HG	Yes (29)	Separable (23)	-180 (98)

Table 3.2 Summary of single neuron coordinate frame criteria during the saccade task
Results shown for each individual participant. Number in parenthesis is number of neurons that met that criterion. Number of neurons that fulfilled at least 8/9 criteria for a coordinate frame are summarized in the left column.

Supplemental Figures

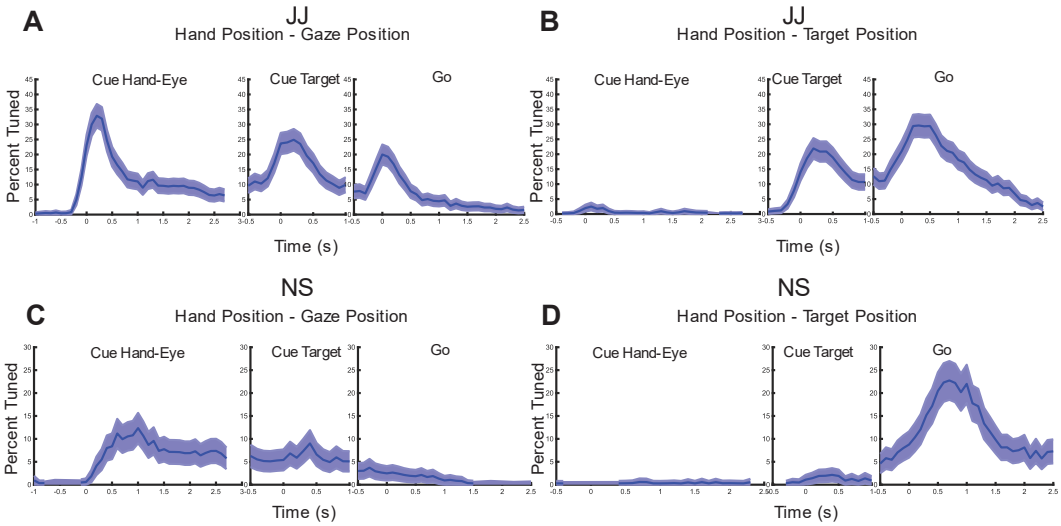

Supplemental Figure 3.1. Linear tuning properties of individual participants during reach task The percent of neurons tuned during the task were determined using an n-way anova ($p<0.05$ adjusted for multiple comparisons). Each section corresponds to a different task phse (left: Cue Hand eye, middle: Cue Target) A: Percent of neurons in JJ-PPC tuned to hand position relative to gaze position. B: Percent of neurons in JJ-PPC tuned to hand position relative to target position. C: Percent of neurons in NS-PPC tuned to hand position relative to gaze position. D: Percent of neurons in NS-PPC tuned to hand position relative to target position.

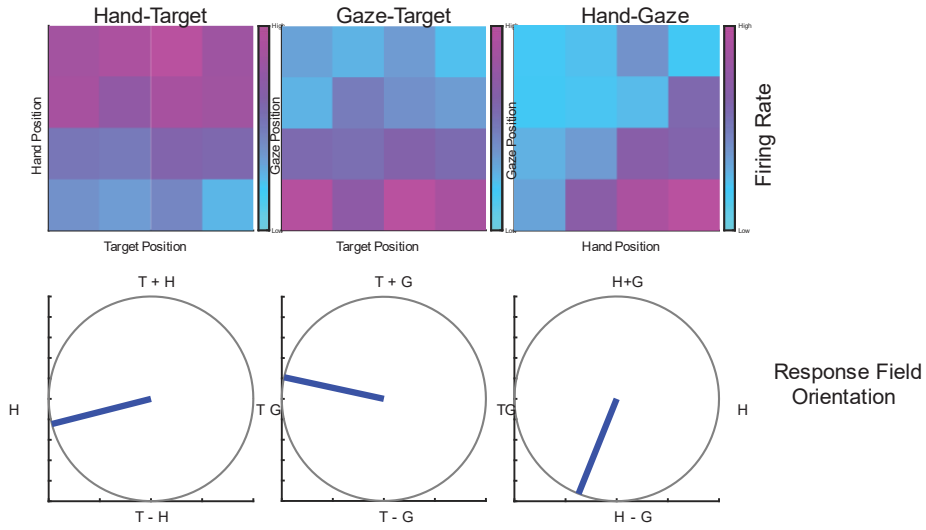

Supplemental Figure 3.2. Response field orientation for example hand-gaze neuron. Gradient results for the hand-gaze neuron show n in figure 2C.

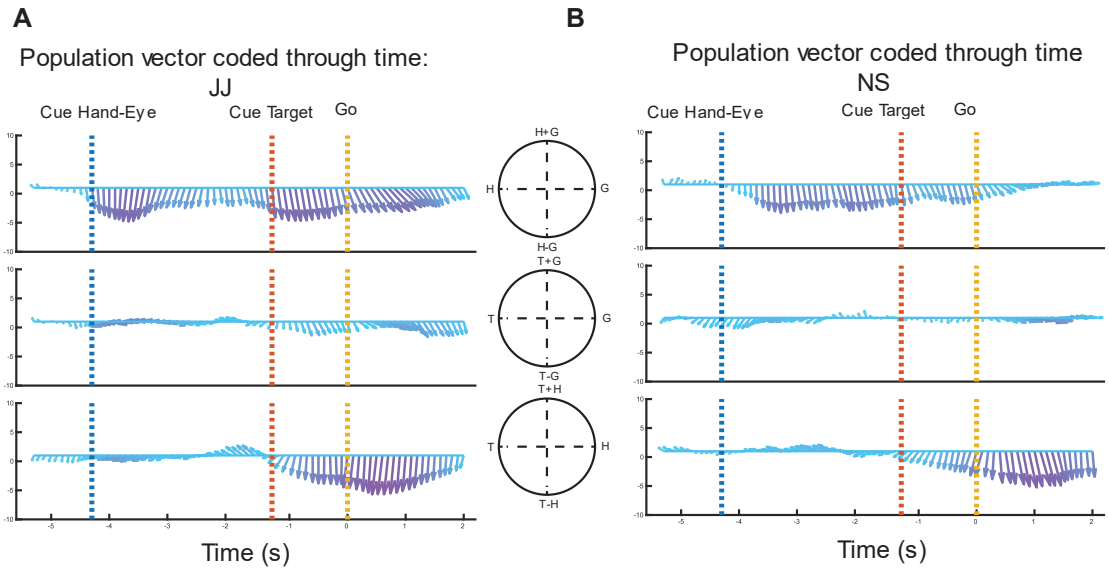

Supplemental Figure 3.3. Population gradient results for individual participants during delayed reach task
A: Population vector through time for JJ-PPC. B: Population vector through time for NS-PPC

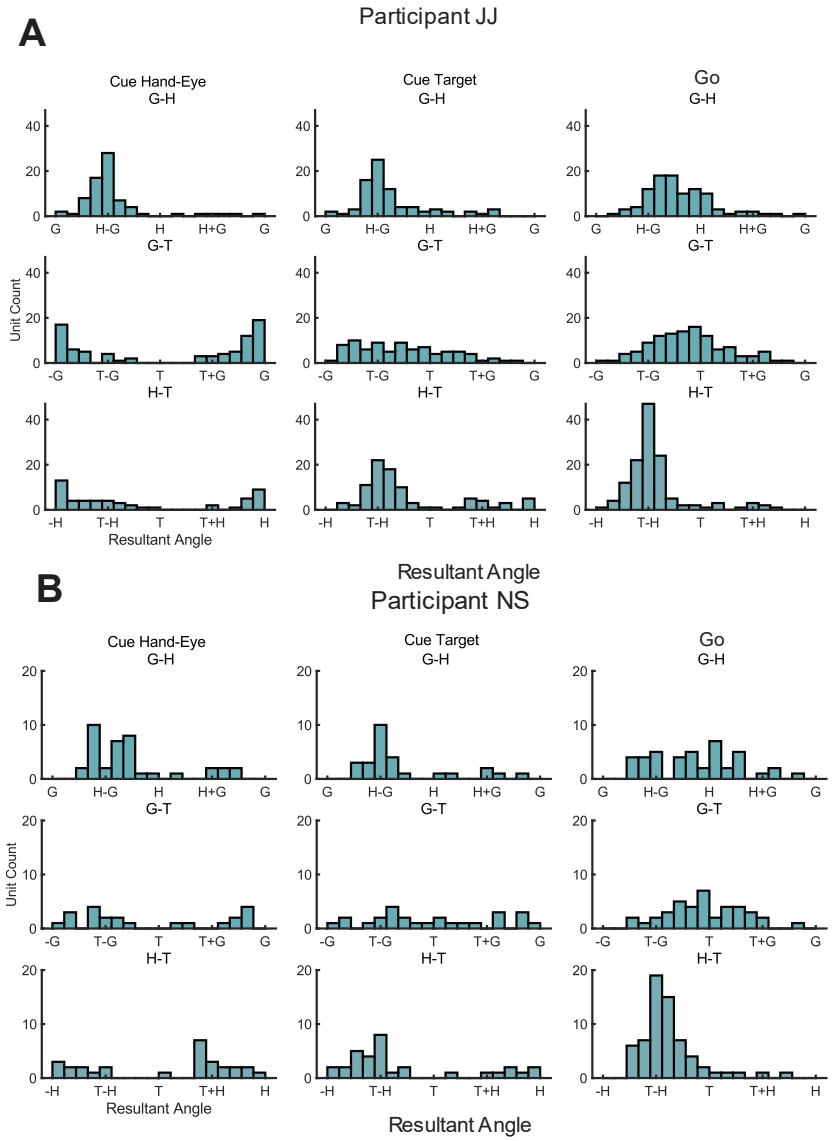

Supplemental Figure 3.4. Population resultant angles for individual participants during reach task Each row shows a different variable pair (top: H-G, middle: G-T, bottom: H-T). Each column shows a different phase (left: Cue Hand Eye, middle: Cue Target, right: Go). Only neurons found to be significantly tuned to the variable pair were included for each row. A: Resultant angles for JJ-PPC. B: Resultant angles for NS-PPC.

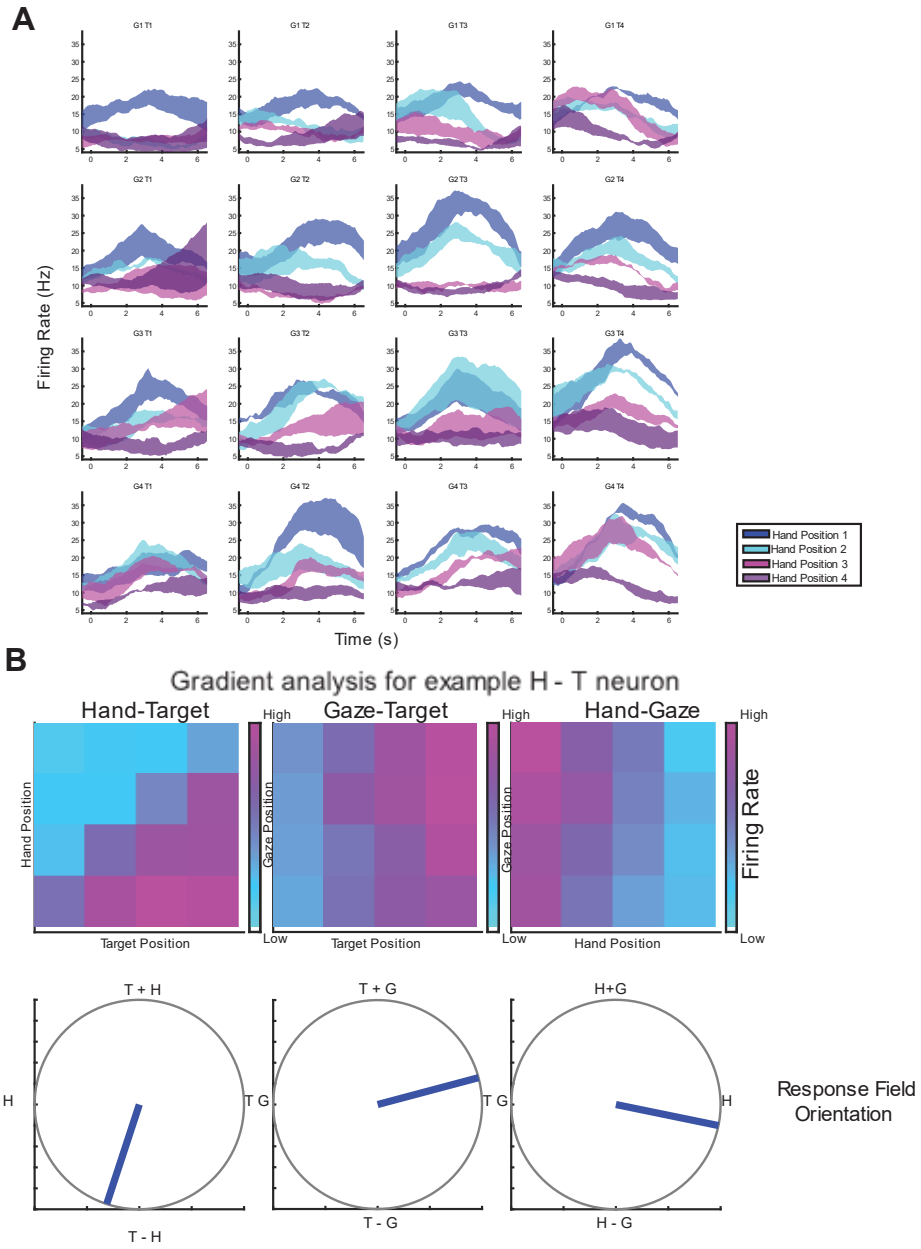

Supplemental Figure 3.5. Responses of example hand-target neuron.
A. Event related average for neuron tuned to hand position relative to target position for every combination of hand, gaze, and target position. Each trace corresponds to one of the four hand positions. B. Response field derived from gradient resultant angles for hand-target neuron.

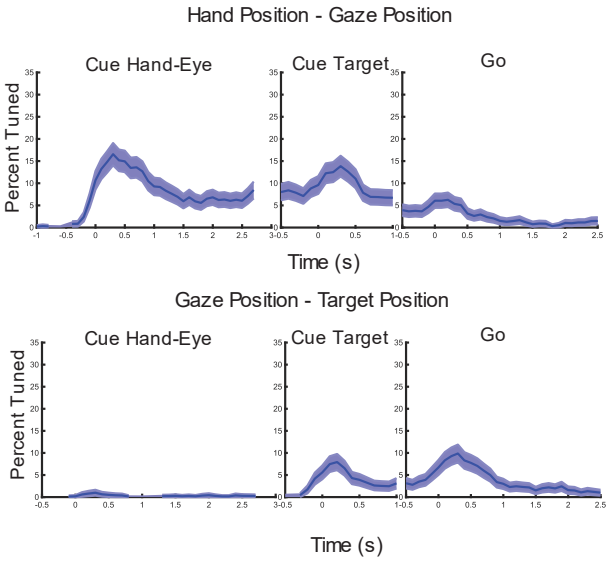

Supplemental Figure 3.6. Linear tuning to relative positions during saccade task. A: Percent tuned to gaze position relative to hand position (anova $p<0.05$). B: Percent tuned to gaze position relative to target position (anova $p<0.05$).

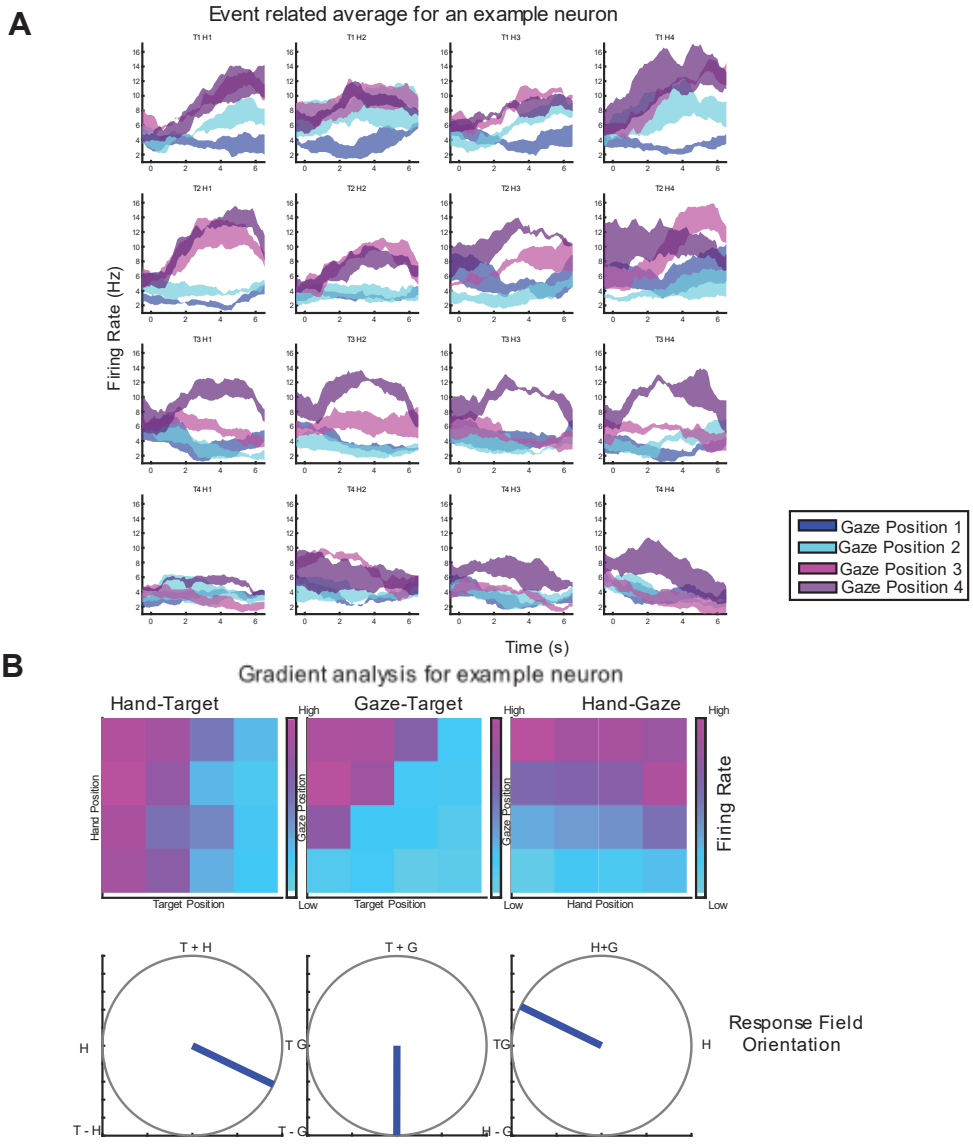

Supplemental Figure 3.7. Responses of example gaze-target neuron. A. Event related average for neuron tuned to gaze position relative to target position for every combination of hand, gaze, and target position. Each trace corresponds to one of the four gaze positions. B. Response field derived from gradient resultant angles

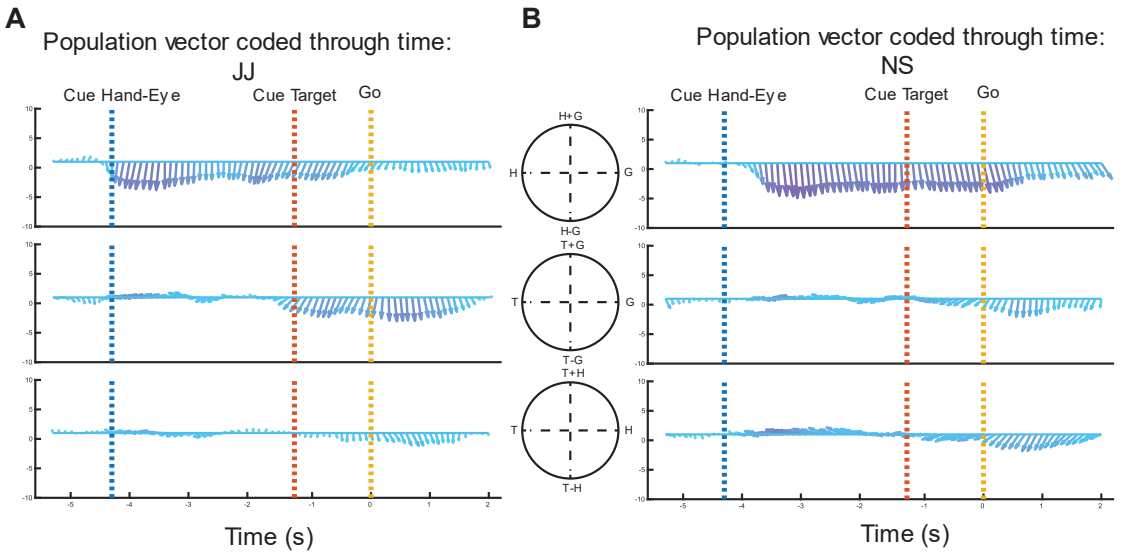

Supplemental Figure 3.8. Population gradient results for individual participants during delayed saccade task
A: Population vector through time for JJ-PPC. B: Population vector through time for NS-PPC

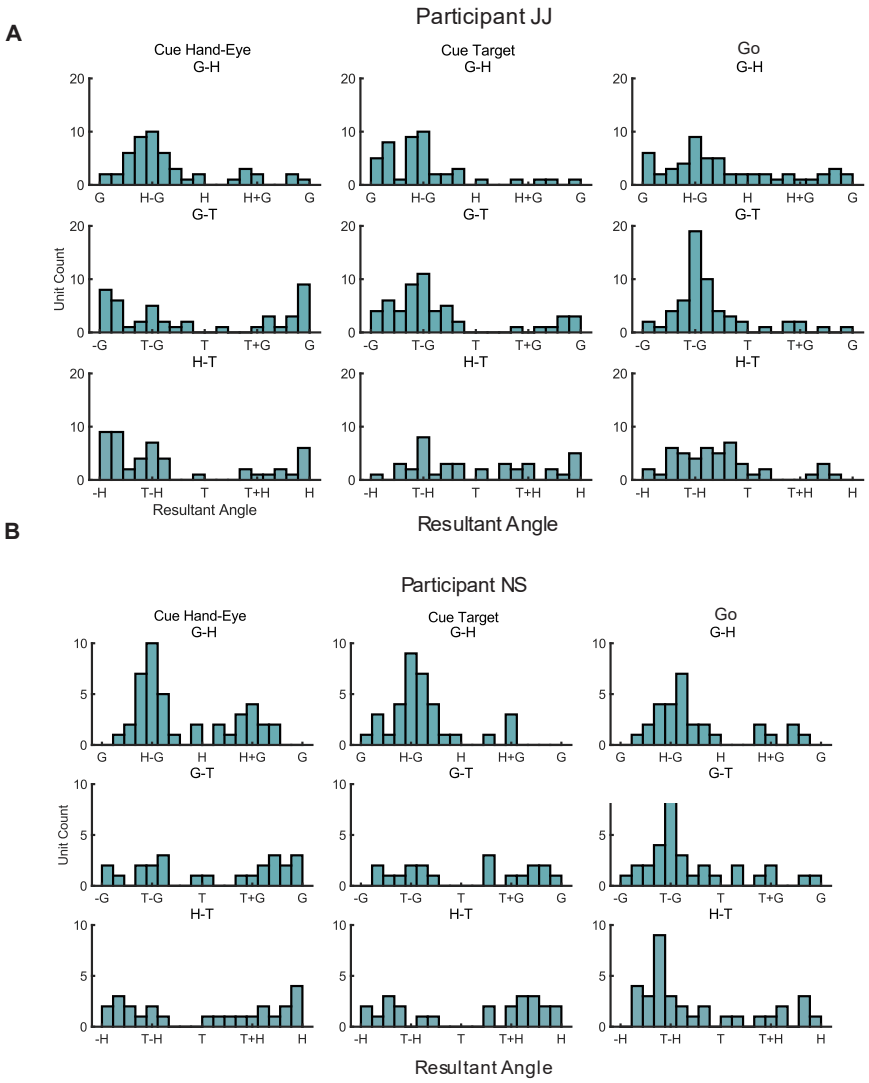

Supplemental Figure 3.9 Single neuron resultant angles for individual participants during delayed saccade task A: Resultant angles for JJ-PPC. B: Resultant angles for NS-PPC.

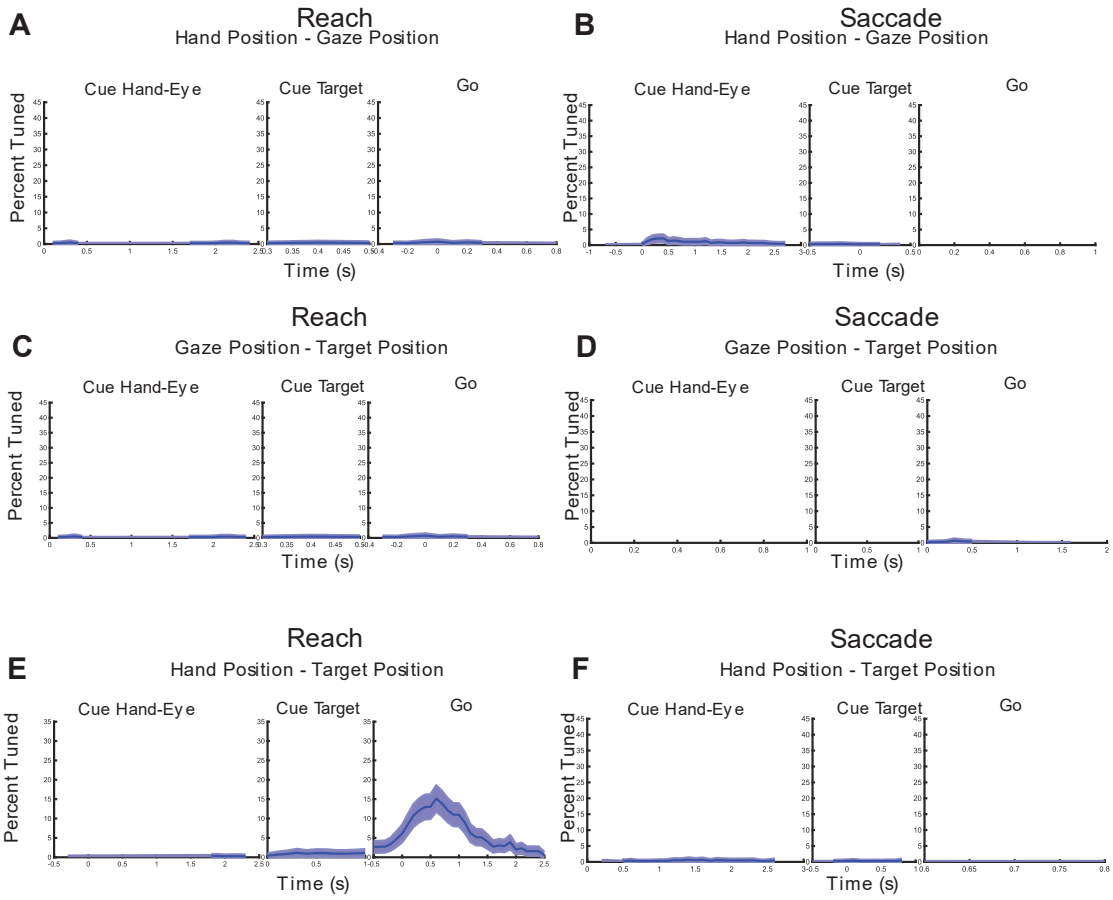

Supplemental Figure 3.10. Linear tuning to hand position relative to target position during reaches in MC

A: Percent of neurons tuned in JJ-MC to hand position relative to gaze position during the imagined reach task (n-way anova $p<0.05$). B: Percent of neurons tuned in JJ-MC to hand position relative to gaze position during the saccade task (n-way anova $p<0.05$). C Percent of neurons tuned in JJ-MC to gaze position relative to target position during the imagined reach task (n-way anova $p<0.05$). D: Percent of neurons tuned in JJ-MC to gaze position relative to target position during the saccade task (n-way anova $p<0.05$). E: Percent of neurons tuned in JJ-MC to hand position relative to target position during the imagined reach task (n-way anova $p<0.05$). F: Percent of neurons tuned in JJ-MC to hand position relative to target position during the saccade task (n-way anova $p<0.05$).

C h a p t e r 4

COMPARING SINGLE NEURON AND POPULATION COORDINATE FRAMES FROM DIFFERENT MOTOR AREAS OF HUMAN CORTEX

Summary

In this study, we revisit the question of how the coordinate frames for different effectors are encoded within small populations of neurons in motor areas of cortex. In Chapter 3, we found that the same population of neurons in PPC can flexibly encode different coordinate frames during imagined reaches or saccades, however, due to the design of the task, the dataset did not allow us to interpret this as the level of single neurons. We adapted the behavioral paradigm to allow for such interpretations to be made, and this adaptation was run in an additional participant with intracortical arrays implanted in both MC and PPC. We found that once again, the population level coordinate frame shifts from hand-centered during reaches to gaze-centered during saccades, and that this is driven by largely separate populations of neurons. For this participant we also had access to recordings from the supramarginal gyrus (SMG), a region of PPC not explored in Chapter 3. The responses found in SMG demonstrated that the flexible coordinate frames we have found are not seen in all regions of PPC. Finally, although most of the population in MC is only active during imagined reaches and not saccades, we consistently recorded a small number of neurons within MC that code position of a visual goal relative to the gaze position. The distinct coordinate frames seen in each bran area offer further clarity to the results in the previous chapters in this thesis, and introduce new questions about the functional role of flexible coordinate frames in certain neural populations within PPC.

4.1 Introduction

The study presented in Chapter 3 was the first to show how single neurons in PPC represent coordinate frames for movements of different effectors. The finding of flexible coding for the location of a visual target relative to the hand during reaches and relative to the gaze during saccades demonstrates a divergence from expectations for separation of hand and gaze centered reference frames between the anterior and posterior regions around the intraparietal sulcus (Andersen et al., 2007; S. W. C. Chang et al., 2008; Levy et al., 2007). As discussed in previous chapters, the separation of representations of hand and eye movements and their respective coordinate frames has been reported in PPC from early in its investigation. Much of these findings have been in nonhuman primates, however, and effector specific coordinate frames have been more elusive in human PPC, with both fMRI and single neuron recordings showing extensive overlap between hand-centered and eye-centered representations within a region (Bernier & Grafton, 2010; Vingerhoets, 2014).

In Chapter 3, we found that overlap in the coordinate frames coded during a held posture and during a movement were largely the result of different populations of neurons active during each task phase. Although we tested whether this temporal shift in coordinate frames occurred for both reaches and saccades, the data for each task version were collected on separate days (and even years), meaning responses are taken from different populations of neurons (or assumed to be, due to neural drift of intracortical electrodes among other factors). So, it remains an open question whether the responses seen during saccades and reaches were driven by the same or distinct single neurons. In the study from Chapter 2, we found that single neurons in PPC were tuned to random combinations of effectors. It seems reasonable to hypothesize this would extend to the coding for coordinate frames for these effectors as well, and that the coordinate frames for gaze and reach are largely coded by different subpopulations of neurons that occupy the same small region within PPC. Understanding whether these representations are from shared or separate neurons can allow for more in-depth interpretations

of the functional role of these mixed representations. For example, if the different coordinate frames are coded by different neurons, these neurons can also have different downstream targets in regions that are more specialized by effector (Vingerhoets, 2014).

To answer the question of whether single neurons demonstrated both hand-centered and gaze-centered depending on the effector being moved, we recorded from intracortical arrays implanted in two parts of PPC and two locations within the hand knob of motor cortex. One of the arrays in PPC is within the superior parietal lobule (SPL), near the location of the PPC recording in the previous study in Chapter 3. The other is in the supramarginal gyrus (SMG) and offers the opportunity to compare the dynamics of coordinate frames in two different regions of PPC. Recordings were made while the participant performed a delayed imagined reach task as well as a delayed saccade task, to evaluate whether single neurons showed any shift in their relative coding of direction.

At the population level, such a coordinate shift was observed in SPL but not SMG. Analysis of single neurons revealed that this shift in SPL was the result of two almost entirely separate populations of neurons. The delayed reach and saccade paradigms begin with the same spatial information presented to the participant, and the instruction does not vary until the final phase of the task. Somewhat surprisingly, even though the population vector appeared the same for this part of each task, this too was the result for distinct populations of neurons recruited during each task version. These results highlight the benefit of single neuron recordings, as otherwise this conclusion would be difficult to draw from the observation of overlapping activity alone. In RD-SMG, the population is dominated by neurons coding hand position relative to gaze position, with very few neurons tuned to the relative position of an effector and target.

This is in sharp contrast to the responses in MC, where the population was almost entirely restricted to coding hand position relative to target position during imagined reaches. A few single neurons strayed from this stereotype coded either the relative position of hand and gaze or gaze and target, but these were much less prominent and their role a bit more ambiguous in the context of other findings in MC. Altogether, these results offer insights into how the spatial coding of single neurons contributes to the overlapping representations we find at the population level in these brain regions.

4.2 Results

The data for this study was collected from participant RD, a tetraplegic male enrolled in an ongoing brain machine interface clinical trial. RD has four 64 channel intracortical Utah arrays implanted in his left hemisphere (Figure 4.1a). Two of these implants are located within the hand knob of the precentral gyrus in MC, and are denoted RD-MCL and RD-MCM (corresponding to the relatively more lateral and medial array respectively). RD has two implants in PPC, one located within the superior parietal lobule and the other within the supramarginal gyrus (RD-SPL and RD-SMG respectively). In addition to anatomical features, a presurgical functional MRI was used to localize areas for their involvement in hand movements (using a motor imagery grasping task), with the exception of RD-SMG which was targeted for activation during speech.

Recordings were made from each array simultaneously while participant RD performed two versions of a delayed movement paradigm, one for imagined reaches and the other for saccades (Figure 4.1b). The initial phase of both versions is the same, during which the participant is cued a hand position and a gaze position by two icons on a computer screen, a hand and a circle. The participant is instructed to fixate their gaze on the circle and imagine holding their hand at the hand icon. A combination of four hand and four gaze positions are possible during this phase. After two seconds, a gray circle appears at one of four possible positions, indicating the target for the participant's

movement. They maintain both their hand and gaze position for 1.5s until the fixation point changes color. At this time the participant's action depends on the task version. In the reach version of the task, the participant maintains gaze position and imagines reaching to the target location. In the saccade version of the task, the participant maintains imagined hand position while making a saccade to the target. Both versions of the task were run within the same session (i.e. data collection period of about two hours) to be able to compare between the single neuron activity for each version. It should be noted that because the participant is tetraplegic, all reaches mentioned in the results of this chapter are imagined reaches and not overt.

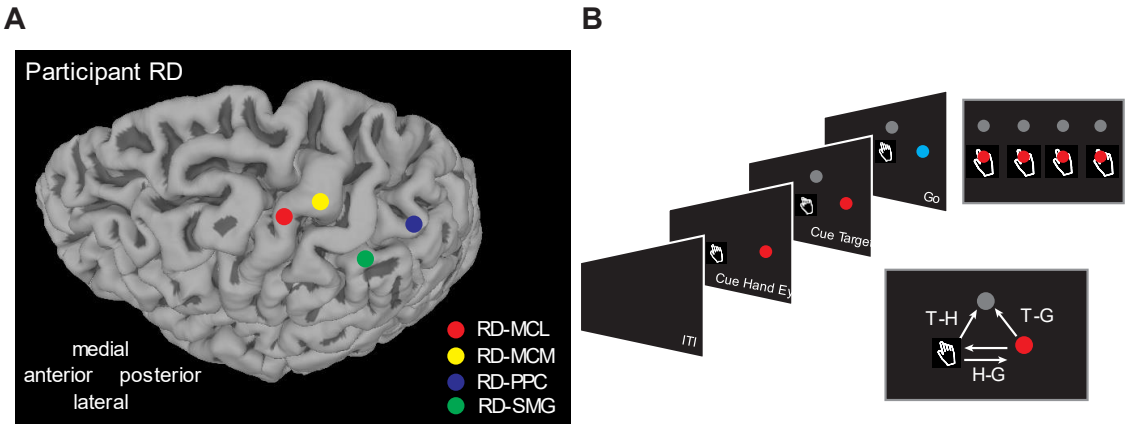

Figure 4.1. Implant locations and behavioral task
A: Location of electrode arrays in participant RD. Red= RD-MCL, Yellow= RD-MCM, Blue = RD-PPC, Green = RD-PPC. B. Delayed imagined reach/saccade paradigm. Left shows different phases of task. Upper right shows differing combinations of hand, gaze, and target positions. Bottom right shows directional vectors relating each position.

Linear tuning to relative position in PPC during reaches and saccades

The first question we addressed was whether there were any differences in the linear tuning properties of neurons in each location in PPC during the reach and saccade task. Each neuron was evaluated for tuning to either hand position relative to gaze position, hand position relative to target position, or gaze position relative to target position (n-way anova, adjusted for multiple comparisons). In both the

reach and saccade version of the task, we found around 20% of neurons in RD-SPL and RD-SMG tuned to the hand position relative to the gaze position after the hand and gaze position are cued on the screen in the initial task phase (Figure 4.2 A and C). During the reach version of the task, around 15% of neurons in RD-SPL and 5% of neurons in RD-SMG were also tuned to the relative position of the hand and gaze during the cue target and go phases of the task. In the saccade version of the task, less than 10% of neurons in RD-SPL and less than 5% of neurons in RD-SMG showed such tuning. In RD-SPL there was also significant tuning seen to the hand position relative to target position during reaches, and the gaze position relative to the target position during saccades (Figure 4. 2B and D). Tuning to the relative hand/gaze and target positions began in the cue target phase after the target was shown, and then increased after the go cue was given. In RD-SPL just under 20% of neurons were tuned to the relative positions of the hand and target during reaches, and 25% were tuned to relative positions of gaze and target during saccades. Less than 2% of neurons in RD-SMG were found to be tuned relative to the target location in either task (Figure 4.2B and D).

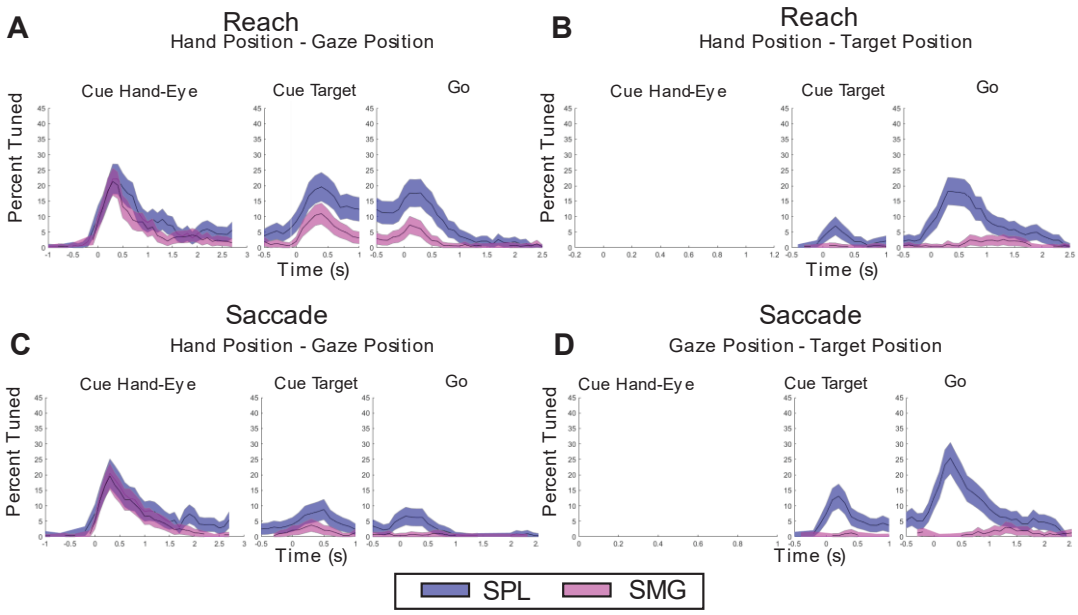

Figure 2. Linear tuning of neurons in SPL and SMG during imagined reach and saccade tasks
Percent tuned to relevant relative variable positions throughout each task (n-way anova, $p<0.05$

adjusted for multiple comparisons). Mean shown as solid trace and standard error of the mean plotted as shaded error bars. RD-SPL in blue and RD-SMG in pink. A: Tuning to hand position relative to gaze position during imagined reach task. B: Tuning to hand position relative to target position during imagined reach task. C: Tuning to hand position relative to gaze position during saccade task. D: Tuning to gaze position relative to target position during saccade task.

Flexible coding for hand-gaze, hand-target, and gaze-target vectors in SPL but not SMG

The linear tuning properties of each area suggest differences in underlying coordinate frames used. The coordinate frame can be determined by finding a vector that describes how positions of different variables are encoded relative to each other across neural responses. In order to find these vectors between each of the relevant position variables (i.e. hand-gaze, hand-target, gaze-target), we used a gradient analysis applied on binned time windows of 100 ms that stretched through the duration of the task. This analysis is described in detail in Chapter 3, but in summary, neural firing rates are organized into three four by four by four matrices, where in each matrix two of the three position variables were varied while one was maintained (Figure 4.3). As an example, the leftmost matrix shown in Figure 4.3 shows the firing rates of a neuron while hand and gaze position are varied, but target position is constant. Next, we compute the gradient of each matrix. The resultant angle and length of the gradient gives a 2 dimensional vector that can be interpreted as the relative coding of position for that neuron.

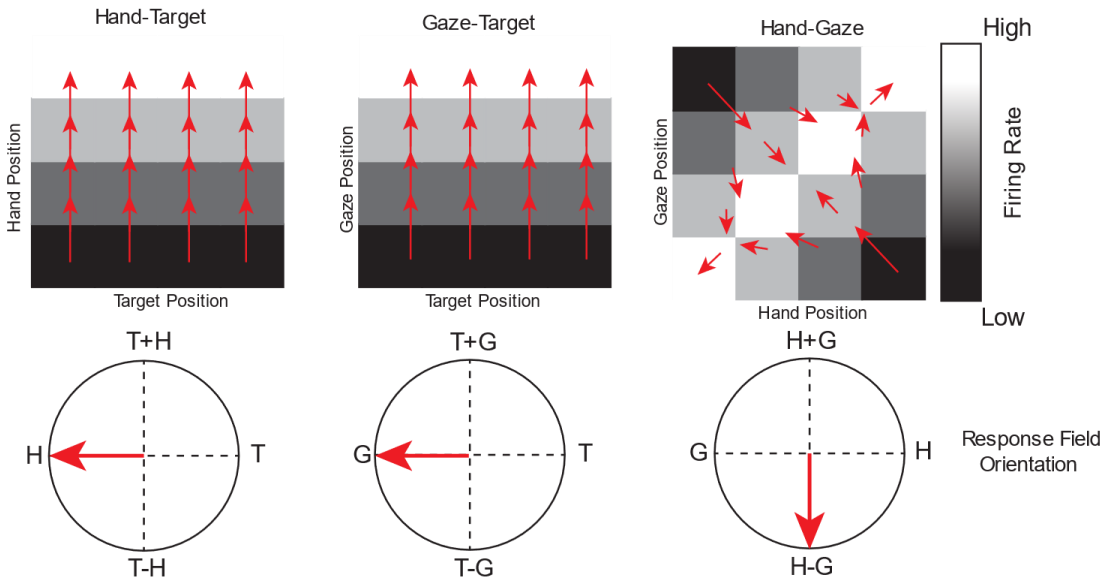

Figure 4.3 Response of an ideal hand-gaze centered neuron.
This shows the response field orientations for an idealized neuron that represents hand and gaze position relative to each other. These response fields are found for each variable pair by performing a gradient analysis on the firing rate matrices shown in the top row (right: hand-target, middle gaze-target, left: hand-gaze). The resultant from the gradient analysis shown in red can be used to derive the response fields shown in the bottom row.

The example neuron in Figure 4.3 is an idealized hand-target coding neuron, so in this case, gradient descent of the hand-gaze matrix results in an angle of 0 degrees, which corresponds to that neuron's firing rate being driven by changes in hand but not gaze position. The resultant angle for the gradient of the gaze-target matrix is 0 because changes in target but not gaze position drive changes in firing rate. However, when hand and target position are varied, the resultant angle of -90 degrees shows that both variables drive that neuron's firing rate. Taken together, these resultant angles demonstrate an ideal response for a neuron coding a hand-target vector. As stated, this was done for each neuron for 100ms time windows across the task. Then, the resultant vector coded by the population was found by summing the resultants of individual neurons and then dividing by the number of neurons.

This analysis found that in the population vector coded shifted depending on the task context in RD-SPL but not RD-SMG. For both the reach and saccade tasks, during the cue hand eye phase, populations in both RD-SPL and RD-SMG coded a H-G vector that gradually declined in magnitude as the task progressed (Figure 4.4). In RD-SPL, depending on the task version, this vector is replaced by either a H-T vector or a G-T that first appears when the target is cued and increases in magnitude through the execution of the imagined reach or saccade respectively (Figure 4.4a and c). In contrast, no such vectors from effector to target are observed in RD-SMG for either task. This population level analysis leads to several questions about how single neurons contribute to the flexible coordinate frames coded in RD-SPL, and how these compare to those that make up the stable vector coding seen in RD-SMG.

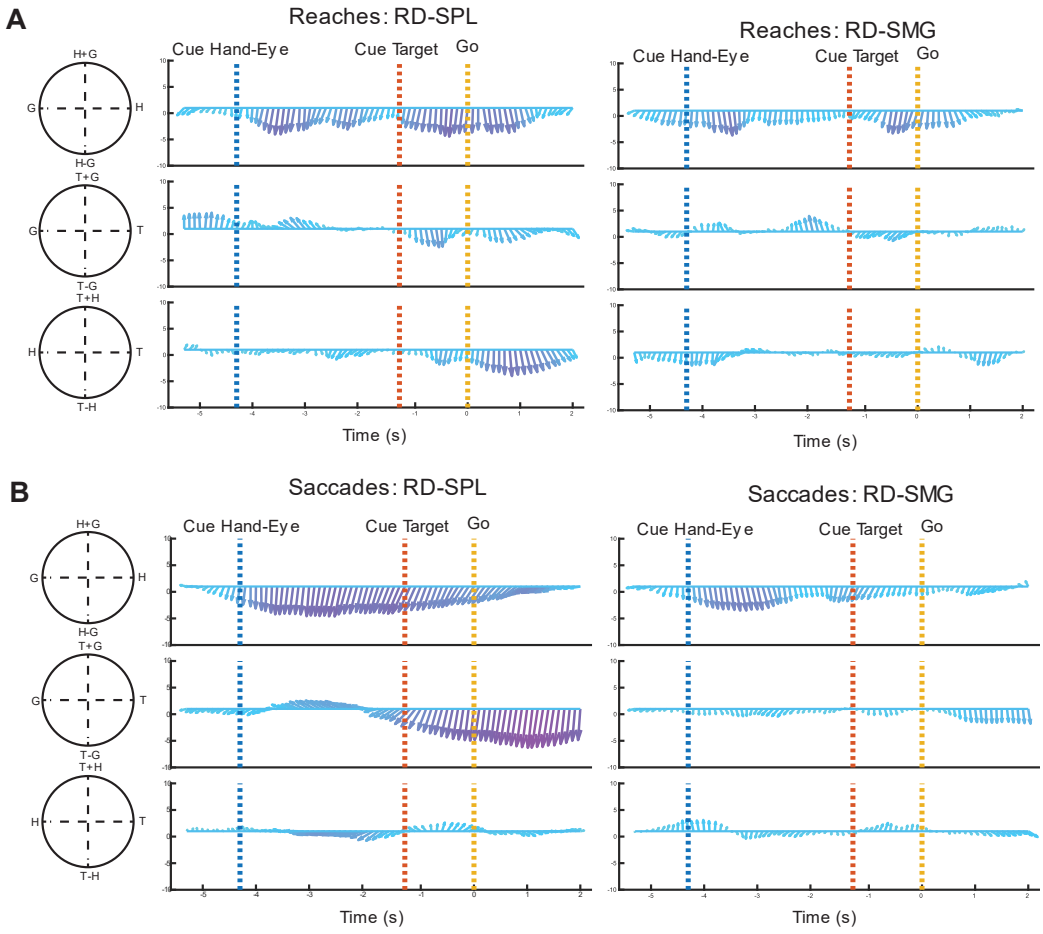

Figure 4.4. Population vectors coded during delayed imagined reach and saccade tasks in PPC Results from gradient analysis through time (100ms windows). Angle of arrows shows the average resultant angle across neurons and the length and color of each arrow indicates the average resultant magnitude. A: Population vector for RD-SPL (left) and RD-SMG (right) during the delayed reach version of the task. B: Population vector for RD-SPL (left) and RD-SMG (right) during the delayed saccade version of the task.

Coding of hand-gaze, hand-target, and gaze-target vectors by distinct subpopulations in SPL

Next, we asked how the shift in population vector coding seen in SPL was achieved at the single neuron level. Are hand-gaze, hand-target, and gaze-target vectors coded by the same neurons? Or are different subpopulations of neurons active during different task contexts? To categorize neurons as vector coding and answer this question, we performed the gradient analysis described in Figure 4.3 for 1 second time windows from each phase of the task to find each neuron's response field during each phase. A neuron was considered to have a significant response field if the magnitude of the resultant vector was greater than that for a shuffled firing rate matrix (randomization test). Singular value decomposition (SVD) was also performed for each neuron and each variable pair to determine whether the response field seen was a result of true vector coding or gain modulation. For a response field to also be considered the result of vector coding for a variable pair, SVD must not be able to separate the impact of the two variables on the neurons firing rate.

This analysis shows that despite the similarities between task versions and the population level vector coding seen, this was the result of largely distinct populations of neurons. Of the neurons significantly tuned to the H-G variable pair during the initial phase of each version of the task (reaches n = 19; saccades n = 29), only three neurons were shared between each task version (Figure 4.5a). One of these three neurons met the criteria to be considered a H-G vector coding neuron. In agreement with the vector magnitudes seen for the population results, there were more neurons coding a H-G vector during the cue phase of the saccade task than the reach task (n=7 and n=2 respectively). This is also reflected in the distributions of the resultant angles of single units. For H-G tuning, the expected

resultant angle is -90. In the cue phase for the saccade phase of the task, the mean response field or the H-G variable pair was -73.9° (19.9° 95% CI) and response fields were unimodally distributed ($p<0.05$; Rayleigh test) and nonuniform ($p<0.05$; Omnibus test) (Supplemental Figure 4.1). For the reach phase of the task, the mean response field was -120.9° (44.4° 95% CI) and response fields were unimodally distributed ($p<0.05$; Rayleigh test) and uniformly distributed ($p>0.05$; Omnibus test).

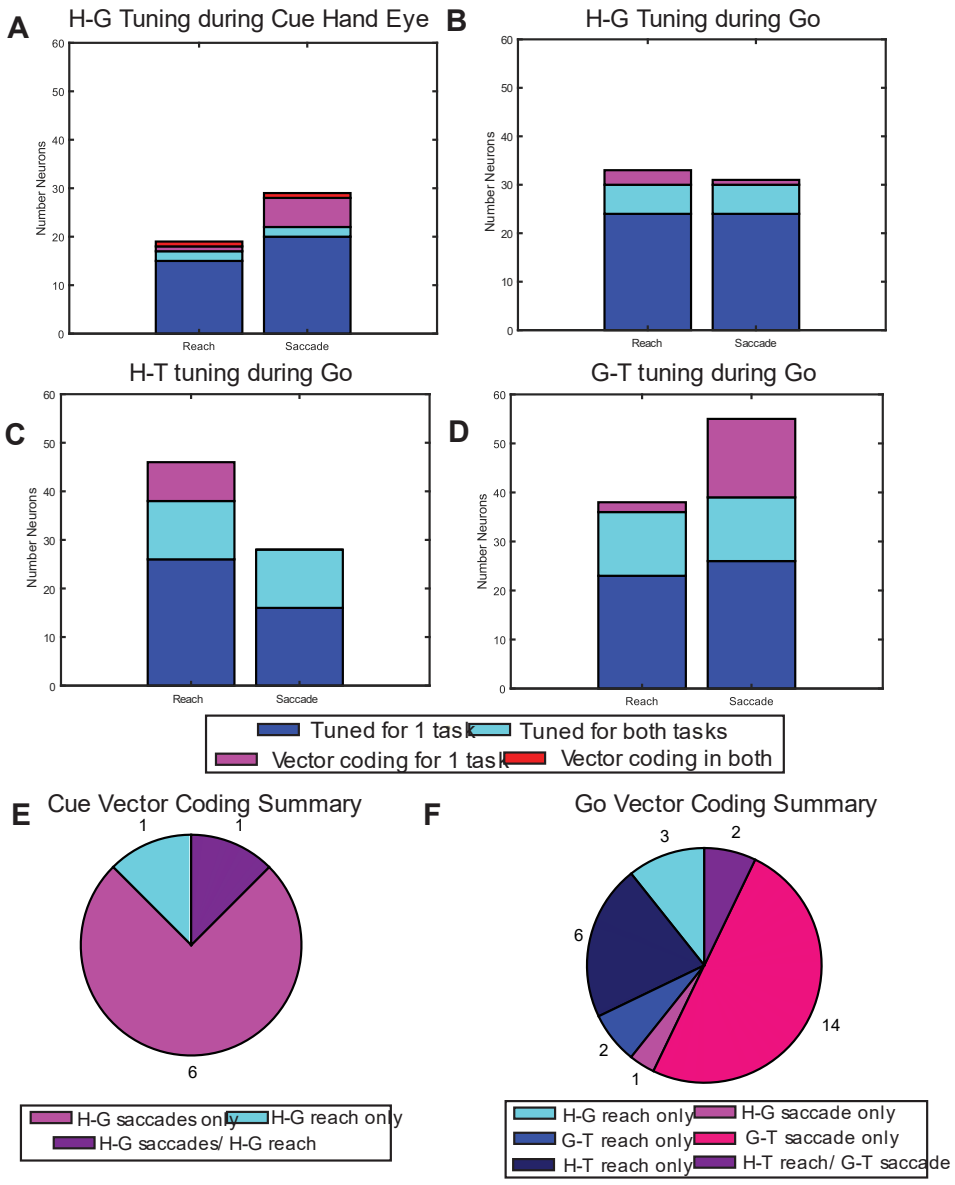

Figure 4.5 Vector coding in single neurons of SPL
A-D: Number of neurons significantly tuned to each variable pair during its relevant phase . Significant neurons are divided into tuned during 1 task only (dark blue), tuned for both task (light blue), and vector coding for 1 task (pink) vector coding for both tasks (red). Reaches on left bar, saccades on right bar . A: Tuning to H-G variable pair during Go , B: Tuning to H-G variable pair during Go, C: Tuning to H-T during Go, D: tuning to G-T during Go. E: Number of neurons that coded H-G variable during the cue phase of each task . F: Number of neurons that coded a vector during Go.

The execution phase of each task also suggested largely different populations being recruited for reaches and saccades (Figure 4.5b-d). Of the neurons tuned to the H-T pair (reaches n = 46, saccades n = 28), twelve neurons were tuned during each task version (Figure 4.c). None of these shared neurons were categorized as H-T vector coding, as no H-T vector coding neurons were seen during saccades. In contrast during reaches, eight neurons coded for a H-T vector. This is once again seen in the distributions of response fields for single units for the H-T variable pair, with a mean angle of -90.6° (12.9° 95% CI, unimodally distributed: $p<0.05$; Rayleigh test, and nonuniform: $p<0.05$; Omnibus test) seen during reaches and of -70° (49.6° 95% CI, unimodally distributed: $p<0.05$; Rayleigh test, and uniform: $p>0.05$; Omnibus test) (Supplemental Figure 4.1). The expected angle for a H-T vector would be -90, in line with the response field of neuron during reaches more so than during saccades.

Much like H-T tuning, neurons tuned to the G-T variable pair were largely distinct between the two task versions with 13 of 78 total G-T tuned neurons being shared between the tasks (reaches n = 36, saccades n = 55) (Figure 4.5d). Further, no neurons were categorized as G-T vector coding for both tasks (reaches n = 2, saccades n = 16). During saccades, the mean response field or the G-T variable pair was -90.8° (11.4° 95% CI) and response fields were unimodally distributed ($p<0.05$; Rayleigh test) and nonuniform ($p<0.05$; Omnibus test), while during reaches the mean response field or the G-T variable pair was -34.2° (82.2° 95% CI, non-unimodally distributed $p>0.05$; Rayleigh test and uniform $p>0.05$; Omnibus test) (Supplemental Figure 4.1). The relative preference of single neurons for gaze over reach vector coding illustrates the difference between these findings and those in the study presented in Chapter 3 where we saw an emphasis of coding for the reach vector over the gaze vector.

Notably, three neurons coded a H-G vector during reaches, an increase from the cue phase (mean response field = -65.6° 18.9° 95% CI, unimodally distributed: $p<0.05$; Rayleigh test, and nonuniform: $p<0.05$; Omnibus test) (Figure 4.5b, Supplemental Figure 4.1). This illustrates a difference between the two tasks, as during the saccade version of the task the number of H-G vector neurons drops from 7 to 1 between the cue and execution phases. (mean response field = -140.2° 27.3° 95% CI, unimodally distributed: $p<0.05$; Rayleigh test, and uniform: $p>0.05$; Omnibus test). This contrast was not seen in a previous study with two other participants, and possible reasons will be explored in the discussion.

The finding that single neurons do not code for the same vectors regardless of task version introduces the possibility for neurons to code for different vectors depending on the task phase or version. In a previous study we found that a small subpopulation of neurons that coded a H-G vector during the initial phase of the task changed to coding a H-T vector during reaches. This was examined for RD in the present study, however no such neurons were found in either version of the task (Figure 4.5e). Another possible case of switching that we can evaluate with the current data is whether a neuron could code a H-T vector during imagined reaches but a G-T vector during saccades. This does not seem to explain the majority of the vector coding seen, however, as only two neurons were shown to switch from H-T during reaches to G-T during saccades (Figure 4.5f, and response field for neurons during each task shown in Figure 4. 6 and Supplemental Figure 4.2). Finally, we assessed whether any neurons could be categorized for a single reference frame (hand-centered, gaze-centered, hand-gaze). Despite the presence of vector coding neurons in both versions of the task, none of these neurons were fully described by a single reference frame.

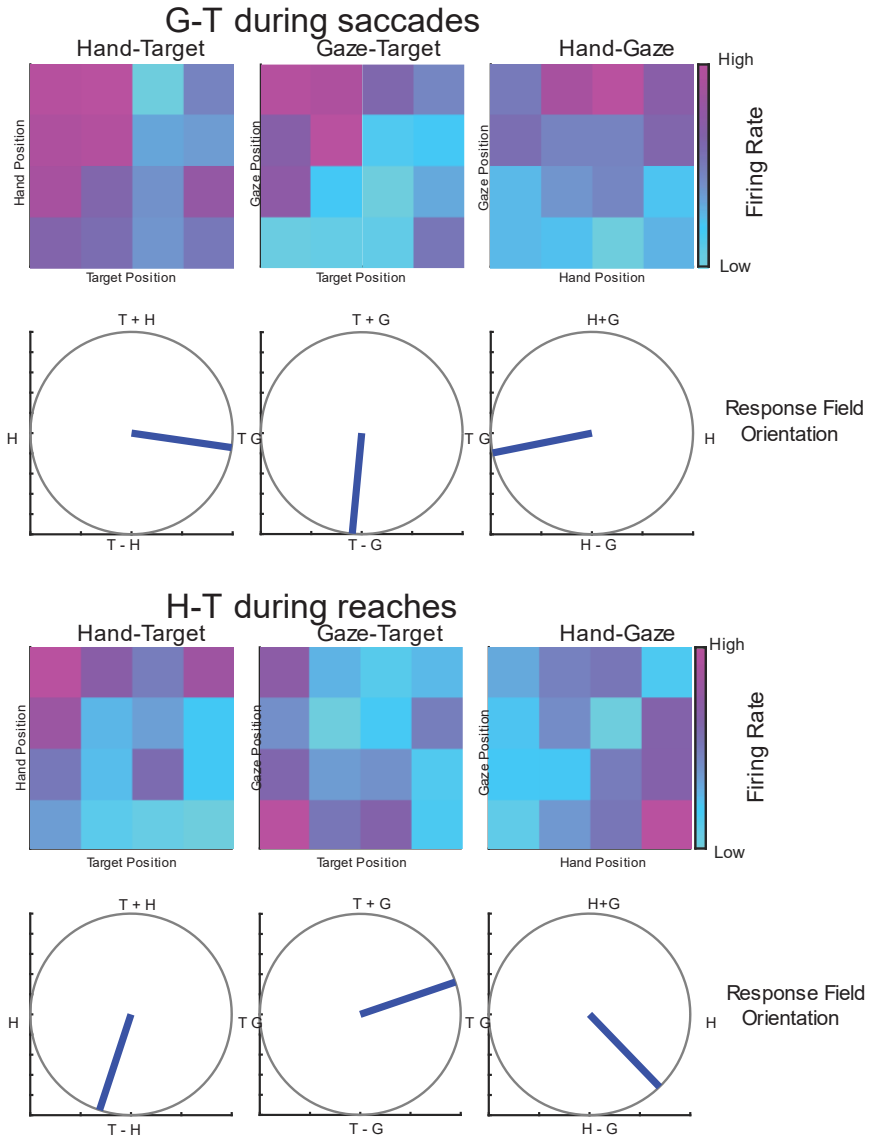

Figure 4.6 Response field for a single neuron in SPl that codes a hand-target vector during reaches and a gaze-target vector during saccades.
Top: Response field for neuron demonstrating a gaze -target vector being coded during saccades. Bottom: Response field from that same neuron during reaches show ing handtarget vector coding.

Hand-gaze vector coding in SMG

The population level vector coded by RD-SMG differed from that in RD-SPL, but it does not necessarily rule out the presence of single neurons that code each coordinate frame. The vector coding of single neurons was evaluated using the same methods described for RD-SPL. This revealed that a

majority of neurons in RD-SMG coded a hand-gaze vector. Like in RD-SPL, there was little overlap between the neurons active during each version of the task. Between 23 neurons tuned to the H-G variable pair during the initial phase for the reach task and the 30 tuned to H-G during the initial phase for the saccade task, only six were in common (Figure 4.7a). There were no neurons that were tuned to the G-T variable pair during both imagined reaches and saccades, and only one neuron tuned to the H-T pair during both movement types.

Unlike in RD-SPL where we saw a sharp drop in the number of H-G vector neurons between the initial and execution phases (from 7 to 1), in RD-SMG there is an increase from 2 H-G vector coding neurons during the cue phase to 4 during saccades (Figure 4.7a,b,e,f). This is seen in a similar mean response field for single neurons for the H-G variable pair during both the cue phase and the go phase of the task (Cue: -72° 24.8° 95% CI, unimodally distributed: $p<0.05$; Rayleigh test, and nonuniform: $p<0.05$; Omnibus test, Go: -22.2° 21.1° 95% CI, unimodally distributed: $p<0.05$; Rayleigh test, and nonuniform: $p<0.05$; Omnibus test) (Supplemental Figure 4.1).

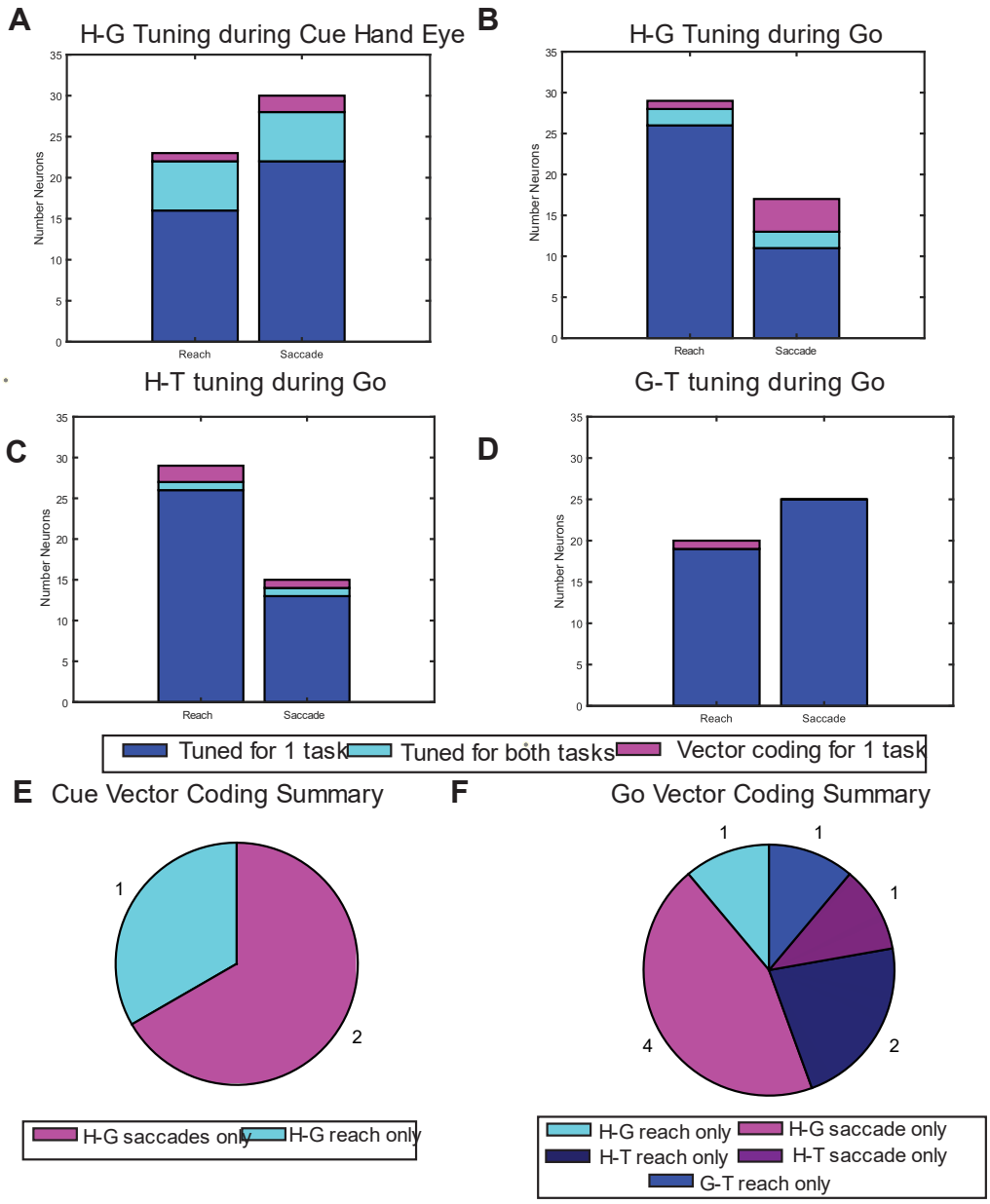

Figure 4.7 Vector coding in single neurons of SMG
A-D: Number of neurons significantly tuned to each variable pair during its relevant phase . Significant neurons are divided into tuned during 1 task only (dark blue), tuned for both task (light blue), and vector coding (pink, only existed for one task only). Results for reaches on left bar , saccades on right bar. A: Tuning to H-G variable pair during Go , B: Tuning to H-G variable pair during Go, C: Tuning to H-T during Go, D: tuning to G-T during Go. E: Number of neurons that coded H-G variable during the cue phase of each task. F: Number of neurons that coded a vector during Go.

The response fields seen during reaches and saccades differed greatly from those seen in RD-SPL, and did not correspond to H-T or G-T vectors respectively (Reach H-T: -57° 54.2° 95% CI, non-unimodally distributed: $p>0.05$; Rayleigh test, and uniform: $p>0.05$; Omnibus test, Saccade G-T: 65.8° 41.1° 95% CI, non-unimodally distributed: $p>0.05$; Rayleigh test, and uniform: $p>0.05$; Omnibus test) (Supplemental Figure 4.1). Indeed, no G-T vector coding neurons were found during saccades. Only one G-T vector coding neuron was observed in RD-SMG, and this was during imagined reaches. There was one H-T vector coding neuron found during saccades, and two during imagined reaches (Figure 4.7f). The reach version of the task did not show the same pattern of increase in H-G vector coding neurons between the initial and execution phases, with one neuron meeting H-G vector criteria during each phase (Figure 4.7 c,d,e,f). The preference for H-G over H-T and G-T vector coding in SMG reported here both at a population and single neuron level are consistent with reports of egocentric coordinate frames being used in this region. The differences seen here between RD-SPL and RD-SMG will be expanded on in the discussion in the context of broader PPC literature and the expected function of each area as it pertains to visually guided movements.

MC predominantly codes a hand-target vector during imagined reaches

Thus far, all results presented in this chapter have been from the PPC, but we also recorded from electrodes implanted in the hand knob of motor cortex. These recordings act as a sort of proxy for behavior during reaches, because although eye movements were overt and thus measured, all reaches were purely motor imagery due to the participants spinal cord injury. The distinctions in hand-target and gaze-target coding seen in RD-SPL suggest correct task behavior, the results from MC can help confirm this further. Because the arrays are located in the hand knob, an area well established for its role in representing hand movements and not eye movements, if behavior was correct we should see a reach vector that is encoded during imagined reaches, but not during saccades, and overall greatest tuning during the execution phase of the reach version of the task.

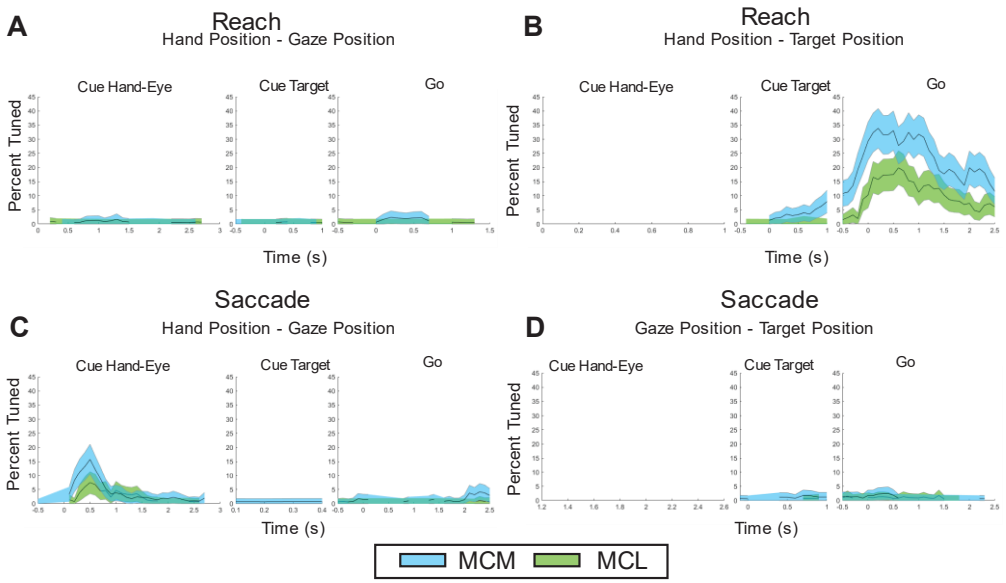

Figure 4.8. Linear tuning of neurons in MCM and MCL during imagined reach and saccade tasks
Percent tuned to relevant relative variable positions throughout each task (n-way anova, $p<0.05$ adjusted for multiple comparisons) Mean shown as solid trace and standard error of the mean plotted as shaded error bars. RD-MCM in blue and RD-MCL in green. A: Tuning to hand position relative to gaze position during imagined reach task. B: Tuning to hand position relative to target position during imagined reach task. C: Tuning to hand position relative to gaze position during saccade task. D: Tuning to gaze position relative to target position during saccade task.

As expected, a majority of neurons in both MC arrays are active exclusively during the execution of imagined reaches (Figure 4.8). Interestingly, there is a slight peak in tuning of hand position relative to gaze position, but only for the saccade version of the task, and much more so in RD-MCM than RD-MCL (Figure 4.8a and c). The results from the population gradient analysis through time also reflect a similar pattern, with the most prominent vector coded being a hand-target vector during imagined reaches (Figure 4.9). This reach vector is notably absent during saccades. Interestingly, there does appear to be a weak gaze-target vector present during saccades at the population level in RD-MCM. Additionally, in agreement with the linear tuning analysis, a weak population vector for hand position relative to gaze position appears at the start of the task.

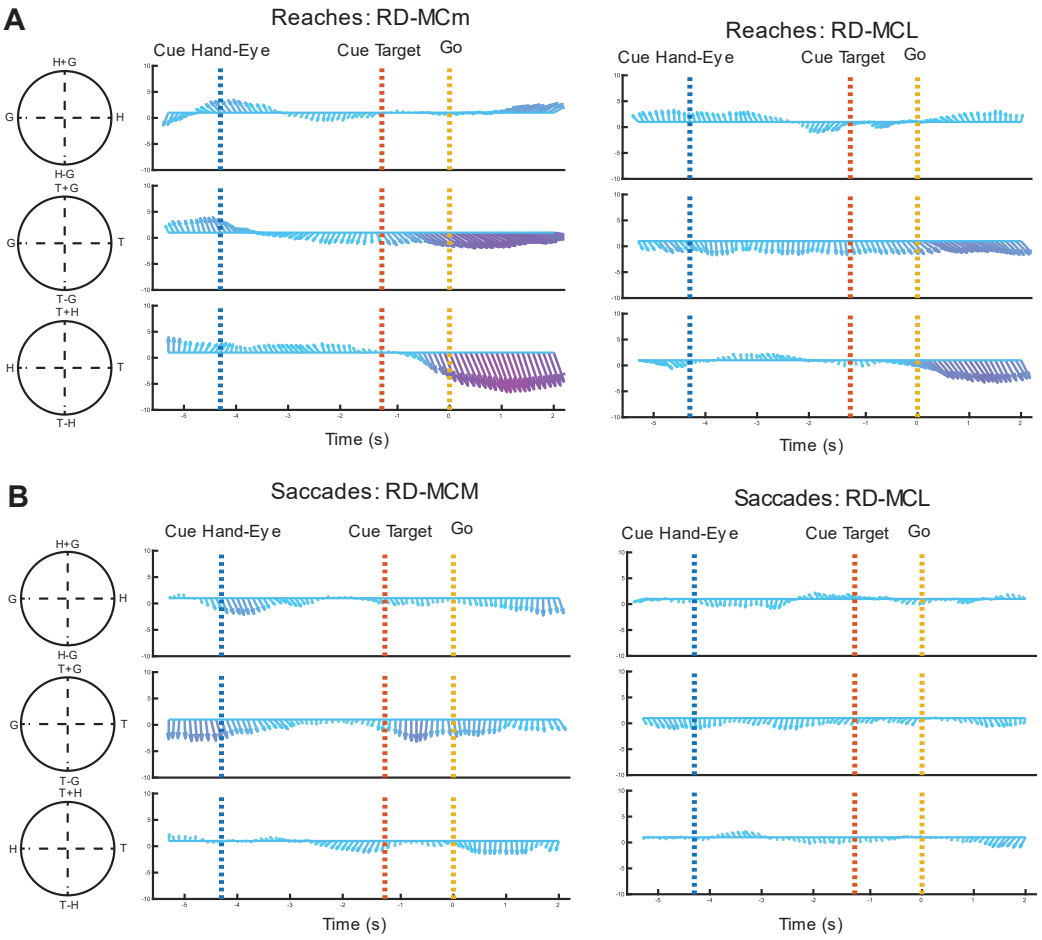

Figure 4.9. Population vectors coded during delayed imagined reach and saccade tasks in MC Results from gradient analysis through time (100ms windows). Angle of arrows shows the average resultant angle across neurons and the length and color of each arrow indicates the average resultant magnitude. A: Population vector for RD-MCM (left) and RD-MCL (right) during the delayed reach version of the task. B: Population vector for RD-MCM (left) and RD-MCL (right) during the delayed saccade version of the task.

The response fields seen for individual neurons also emphasized the execution phase of the task, with the most prominent vector coded being from the hand to the target during imagined reach (example H-T neuron shown in Figure 4.10a). These were once again evaluated using gradient analysis for 1s windows for each phase of the task. This gave 15 neurons in RD-MCM and 10 in RD-MCL that coded the H-T vector during reaches (Figure 4.10b and c) (it should be noted that slightly more single neurons were recorded from RD-MCL than RD-MCM, so this seems unlikely to have been caused

by differences in signal yield). In contrast, each array showed only one neuron that coded a H-T vector during saccades, and this was not shared with the reach task. There are few neurons in MCM or MCL that code for a H-G vector. Somewhat interestingly, in MCL these neurons are only observed during the saccade version of the task (n = 3 during cue, n = 1 during go). H-G vector neurons were only seen in RD-MCM during the cue phase (Supplemental Figure 4.3) (reach: n=2, Saccade: n=1).

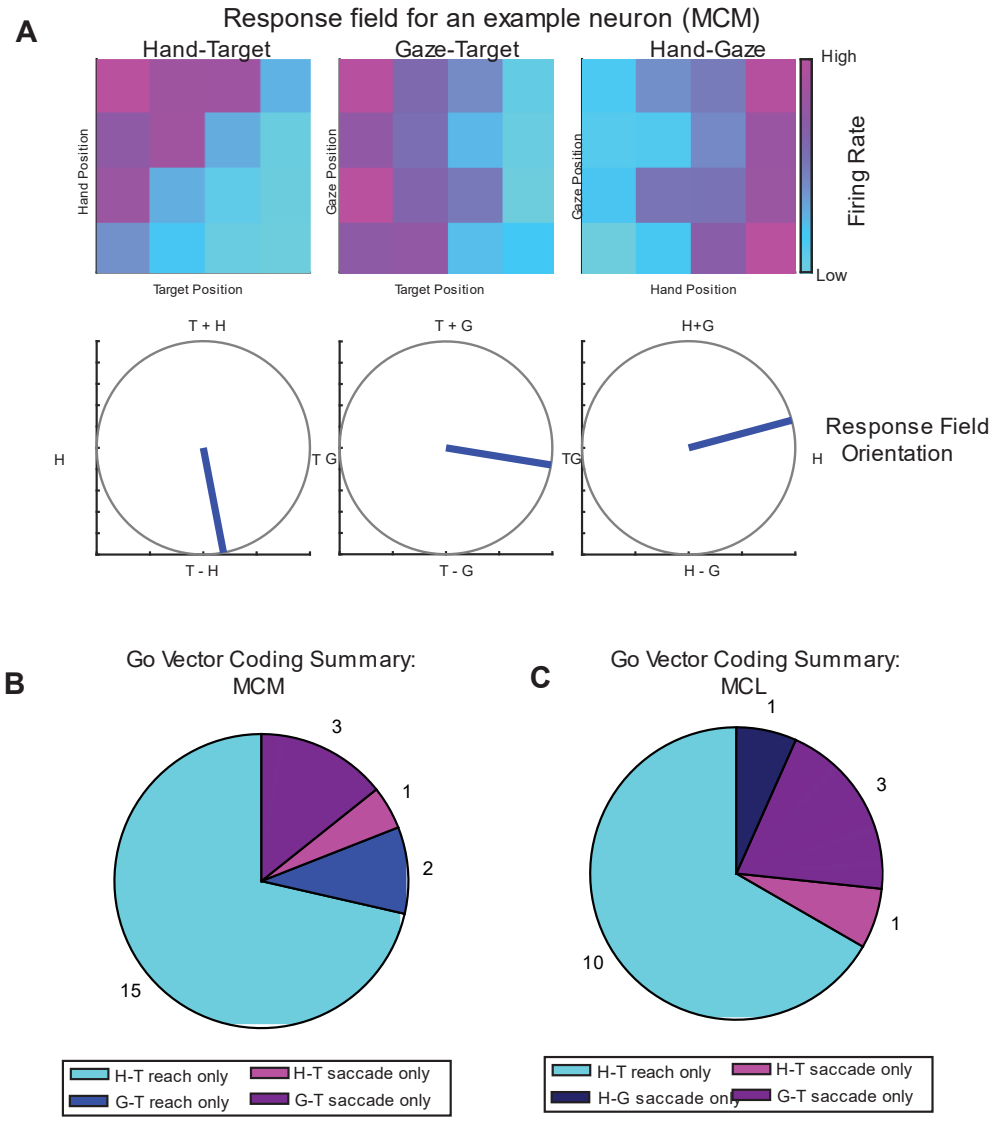

Figure 4.10 Vector coding in single neurons of MC
A: Response field for an example hand-target vector coding neuron , the most common type in MC. B and C show a summary of neurons that coded a vector during both task versions . Light blue: H-T reach only, Blue: G-T reach only, Dark Blue: H-G reach only, Purple: G-T saccade only, Pink: H-T saccade only. C: RD-MCM, D: RD-MCL

Although there were relatively few neurons that coded a gaze vector during reaches, they were not entirely absent. In both RD-MCM and RD-MCL three neurons (six total) were found to code a G-T vector during saccades, and in RD-MCM two neurons coded a G-T vector during reaches (Figure 4.10b and c, example shown in Supplemental Figure 4.4). These neurons were not shared between

the tasks (Supplemental Figure 4.3). Although the number of G-T neurons are relatively small in comparison to the H-T neurons, this is a consistent pattern across several results presented in this thesis and bring up questions about the functional role of this representation as classic views would suggest something other than it being the same motor command as the reach vector. The interpretation of G-T coding seen in MC will be expanded on in a discussion section.

4.3 Discussion

The results in this study add to our growing understanding of how coordinate frame transformations are encoded in the human cortex. The differences seen between each area can help in our constant search for the functional organization of brain regions, and also better understand what computational properties are characteristic of each function. The findings in this study also highlight that even within small anatomical patches of cortex, functions of individual neurons can show great variability. Importantly this is more so the case for some regions than others, with the rich responses in SPL indicating potentially higher cognitive representations of movement than either SMG or MC.

Separate populations of hand and gaze centered neurons in SPL are active during reaches and saccades

One of the primary motivations of the current study was to better understand the single neuron responses that resulted in the flexible coordinate frames we observed at the population level in PPC in Chapter 3. We found that largely distinct subpopulations of neurons are active during each version of the task. This offers an important insight to previous findings in fMRI work that also showed mixed coordinate frame representations within the same regions of PPC, and demonstrates that this is not the result of a purely functional code implemented across all neurons (Bernier & Grafton, 2010; Vingerhoets, 2014). Rather, single neurons are engaged depending on the function that is being utilized. One interpretation of this separation within the population is that these neurons may have

downstream targets in entirely separate areas. Another question that arises is what is the role of the neurons that are active during each task? Only two neurons were found to flexibly change from coding reach vector to saccade vectors. Although this small number may seem trivial at first, computationally, switching neurons are shown to provide a boost in efficiency, and may even be necessary for activating the proper subpopulations of non-switching neurons (Brozović et al., 2007).

In the study in Chapter 3, we found a small number of neurons switched their relative coding of position for different task contexts. More specifically, we found that neurons switched from representing hand position relative to gaze position during posture maintenance to representing hand position relative to target position during imagined reaches. In this study, we found no neurons that exhibited such a behavior. There were also a smaller number of hand-gaze and hand-target coding neurons recorded in RD in general, which could indicate the use of a more inter-mixed coordinate frame that is not well assessed by our task. This is supported by the lack of any neurons found to full described by a single reference frame. One caveat is that the movements tested were performed in isolation, and it could be that to fully evaluate the coordinate frames for intermixing neurons, coordinated hand and eye movements must be tested.

In SMG we found no neurons that exhibited any switching behavior in any capacity, which also brings up the question of whether this type of neuron is characteristic across PPC, or is specific to certain areas. If this is the case, perhaps there are some regions where switching occurs between movement contexts and others where switching occurs between effectors. Regardless, this does not represent the only difference between the results in Chapters 3 and 4, which brings up the need to explore anatomical factors that may influence our findings. This is the topic of the next section.

Distinctions in coordinate frame coding in different anatomical locations of PPC

In this study we were able to directly compare the coordinate frames encoded in both SPL and SMG. We found multiple coordinate frames coded in SPL but almost exclusively hand-gaze coding in SMG. This is in agreement with most work in SMG reporting strong egocentric, or self-centered, coding, and much more varying reports for the coding within SPL (Bernier & Grafton, 2010; Celsis et al., 1999). In SPL, movements of the hand are seen to overlap with movements of other parts of the body, although there is some heterogeneity in evidence as to whether there is separation of hand and eye movements specifically (Heed et al., 2016; Striem-Amit et al., 2018). Damage to either region causes distinct deficits that further emphasize the more egocentric nature of SMG compared with SPL. Damage to SPL tends to result in a variety of different deficits including optic ataxia, while damage to SMG results is associated with egocentric but not allocentric contralateral neglect (Andersen et al., 2014; Medina et al., 2009; Yeo et al., 2014).

Chapter 3 presented results from PPC in two additional participants. One of these was also within SPL, although notably located more medially than RD-SPL (i.e. further removed from the intraparietal sulcus (IPS)). Although the population coordinate frames were similar in both areas, we found slightly different patterns of effector emphasis. RD-SPL, which is closer to the IPS, showed preference for saccades while recordings from SPL in the previous participant showed a preference for reaches. This offers some insight into the heterogeneity of findings with the PPC, as this could either indicate that these regions close in anatomical location are in fact different subregions, or that a single region has some variability in its coding of spatial information.

The recordings for the second participant in Chapter 3 were taken from an area at the junction of the IPS and postcentral gyrus. This is located in the anterior portion of the IPS, while RD-SPL is slightly posterior to this junction (in the middle portion of IPS). We found that there is the greatest emphasis

of the hand in PC-IP compared with RD-SPL which showed the greatest emphasis of eyes. These findings are in line with the expectation that as one progresses from the posterior to anterior portions of the IPS, the representation gradually shifts from being for the eyes to being for the hand (Filimon, 2010; Konen et al., 2013; Vingerhoets, 2014). Most work in NHPs that demonstrates the greatest effector specificity is within the sulcus, so maybe these regions are the best approximation and perhaps if we had access to deeper, we would see even more specificity (Kastner et al., 2017).

Evidence for somatotopy in imagined reaches and weak but consistent finding of neurons tuned to eye movements in hand knob of MC

The results from motor cortex largely fit with expectations set by the literature, with the neural population encoding a reach vector during imagined reaches and weak response seen during saccades. One distinction between much of this work and the present study is the use of motor imagery as opposed to overt movements. The representation of motor imagery in MC is less well understood, in part because the concept is limited to human studies and cannot be further explored in NHPs. In a study that compared attempted, imagined, and observed movements, it was found that MC represented attempted movements the strongest, followed by imagined, with observed actions evoking the least response (Park et al., 2015; Rastogi et al., 2020; Vargas-Irwin et al., 2018). Thus, it is possible that if we were able to use overt reaches in this paradigm, we would see an even stronger representation of a reach vector.

One surprise was the presence of any neurons that coded a gaze vector during saccades. In Chapter 2, we showed that eye movements can be detected in the population responses of MC, and here we demonstrate that these signals are in fact spatially tuned for the eyes. One limitation of the current study that makes this difficult to fully interpret is that head position was not fixed throughout the task.

Thus, it could be the case that these signals are driven by slight head movements that correspond to the direction of the participants' saccades. This explanation is important to consider, as while there is little evidence across the literature for control of eye movements in MC, there is substantial evidence of signals in MC for the control of the head and face. That said, the finding of a small group of neurons in this region of MC is consistent across two participants and two different task types (both the presently discussed paradigm as well as thar from Chapter 2), suggesting there is more to be explored for how gaze position is coded in MC.

Conclusions

Much of our access to the human brain is limited to measures of large populations of neurons. The results in this study show that the observation of similar representations in different neural populations can demonstrate very different patterns of single neuron activity. This may explain some of the differences seen between NHP and human results, as while at the population level it was difficult to detect any preference for a particular coordinate frame, these preferences became clearer in the single neuron responses. Future work is needed to evaluate how the overlap of these neurons within a population is utilized for both simultaneous movements of the hands and the eyes, as well as coordinating the eyes with other effectors.

4.4 Methods

Study participants

Data for this study was collected from participant RD, a right-handed 35-year old male with a C3-C4 spinal cord injury (approximately 10 years before enrollment). The procedures in this study were approved by review boards of California Institute of Technology, Casa Colina Hospital and Centers for Healthcare, and University of California, Los Angeles.

Implant Locations

Participant RD had four 64-channel NeuroPort Utah electrode arrays implanted in his left hemisphere in six months before data collection for this study began. One array was placed in the left superior parietal lobule (RD-SPL). One array was placed in the supramarginal gyrus (RD-SMG). Finally, two arrays were placed within the hand knob of left precentral gyrus, with one relatively more lateral and the other more medial (RD-MCL and RD-MCM respectively). A presurgical fMRI was used to identify brain regions active during a grasping imagery task to serve as a functional guide to our target implant location.

Neural signal recording and preprocessing

Neural signals were recorded from the implanted microelectrode arrays. These signals were then amplified, bandpass filtered and digitized (0.3 Hz–7.5 kHz, and 30 kHz, 16 bits/sample respectively) (NeuroPort Neural Signal Processors, Blackrock Microsystems Inc.). The signal was then high pass filtered at 250 Hz and thresholded at -3.5 times the root-mean square voltage in order to detect spikes.This was done for each electrode. Single neurons were then identified using the k-medoids clustering method and the total number of waveforms was determined by the gap criteria. This was done for the first $n \in \{2, 3, 4\}$ principal components, (n was selected to account for 95% of waveform variance). Neurons that had an average firing rate of less than 0.25 Hz across an entire task were considered noise and excluded.

For single unit gradients during each phase, behavioral epochs were defined as 1000ms starting 300ms after the onset of the phase. This was defined by the hand and gaze position appearing on screen for the first phase, the target appearing on screen for the second phase, and the go cue being given for the final phase.

Behavioral Tasks

Two behavioral tasks were used, a delayed reaching task and a delayed saccade task. For both, the participant sat in front of an LED monitor that displayed instructed positions for the hand and gaze. A white hand icon and blue fixation point were placed in one of four possible locations all at the same vertical location on the screen. First, the participant imagined the position their hands at the location indicated and fixed their gaze on the fixation point. He maintained this initial set up position until a go cue was given after 2s. Before the go cue was given, a target appeared on the screen at one of four locations above the hand and gaze positions.

Then, 1.5s after the target appeared, the go cue was shown. This is where the two tasks differed. In the reach version of the task, the participant was instructed to imagine reaching to the target with their right arm. During the imagined reach, he was to maintain gaze fixation. Imagined reaches were used because RD was not able to overtly reach due to their injuries. During the saccade task, he was instructed to saccade to the target and maintain their initial imagined hand position. The participant was able to move his eyes, and so overt movements were used for this task.

The four hand, gaze, and target positions yield 64 possible layouts. Each position combination was repeated six times across three runs for each session of the two tasks. Both versions of the task were run within the same study session, for three total study sessions. As each run of the task lasts approximately 10-12 minutes, each session is equivalent to approximately one hour of task-related neural recordings from each array.

Eye Tracking and Fixation-break triggered trial cancellations

Eye tracking data was obtained using a Tobii Eye Tracker 5. During the delayed reach task, any fixation break would trigger a cancellation of that trial and the trial would be repeated again later in

the task. This ensured that the participant had the correct gaze position during the task and did not saccade to the target during their reach. For the delayed saccade task fixation breaks before the go cue would trigger the end of a trial, but in this case saccading during the go was not penalized as a canceled trial.

Single unit significance

As a first means of quantifying the population tuning across hand, gaze, and target position, an n-way anova was performed on time windows of 100ms throughout the task. In addition, significant responses for hand relative to gaze, gaze relative to target, and hand relative to target positions are also considered (relative vector calculated by subtracting one position from the other). P-values were corrected for multiple comparisons before a threshold of 0.05 was used to determine whether a neuron was significantly tuned. The mean percentage of the population that was tuned was plotted with confidence intervals, both calculated from the empirical cdf (MATLAB ecdf).

Gradient analysis for determining population vector coded through time

To determine the degree to which the different position variables (hand, gaze, and target) influence neural firing rates, a gradient analysis was performed (Bremner & Andersen, 2014). This was done to assess three pairs of relative coding: hand relative to gaze (hand-gaze vector), gaze relative to target (gaze-target vector), and hand relative to target (hand-target vector). To assess the impact of two position variables at a time, neural responses were gathered into matrices where two position variables changed and the other was held constant. In other words, we created 4x4 matrices of mean firing rates for all combinations of two position variables, averaging across all trials and the third non-varied position. The gradient was then calculated using MATLAB's gradient function yielding a resultant angle and length that can be used to quantify the modulation by each position variable and its strength respectively In order to account for symmetrical responses, each angle is doubled in order to prevent

instances of perfectly opposing resultants from summing to zero. Additionally, vector magnitudes were normalized. In order to assess the population vector through the different phases of the task, we performed this analysis on sliding windows across the task as in Bremner and Andersen 2014. These resultant angles and vector magnitudes were then summed across all neurons and divided by the total number of neurons to find the average vector coded by the population.

Determining single neuron vector coding

In order to assess the vector coding of single neurons, the gradient analysis described above was done for 1 second windows during each phase of the task. A neuron was considered to be tuned to a variable pair if the resultant length was significantly greater than that for a randomized matrix. The tuning and resultant angles yielded from the gradient analysis are not sufficient to fully categorize a neuron as vector coding. Prior work has used singular value decomposition (SVD) to determine whether a neuron is vector coding or gain-modulated. SVD can be used to assess the separability of the impact of position in a variable pair on a neuron's firing rate. If a neuron is vector coding for a certain pair of variables, the matrix of weighted sums resulting from the SVD will reveal that multiple values are needed in order to describe that neuron’s response to each variable, and thus is inseparable for that .

In order for a neuron to be classified as a vector coding neuron for a certain variable pair, it had to meet five criteria: 1) significant tuning to that pair , 2) inseparable result from SVD analysis for that pair, and 3-5) the correct resultant angles for each matrix gradient (within a margin of 60 degrees. This is based on criteria used by Bremner 2012 to identify vector coding neurons. This was done for the angles found during the 1 s time bins for each of the three task phases.

Author contributions

K.K., J.G., and R.A.A. designed the study. K.K. J.G. developed the experimental tasks. K.K. and J.G. analyzed the results. K.K., J.G., and R.A.A. interpreted the results. K.P. coordinated regulatory requirements of clinical trials. A.B. performed the surgery to implant the recording arrays

Supplemental Figures

Supplemental Figure 4.1. Distribution of resultant angles for each variable pair across tuned single neurons during each phase of the task.
Histograms showing resultant angles for significantly tuned neurons for each variable pair (top: H-G, middle: G-T, bottom: H-T) during each phase (left: Cue Hand Eye, middle: Cue Target, right: Go). A: Resultants for RD-SPL during reaches. B: Resultants for RD-SPL during saccades. C: RD-SMG reaches. D: RD-SMG saccades

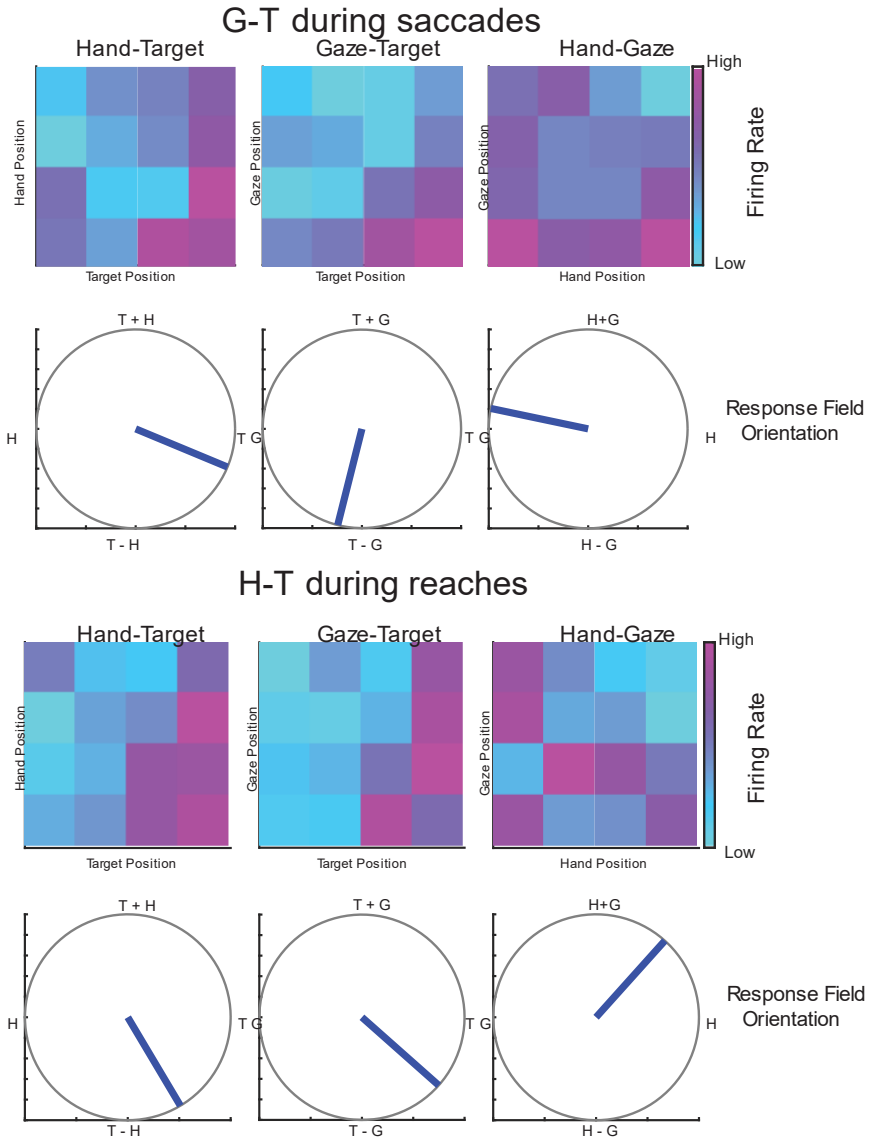

Supplemental Figure 4.2. Response fields for the second neuron in RD-SPL that switched vector coding between tasks. Top: Response field showing gaze-target coding during saccades, bottom: response field of the same neuron showing hand-target coding during imagined reaches.

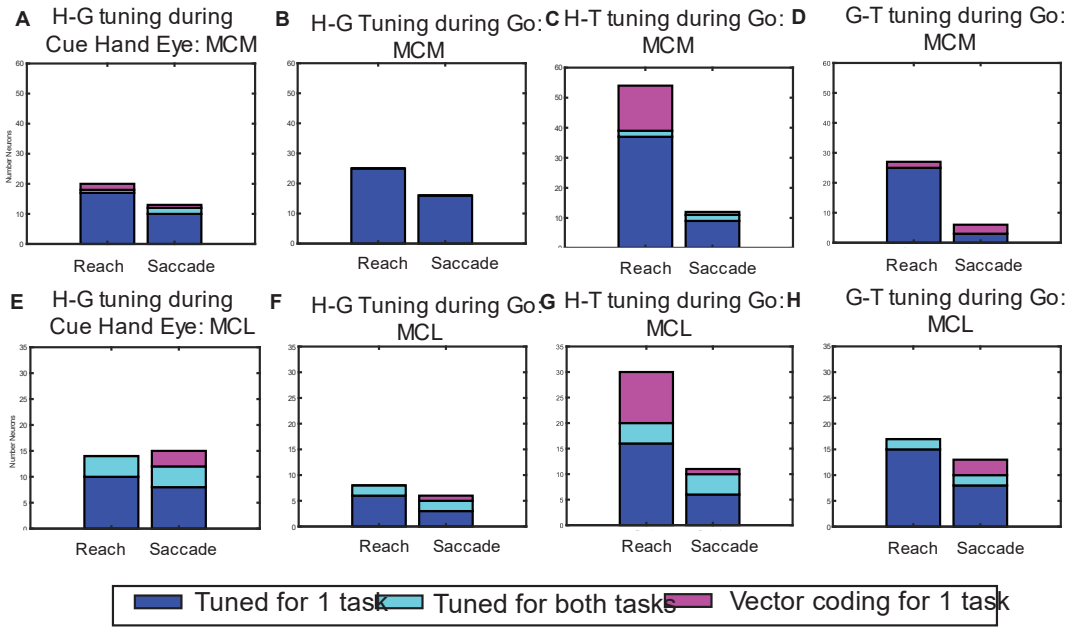

Supplemental Figure 4.3Tuning for MC neurons
Number of neurons significantly tuned to each variable pair during its relevant phase . Significant neurons are divided into tuned during 1 task only (dark blue), tuned for both task (light blue), and vector coding (pink, only existed for one task only). Results for reaches on left bar , saccades on right bar. A-D: RD-MCM, A: Tuning to H-G variable pair during Go , B: Tuning to H-G variable pair during Go, C: Tuning to H-T during Go, D: tuning to G-T during Go. E-H, RD-MCL, E: Number of neurons that coded H-G variable during the cue phase of each task F: Number of neurons that coded a vector during Go .

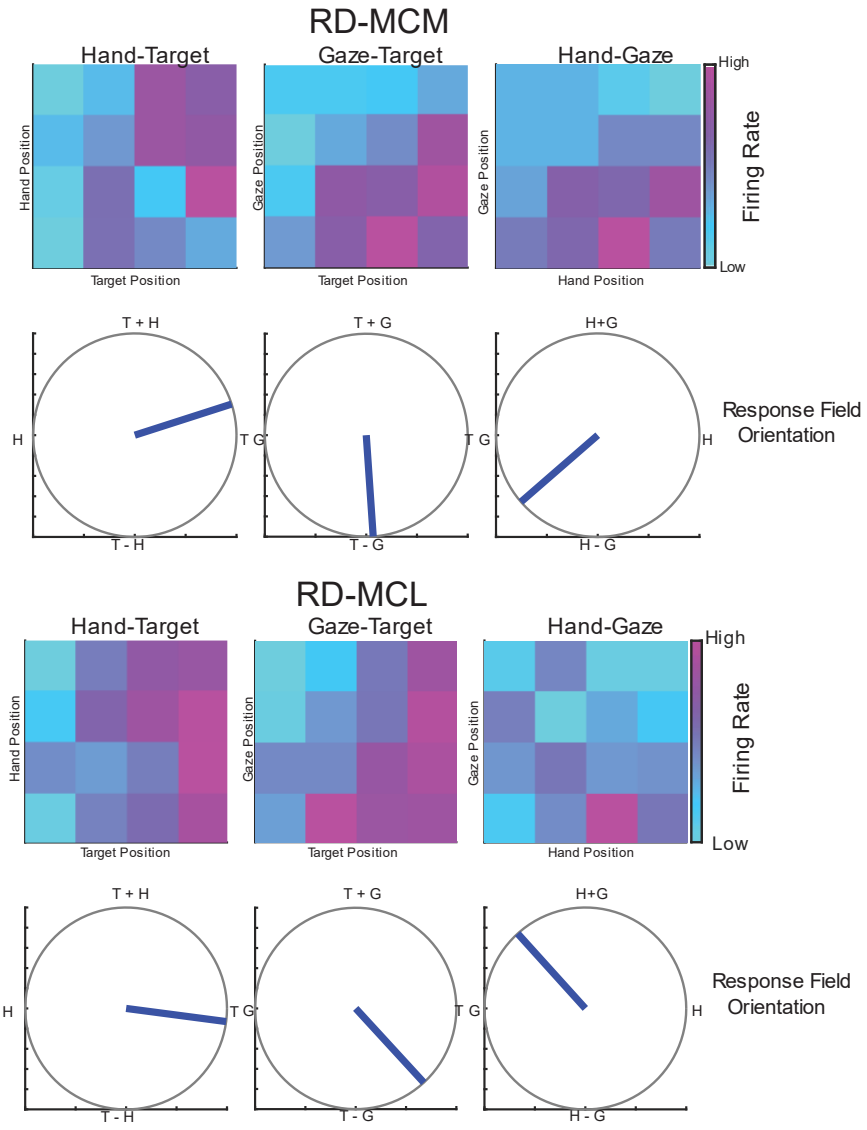

Supplemental Figure 4.4. Examples of neurons coding gaze -target vector during saccades in MC . Top: Response field for neuron in RD -MCM that codes a gaze-target vector during saccades. Bottom: Response field for neuron in RD-MCL that codes a gaze-target vector during saccades .

Chapter 5

CONCLUSION

Summary

The studies covered in this thesis contribute to our growing understanding of the organization and representation of motor variables in human motor cortex and posterior parietal cortex. The complexity seen in these results illustrate why this has been a topic of debate for decades. The following sections will discuss the implications of these results in the context of larger topics in neuroscience research as well as suggestions for future directions both for scientific investigation and BMI advancement.

Complexity vs Topography in high vs low level motor areas

One of the motivations for the studies presented in this thesis was the growing evidence that small neural populations can occupy complex and high dimensional representation spaces. Although there has previously been an emphasis on how the activity of large neural populations can be summarized by a low-dimensional response space (e.g. L. Chang & Tsao, 2017; Cunningham & Yu, 2014), many of these studies have also utilized simple tasks that are themselves limited in dimensionality. As researchers have been able to implement more complex tasks and even examine natural/non-task driven behavior, they have observed that many processes recruit brain areas across the entirety of cortex (Gao & Ganguli, 2015; Musall et al., 2019; Stringer et al., 2019). This has led to a reevaluation of cortical maps from across the field, and blurred the distinction in functional roles of each area (Hayden, 2023).

Motor cortex and posterior parietal cortex are two such areas for which the functional organization has been called into question. Work over the last decade in the Andersen lab has demonstrated a wide

variety of variables that can be decoded from human PPC within patches previously thought to be largely important for hand movements (T. Aflalo et al., 2020; Wandelt et al., 2024; Zhang et al., 2017). Although these findings have held some surprises, they support a more classic view that PPC plays a higher-level role in motor control than primary motor areas and thus represents more cognitive attributes of movements, further supported by its anatomical connections. However, recent investigations of neurons in the hand knob of MC also revealed a similar repertoire of unexpected responses, bringing into question whether it is correct to consider PPC and MC high and low level respectively (Gordon et al., 2023; Willett et al., 2020). If this assessment of each area is appropriate, the expectation would be for more complexity in PPC and more redundancy in MC. By directly comparing between the two areas across different movement contexts, the results in this thesis provide novel insights into this assessment.

For one, the pattern of full body representation found in each area was distinct and followed the expectation that effector specialization would be more prominent in MC than PPC reflecting lower-level coding in MC. The majority of responses in MC were restricted to a single limb in agreement with a broad somatotopic organization across cortex. Although the effectors in this study did not include multiple fingers from the same hand, it is also notable that another recent study in the lab from one of the participants included in this thesis (JJ) found strong tuning across all five digits, in line with expectations from a hand specific area (Guan et al., 2023).

In contrast to the relatively predictable nature of most responses seen in our MC arrays, the responses in PPC showed a higher level of complexity. Although higher cognitive than MC, the results support placing PPC as an intermediate stage relative to the prefrontal cortex as representations are not fully abstracted to goal as one would expect from an area like the prefrontal cortex. The studies presented here demonstrate this in the context of movement and sensorimotor integration, but it should be

emphasized that alongside these results, other findings from the lab including some from the participants in this thesis have only further illustrated the variety of functions found in PPC (T. Aflalo et al., 2020; Guan et al., 2023; Zhang et al., 2017). Although the scope of representations that will be found in PPC has yet to be seen, the label of associative holds accurate.

Complexity in humans vs NHPs

Much of our expectations for the organization of motor areas of human cortex has come from studies in NHPs. A natural question is whether the complexity seen in both MC and PPC is unique to humans or extends to NHPs. First, it should be noted that the answer could vary substantially for each area. Anatomically, the MC of humans and NHPs is much more analogous than the PPC, although both are more extensive and more segmented in humans (Kastner et al., 2017; Meier et al., 2008a).

One possible answer is that humans have more complex organization of motor areas because our motor repertoire is more extensive than that of NHPs (Graziano & Aflalo, 2007). One of the principles in neuroscience that contributed to the acceptance of a somatotopic organization was the finding that in the brain "like attracts like". This is to say that neurons that are close in physical location are similar in function. Thus, as our behaviors became more complex, and we also began to move effectors together in ways we previously did not, we created a new functional demand that was met by more overlapping effector representations. This could especially be true for PPC, which is heavily implicated in tool use and even speech and semantics, all of which are much more relevant to humans than NHPs. The growth of the parietal bone is associated with the time in our evolution when our intelligence began to diverge from our primate ancestors, and perhaps as its surface area expanded so did its function (Bruner et al., 2023).

It may also be that the complexity seen in humans results from the use of more complex and high dimensional tasks (Elsayed & Cunningham, 2017; Gao & Ganguli, 2015). In animals, training can limit the variables tested by a single assay and artificially simplify a neural response space. One way this has been addressed is to record the non-task related behaviors the animal does such as spontaneous movements. In rodents, these non-task related behaviors showed much more widespread cortical activation than movements for task-instructed behaviors, suggesting a limitation in comparing tasks with natural behaviors (Musall et al., 2019). As discussed throughout Chapters 2, 3, and 4, there is also some possibility that we have yet to identify the correct analogous effector specialized regions in humans. Our access to cortical mapping in humans is more limited than animal models, and as we continue to investigate, it may be we uncover even more subregions within the motor areas.

Understanding whether overlapping effector representations are a feature of human cortex or preserved across other species can provide evolutionary insights into the functional basis and organization of these cortical areas. For example, if humans show more complex overlapping effector representations than other animals, this is perhaps driven by the increased behavioral repertoire of humans and thus suggest an ethological organization. However, if more overlapping representations are seen across species, this could be a somatotopic structure that originated from our quadrupedal ancestors with greater overlap in effector functions (or even further back to those without limbs), and was simply built upon as new functions for these effectors were evolved. It is not unlikely that the answer includes both hypotheses.

Interpreting overlapping representations in the context of cortical remapping

The debate over how motor areas of cortex are organized has been accompanied by differing views on the extent to which reorganization is possible in cases where functional importance of effectors

changes. For example, does the body map seen in people who lose their arms reflect repurposing of regions previously used to control the hands to instead control the remaining effectors like the mouth or feet? If this is the case, the overlap seen in the studies of this thesis could be interpreted as a reflection of cortical reorganization after paralysis. While this interpretation cannot be fully ruled out, it seems unlikely both because most evidence suggests that cortical body maps in primary sensorimotor areas are largely stable by adulthood (Muret & Makin, 2021). Additionally, fMRI work in human M1 has shown overlapping effector representations in motor intact individuals (Gordon et al., 2023; Meier et al., 2008b). This is also true for PPC, with both hand and foot movements activating similar areas (Heed et al., 2016).

Another study from the lab that involved participant NS also demonstrated that years after loss of movements, the biomechanical properties of finger movements were still apparent in their neural representations in PPC (Guan et al., 2022). This preservation is even seen in primary sensorimotor areas as well, as it was found that S1 responded to imagined reaches without any proprioceptive feedback (Jafari et al., 2020). As a final note as to why this interpretation seems unlikely, we found no evidence for representation of the shoulder or head being more emphasized than other effectors in these "hand areas", despite these being the only effectors that can be overtly moved. Nonetheless, more work is needed to truly understand how these overlapping representations are related to naturalistic movements.

BCI work and scientific research are mutually beneficial

In addition to the contributions these studies make to the literature on the organization of motor areas of cortex, the results have important and exciting implications for advancing BMIs for motor applications. Much BMI work has focused on single-effector use cases, largely because of the expectation for body maps as the organizing principle in motor regions. Although evidence for

overlap has existed since the original body maps were proposed, the potential function of this overlapping representation for extending BMI design has only recently begun to be realized, and this has been almost exclusively in motor cortex. The results in this study demonstrate that PPC even more so than MC operates in a way that could be taken advantage of for full-body BMI control. One of the results that I did not discuss extensively in this paper but are especially important to note in the context of the design of clinical trials is that our results are not only reproduced across multiple participants, but also showed stability over five years, which is an important consideration in evaluating potential implant locations.

I would also like to comment on how the unique context of BMI studies allows for advances in our understanding of the brain. My choice to study how different parts of the body are organized in human cortex was first motivated by a mini experiment in a BMI session. A regular BMI session involves decoding neural signals for something called closed loop control (Gilja et al., 2012; Guan et al., 2023). First a linear model is trained to associate neural responses with a particular behavior, for example attempting to move the hand. In closed loop control, these predictions of the linear model are translated real-time into the control a computer cursor, allowing the user to move the cursor with the trained behavior. This paradigm allows for a sort of in-session analysis of the presence or absence of neural signals relating to particular variables of interest. As mentioned, most BMI work has focused on hand and fine digit control, and it is not uncommon to test multiple effectors within these limb groups to evaluate the tuning properties of the area. During this process, in a session with participant JJ, I thought it would be interesting to test whether JJ was able to control the BMI by attempting to move his foot rather than his hand. I was surprised when not only was it possible, but it was not even difficult for JJ. I had learned that the organization of motor areas was a well understood area of neuroscience during my undergraduate courses, and this did not meet my expectations whatsoever. However, as I began to investigate the literature more, I realized how much was still unknown.

Concluding remarks

The results presented in these studies feel as though they are only a view of the tip of the iceberg when it comes to understanding neural encoding of movement in cortex, and in particular how this relates to other cognitive processes. How these overlapping representations of the body relate to learning, coordinated movements, and more cognitive components of movement representation like action goal are all unknown and would provide critical context for understanding the functional roles for this overlapping representation. As we explore these avenues, it is important to continue expanding the behaviors we consider relevant to the neural populations to ensure findings of "simple" vs "complex" neural representations are not simply reflections of our prior expectations.

BIBLIOGRAPHY

Abdollahi, R. O., Jastorff, J., & Orban, G. A. (2013). Common and Segregated Processing of Observed Actions in Human SPL. *Cerebral Cortex*, *23*(11), 2734–2753. https://doi.org/10.1093/cercor/bhs264

Aflalo, T., Chivukula, S., Zhang, C., Rosario, E. R., Pouratian, N., & Andersen, R. A. (2022). *Cognition through internal models: Mirror neurons as one manifestation of a broader mechanism*. https://doi.org/10.1101/2022.09.06.506071

Aflalo, T., Kellis, S., Klaes, C., Lee, B., Shi, Y., Pejsa, K., Shanfield, K., Hayes-Jackson, S., Aisen, M., Heck, C., Liu, C., & Andersen, R. A. (2015). Decoding motor imagery from the posterior parietal cortex of a tetraplegic human. *Science (New York, N.Y.)*, *348*(6237), 906–910. https://doi.org/10.1126/science.aaa5417

Aflalo, T. N., & Graziano, M. S. A. (2006). Possible Origins of the Complex Topographic Organization of Motor Cortex: Reduction of a Multidimensional Space onto a Two-Dimensional Array. *Journal of Neuroscience*, *26*(23), 6288–6297. https://doi.org/10.1523/JNEUROSCI.0768-06.2006

Aflalo, T., Zhang, C., Revechkis, B., Rosario, E., Pouratian, N., & Andersen, R. A. (2022). Implicit mechanisms of intention. *Current Biology*, *32*(9), 2051-2060.e6. https://doi.org/10.1016/j.cub.2022.03.047

Aflalo, T., Zhang, C. Y., Rosario, E. R., Pouratian, N., Orban, G. A., & Andersen, R. A. (2020). A shared neural substrate for action verbs and observed actions in human posterior parietal cortex. *Science Advances*, *6*(43), eabb3984. https://doi.org/10.1126/sciadv.abb3984

Alkadhi, H., Crelier, G. R., Hotz Boendermaker, S., Hepp-Reymond, M. C., & Kollias, S. S. (2002). Somatotopy in the ipsilateral primary motor cortex. *NeuroReport*, *13*(16), 2065–2070. https://doi.org/10.1097/00001756-200211150-00015

Ames, K. C., & Churchland, M. M. (2019). Motor cortex signals for each arm are mixed across hemispheres and neurons yet partitioned within the population response. *ELife*, *8*. https://doi.org/10.7554/eLife.46159

Andersen, R. A., Aflalo, T., & Kellis, S. (2019). From thought to action: The brain-machine interface in posterior parietal cortex. *Proceedings of the National Academy of Sciences of the United States of America*, *116*(52), 26274–26279. https://doi.org/10.1073/pnas.1902276116

Andersen, R. A., Andersen, K. N., Hwang, E. J., & Hauschild, M. (2014). Optic Ataxia: From Balint's Syndrome to the Parietal Reach Region. *Neuron*, *81*(5), 967–983. https://doi.org/10.1016/j.neuron.2014.02.025

Andersen, R. A., & Buneo, C. A. (2002). Intentional Maps in Posterior Parietal Cortex. *Annual Review of Neuroscience*, *25*(1), 189–220. https://doi.org/10.1146/annurev.neuro.25.112701.142922

Andersen, R. A., Essick, G. K., & Siegel, R. M. (1985). Encoding of spatial location by posterior parietal neurons. In *Science* (Vol. 230, Issue 4724, pp. 456–458). https://doi.org/10.1126/science.4048942

Andersen, R. A., Snyder, L. H., Batista, A. P., Buneo, C. A., & Cohen, Y. E. (2007). Posterior Parietal Areas Specialized for Eye Movements (Lip) and Reach (PRR) Using a Common Coordinate Frame. In G. R. Bock & J. A. Goode (Eds.), *Novartis Foundation Symposia* (pp. 109–128). John Wiley & Sons, Ltd. https://doi.org/10.1002/9780470515563.ch7

Andersen, R. A., Snyder, L. H., Bradley, D. C., & Xing, J. (1997). MULTIMODAL REPRESENTATION OF SPACE IN THE POSTERIOR PARIETAL CORTEX AND ITS USE IN PLANNING MOVEMENTS. *Annual Review of Neuroscience*, *20*(1), 303–330. https://doi.org/10.1146/annurev.neuro.20.1.303

Andersen, R. A., Snyder, L. H., Li, C.-S., & Stricanne, B. (1993). Coordinate transformations in the representation of spatial information. *Current Opinion in Neurobiology*, *3*(2), 171–176. https://doi.org/10.1016/0959-4388(93)90206-E

Asanuma, H., & Arnold, A. P. (1975). Noxious effects of excessive currents used for intracortical microstimulation. *Brain Research*, *96*(1), 103–107. https://doi.org/10.1016/0006-8993(75)90579-X

Avillac, M., Denève, S., Olivier, E., Pouget, A., & Duhamel, J.-R. (2005). Reference frames for representing visual and tactile locations in parietal cortex. *Nature Neuroscience*, *8*(7), 941–949. https://doi.org/10.1038/nn1480

Baldwin, M. K. L., Cooke, D. F., Goldring, A. B., & Krubitzer, L. (2018). Representations of fine digit movements in posterior and anterior parietal cortex revealed using long-train intracortical microstimulation in macaque monkeys. *Cerebral Cortex*, *28*(12), 4244–4263. https://doi.org/10.1093/cercor/bhx279

Barash, S., Bracewell, R. M., Fogassi, L., Gnadt, J. W., & Andersen, R. A. (1991). Saccade-related activity in the lateral intraparietal area. I. Temporal properties; comparison with area 7a. *Journal of Neurophysiology*, *66*(3), 1095–1108. https://doi.org/10.1152/jn.1991.66.3.1095

Batista, A. P., Buneo, C. A., Snyder, L. H., & Andersen, R. A. (1999). Reach plans in eye-centered coordinates. *Science*, *285*(5425), 257–260. https://doi.org/10.1126/science.285.5425.257

Beevor, C. E., & Horsley, V. A. H. (1887). VI. A minute analysis (experiments) of the various movements produced by stimulating in the monkey different regions of the cortical centre for the upper limb, as defined by Professor Ferrier. *Philosophical Transactions of the Royal Society of London. (B.)*, *178*, 153–167. https://doi.org/10.1098/rstb.1887.0006

Bernier, P.-M., & Grafton, S. T. (2010). Human Posterior Parietal Cortex Flexibly Determines Reference Frames for Reaching Based on Sensory Context. *Neuron*, *68*(4), 776–788. https://doi.org/10.1016/j.neuron.2010.11.002

Beurze, S. M., de Lange, F. P., Toni, I., & Medendorp, W. P. (2009). Spatial and Effector Processing in the Human Parietofrontal Network for Reaches and Saccades. *Journal of Neurophysiology*, *101*(6), 3053–3062. https://doi.org/10.1152/jn.91194.2008

Binkofski, F., Dohle, C., Posse, S., Stephan, K. M., Hefter, H., Seitz, R. J., & Freund, H. J. (1998). Human anterior intraparietal area subserves prehension. *Neurology*, *50*(5), 1253–1259. https://doi.org/10.1212/WNL.50.5.1253

Bosco, A., Piserchia, V., & Fattori, P. (2017). Multiple Coordinate Systems and Motor Strategies for Reaching Movements When Eye and Hand Are Dissociated in Depth and Direction. *Frontiers in Human Neuroscience*, *11*, 323. https://doi.org/10.3389/fnhum.2017.00323

Bremner, L. R., & Andersen, R. A. (2012). Coding of the Reach Vector in Parietal Area 5d. *Neuron*, *75*(2), 342–351. https://doi.org/10.1016/j.neuron.2012.03.041

Bremner, L. R., & Andersen, R. A. (2014). Temporal analysis of reference frames in parietal cortex area 5d during reach planning. *Journal of Neuroscience*, *34*(15), 5273–5284. https://doi.org/10.1523/JNEUROSCI.2068-13.2014

Brozović, M., Gail, A., & Andersen, R. A. (2007). Gain Mechanisms for Contextually Guided Visuomotor Transformations. *Journal of Neuroscience*, *27*(39), 10588–10596. https://doi.org/10.1523/JNEUROSCI.2685-07.2007

Bruner, E., Battaglia-Mayer, A., & Caminiti, R. (2023). The parietal lobe evolution and the emergence of material culture in the human genus. *Brain Structure and Function*, *228*(1), 145–167. https://doi.org/10.1007/s00429-022-02487-w

Buneo, C. A., & Andersen, R. A. (2006). The posterior parietal cortex: Sensorimotor interface for the planning and online control of visually guided movements. *Neuropsychologia*, *44*(13), 2594–2606. https://doi.org/10.1016/j.neuropsychologia.2005.10.011

Buneo, C. A., Jarvis, M. R., Batista, A. P., & Andersen, R. A. (2002). Direct visuomotor transformations for reaching. *Nature*, *416*(6881), Article 6881. https://doi.org/10.1038/416632a

Caminiti, R., Innocenti, G. M., & Battaglia-Mayer, A. (2015). Organization and evolution of parieto-frontal processing streams in macaque monkeys and humans. *Neuroscience & Biobehavioral Reviews*, *56*, 73–96. https://doi.org/10.1016/j.neubiorev.2015.06.014

Campbell, A. W. (1904). Histological Studies on the Localisation of Cerebral Function. *Journal of Mental Science*, *50*(211), 651–662. https://doi.org/10.1192/bjp.50.211.651

Celsis, P., Boulanouar, K., Doyon, B., Ranjeva, J. P., Berry, I., Nespoulous, J. L., & Chollet, F. (1999). Differential fMRI Responses in the Left Posterior Superior Temporal Gyrus and Left Supramarginal Gyrus to Habituation and Change Detection in Syllables and Tones. *NeuroImage*, *9*(1), 135–144. https://doi.org/10.1006/nimg.1998.0389

Chang, L., & Tsao, D. Y. (2017). The Code for Facial Identity in the Primate Brain. *Cell*, *169*(6), 1013-1028.e14. https://doi.org/10.1016/j.cell.2017.05.011

Chang, S. W. C., Dickinson, A. R., & Snyder, L. H. (2008). *Limb-Specific Representation for Reaching in the Posterior Parietal Cortex*. https://doi.org/10.1523/JNEUROSCI.1442-08.2008

Chang, S. W. C., & Snyder, L. H. (2010). Idiosyncratic and systematic aspects of spatial representations in the macaque parietal cortex. *Proceedings of the National Academy of Sciences*, *107*(17), 7951–7956. https://doi.org/10.1073/pnas.0913209107

Chen, X., DeAngelis, G. C., & Angelaki, D. E. (2018). Flexible egocentric and allocentric representations of heading signals in parietal cortex. *Proceedings of the National Academy of Sciences of the United States of America*, *115*(14), E3305–E3312. https://doi.org/10.1073/pnas.1715625115

Cleret de Langavant, L., Trinkler, I., Cesaro, P., & Bachoud-Lévi, A.-C. (2009). Heterotopagnosia: When I point at parts of your body. *Neuropsychologia*, *47*(7), 1745–1755. https://doi.org/10.1016/j.neuropsychologia.2009.02.016

Cohen, Y. E., & Andersen, R. A. (2002). A common reference frame for movement plans in the posterior parietal cortex. *Nature Reviews Neuroscience*, *3*(7), 553–562. https://doi.org/10.1038/nrn873

Collinger, J. L., Wodlinger, B., Downey, J. E., Wang, W., Tyler-Kabara, E. C., Weber, D. J., McMorland, A. J. C., Velliste, M., Boninger, M. L., & Schwartz, A. B. (2013). High-performance neuroprosthetic control by an individual with tetraplegia. *The Lancet*, *381*(9866), 557–564. https://doi.org/10.1016/S0140-6736(12)61816-9

Corradi-Dell'Acqua, C., Hesse, M. D., Rumiati, R. I., & Fink, G. R. (2008). Where is a Nose with Respect to a Foot? The Left Posterior Parietal Cortex Processes Spatial Relationships

among Body Parts. *Cerebral Cortex*, *18*(12), 2879–2890. https://doi.org/10.1093/cercor/bhn046

Cramer, S. C., Finklestein, S. P., Schaechter, J. D., Bush, G., & Rosen, B. R. (1999). Activation of distinct motor cortex regions during ipsilateral and contralateral finger movements. *Journal of Neurophysiology*, *81*(1), 383–387. https://doi.org/10.1152/JN.1999.81.1.383/ASSET/IMAGES/LARGE/JNP.JA02F1.JPEG

Cui, H., & Andersen, R. A. (2011). Different representations of potential and selected motor plans by distinct parietal areas. *Journal of Neuroscience*, *31*(49), 18130–18136. https://doi.org/10.1523/JNEUROSCI.6247-10.2011

Cunningham, J. P., & Yu, B. M. (2014). Dimensionality reduction for large-scale neural recordings. *Nature Neuroscience*, *17*(11), 1500–1509. https://doi.org/10.1038/nn.3776

Dang, W., Li, S., Pu, S., Qi, X. L., & Constantinidis, C. (2022). More Prominent Nonlinear Mixed Selectivity in the Dorsolateral Prefrontal than Posterior Parietal Cortex. *ENeuro*, *9*(2). https://doi.org/10.1523/ENEURO.0517-21.2022

Donchin, O., Gribova, A., Steinberg, O., Bergman, H., & Vaadia, E. (1998). Primary motor cortex is involved in bimanual coordination. *Nature*, *395*(6699), 274–278. https://doi.org/10.1038/26220

Duhamel, J. R., Goldberg, M. E., Fitzgibbon, E. J., Sirigu, A., & Grafman, J. (1992). Saccadic dysmetria in a patient with a right frontoparietal lesion. The importance of corollary discharge for accurate spatial behaviour. *Brain: A Journal of Neurology*, *115 (Pt 5)*, 1387–1402. https://doi.org/10.1093/brain/115.5.1387

Elsayed, G. F., & Cunningham, J. P. (2017). Structure in neural population recordings: An expected byproduct of simpler phenomena? *Nature Neuroscience*, *20*(9), 1310–1318. https://doi.org/10.1038/nn.4617

Evans, C., Milner, A. D., Humphreys, G. W., & Cavina-Pratesi, C. (2013). Optic ataxia affects the lower limbs: Evidence from a single case study. *Cortex*, *49*(5), 1229–1240. https://doi.org/10.1016/J.CORTEX.2012.07.008

Fetz, E. E., & Cheney, P. D. (1980). Postspike facilitation of forelimb muscle activity by primate corticomotoneuronal cells. *Journal of Neurophysiology*, *44*(4), 751–772. https://doi.org/10.1152/jn.1980.44.4.751

Filimon, F. (2010). Human Cortical Control of Hand Movements: Parietofrontal Networks for Reaching, Grasping, and Pointing. *The Neuroscientist*, *16*(4), 388–407. https://doi.org/10.1177/1073858410375468

Fulton, J. F. (1935). A NOTE ON THE DEFINITION OF THE "MOTOR" AND "PREMOTOR" AREAS. *Brain*, *58*(2), 311–316. https://doi.org/10.1093/brain/58.2.311

Fusi, S., Miller, E. K., & Rigotti, M. (2016). Why neurons mix: High dimensionality for higher cognition. *Current Opinion in Neurobiology*, *37*, 66–74. https://doi.org/10.1016/j.conb.2016.01.010

Gallese, V., Murata, A., Kaseda, M., Niki, N., & Sakata, H. (1994). Deficit of hand preshaping after muscimol injection in monkey parietal cortex. *Neuroreport*, *5*(12), 1525–1529. https://doi.org/10.1097/00001756-199407000-00029

Gao, P., & Ganguli, S. (2015). On simplicity and complexity in the brave new world of large-scale neuroscience. *Current Opinion in Neurobiology*, *32*, 148–155. https://doi.org/10.1016/j.conb.2015.04.003

Georgopoulos, A. P., & Grillner, S. (1989). Visuomotor Coordination in Reaching and Locomotion. *Science*, *245*(4923), 1209–1210. https://doi.org/10.1126/science.2675307

Geyer, S., Ledberg, A., Schleicher, A., Kinomura, S., Schormann, T., Burgel, U., Klingberg, T., Larsson, J., Zilles, K., & Roland, P. E. (1996). Two different areas within the primary motor cortex of man. *Nature*, *382*(6594), 805–807. https://doi.org/10.1038/382805a0

Gilja, V., Nuyujukian, P., Chestek, C. A., Cunningham, J. P., Yu, B. M., Fan, J. M., Churchland, M. M., Kaufman, M. T., Kao, J. C., Ryu, S. I., & Shenoy, K. V. (2012). A high-performance neural prosthesis enabled by control algorithm design. *Nature Neuroscience*, *15*(12), 1752–1757. https://doi.org/10.1038/nn.3265

Gordon, E. M., Chauvin, R. J., Van, A. N., Rajesh, A., Nielsen, A., Newbold, D. J., Lynch, C. J., Seider, N. A., Krimmel, S. R., Scheidter, K. M., Monk, J., Miller, R. L., Metoki, A., Montez, D. F., Zheng, A., Elbau, I., Madison, T., Nishino, T., Myers, M. J., … Dosenbach, N. U. F. (2023). A somato-cognitive action network alternates with effector regions in motor cortex. *Nature*, *617*(7960), Article 7960. https://doi.org/10.1038/s41586-023-05964-2

Graziano, M. S. A. (2019). *Rethinking consciousness: A scientific theory of subjective experience* (First Edition). W.W. Norton & Company.

Graziano, M. S. A., & Aflalo, T. N. (2007). Mapping behavioral repertoire onto the cortex. *Neuron*, *56*(2), 239–251. https://doi.org/10.1016/j.neuron.2007.09.013

Graziano, M. S. A., Aflalo, T. N. S., & Cooke, D. F. (2005). Arm movements evoked by electrical stimulation in the motor cortex of monkeys. *Journal of Neurophysiology*, *94*(6), 4209–4223. https://doi.org/10.1152/jn.01303.2004

Graziano, M. S. A., Taylor, C. S. R., & Moore, T. (2002). Complex Movements Evoked by Microstimulation of Precentral Cortex. *Neuron*, *34*(5), 841–851. https://doi.org/10.1016/S0896-6273(02)00698-0

Gréa, H., Pisella, L., Rossetti, Y., Desmurget, M., Tilikete, C., Grafton, S., Prablanc, C., & Vighetto, A. (2002). A lesion of the posterior parietal cortex disrupts on-line adjustments during aiming movements. *Neuropsychologia*, *40*(13), 2471–2480. https://doi.org/10.1016/s0028-3932(02)00009-x

Grefkes, C., & Fink, G. R. (2005). REVIEW: The functional organization of the intraparietal sulcus in humans and monkeys. *Journal of Anatomy*, *207*(1), 3–17. https://doi.org/10.1111/j.1469-7580.2005.00426.x

Guan, C., Aflalo, T., Kadlec, K., Leon, J. G. de, Rosario, E. R., Bari, A., Pouratian, N., & Andersen, R. A. (2023). Decoding and geometry of ten finger movements in human posterior parietal cortex and motor cortex. *Journal of Neural Engineering*, *20*(3), 036020. https://doi.org/10.1088/1741-2552/acd3b1

Guan, C., Aflalo, T., Zhang, C. Y., Amoruso, E., Rosario, E. R., Pouratian, N., & Andersen, R. A. (2022). Stability of motor representations after paralysis. *ELife*, *11*, e74478. https://doi.org/10.7554/eLife.74478

Hanakawa, T., Parikh, S., Bruno, M. K., & Hallett, M. (2005). Finger and Face Representations in the Ipsilateral Precentral Motor Areas in Humans. *J Neurophysiol*, *93*, 2950–2958. https://doi.org/10.1152/jn.00784.2004

Hayden, B. Y. (2023). The Dangers of Cortical Brain Maps. *Journal of Cognitive Neuroscience*, *35*(3), 372–375. https://doi.org/10.1162/jocn_e_01924

Heed, T., Beurze, S. M., Toni, I., Röder, B., & Medendorp, W. P. (2011). Functional rather than effector-specific organization of human posterior parietal cortex. *Journal of Neuroscience*, *31*(8), 3066–3076. https://doi.org/10.1523/JNEUROSCI.4370-10.2011

Heed, T., Leone, F. T. M., Toni, I., & Medendorp, W. P. (2016). Functional versus effector-specific organization of the human posterior parietal cortex: Revisited. *Journal of Neurophysiology*, *116*(4), 1885–1899. https://doi.org/10.1152/jn.00312.2014

Heming, E. A., Cross, K. P., Takei, T., Cook, D. J., & Scott, S. H. (2019). Independent representations of ipsilateral and contralateral limbs in primary motor cortex. *ELife*, *8*. https://doi.org/10.7554/eLife.48190

Hochberg, L. R., Serruya, M. D., Friehs, G. M., Mukand, J. A., Saleh, M., Caplan, A. H., Branner, A., Chen, D., Penn, R. D., & Donoghue, J. P. (2006). Neuronal ensemble control of prosthetic devices by a human with tetraplegia. *Nature*, *442*(7099), 164–171. https://doi.org/10.1038/nature04970

Hwang, E. J., Hauschild, M., Wilke, M., & Andersen, R. A. (2014). Spatial and Temporal Eye–Hand Coordination Relies on the Parietal Reach Region. *The Journal of Neuroscience*, *34*(38), 12884–12892. https://doi.org/10.1523/JNEUROSCI.3719-13.2014

Jafari, M., Aflalo, T., Chivukula, S., Kellis, S. S., Salas, M. A., Norman, S. L., Pejsa, K., Liu, C. Y., & Andersen, R. A. (2020). The human primary somatosensory cortex encodes imagined movement in the absence of sensory information. *Communications Biology*, *3*(1), 1–7. https://doi.org/10.1038/s42003-020-01484-1

Jain, N., Qi, H.-X., Collins, C. E., & Kaas, J. H. (2008). Large-Scale Reorganization in the Somatosensory Cortex and Thalamus after Sensory Loss in Macaque Monkeys. *The Journal of Neuroscience*, *28*(43), 11042–11060. https://doi.org/10.1523/JNEUROSCI.2334-08.2008

Jakobson, L. S., Archibald, Y. M., Carey, D. P., & Goodale, M. A. (1991). A kinematic analysis of reaching and grasping movements in a patient recovering from optic ataxia. *Neuropsychologia*, *29*(8), 803–809. https://doi.org/10.1016/0028-3932(91)90073-h

Jastorff, J., Begliomini, C., Fabbri-Destro, M., Rizzolatti, G., & Orban, G. A. (2010). Coding observed motor acts: Different organizational principles in the parietal and premotor cortex of humans. *Journal of Neurophysiology*, *104*(1), 128–140. https://doi.org/10.1152/JN.00254.2010/SUPPL_FILE/SUPPDATA.PDF

Jeffrey Johnston, W., Palmer, S. E., & Freedman, D. J. (2020). Nonlinear mixed selectivity supports reliable neural computation. *PLoS Computational Biology*, *16*(2), e1007544. https://doi.org/10.1371/journal.pcbi.1007544

Jensen, M. A., Huang, H., Valencia, G. O., Klassen, B. T., van den Boom, M. A., Kaufmann, T. J., Schalk, G., Brunner, P., Worrell, G. A., Hermes, D., & Miller, K. J. (2023). A motor association area in the depths of the central sulcus. *Nature Neuroscience*, *26*(7), Article 7. https://doi.org/10.1038/s41593-023-01346-z

Kagan, I., Iyer, A., Lindner, A., & Andersen, R. A. (2010). Space representation for eye movements is more contralateral in monkeys than in humans. *Proceedings of the National Academy of Sciences*, *107*(17), 7933–7938. https://doi.org/10.1073/pnas.1002825107

Karnath, H.-O., & Perenin, M.-T. (2005). Cortical Control of Visually Guided Reaching: Evidence from Patients with Optic Ataxia. *Cerebral Cortex*, *15*(10), 1561–1569. https://doi.org/10.1093/cercor/bhi034

Kastner, S., Chen, Q., Jeong, S. K., & Mruczek, R. E. B. (2017). A brief comparative review of primate posterior parietal cortex: A novel hypothesis on the human toolmaker. *Neuropsychologia*, *105*, 123–134. https://doi.org/10.1016/J.NEUROPSYCHOLOGIA.2017.01.034

Konen, C. S., Mruczek, R. E. B., Montoya, J. L., & Kastner, S. (2013). Functional organization of human posterior parietal cortex: Grasping- and reaching-related activations relative to topographically organized cortex. *Journal of Neurophysiology*, *109*(12), 2897–2908. https://doi.org/10.1152/jn.00657.2012

Kwan, H. C., MacKay, W. A., Murphy, J. T., & Wong, Y. C. (1978). Spatial organization of precentral cortex in awake primates. II. Motor outputs. *Journal of Neurophysiology*, *41*(5), 1120–1131. https://doi.org/10.1152/jn.1978.41.5.1120

Leoné, F. T. M., Heed, T., Toni, I., & Pieter Medendorp, W. (2014). Understanding effector selectivity in human posterior parietal cortex by combining information patterns and activation measures. *Journal of Neuroscience*, *34*(21), 7102–7112. https://doi.org/10.1523/JNEUROSCI.5242-13.2014

Leoné, F. T. M., Monaco, S., Henriques, D. Y. P., Toni, I., & Medendorp, W. P. (2015). Flexible Reference Frames for Grasp Planning in Human Parietofrontal Cortex. *ENeuro*, *2*(3). https://doi.org/10.1523/ENEURO.0008-15.2015

Levy, I., Schluppeck, D., Heeger, D. J., & Glimcher, P. W. (2007). Specificity of Human Cortical Areas for Reaches and Saccades. *Journal of Neuroscience*, *27*(17), 4687–4696. https://doi.org/10.1523/JNEUROSCI.0459-07.2007

Leyton, A. S. F., & Sherrington, C. S. (1917). Observations on the Excitable Cortex of the Chimpanzee, Orang-Utan, and Gorilla. *Quarterly Journal of Experimental Physiology*, *11*(2), 135–222. https://doi.org/10.1113/expphysiol.1917.sp000240

Li, K., & Malhotra, P. A. (2015). Spatial neglect. *Practical Neurology*, *15*(5), 333–339. https://doi.org/10.1136/practneurol-2015-001115

Liu, Y., Caracoglia, J., Sen, S., Erez Freud, ·, & Striem-Amit, E. (2022). Are reaching and grasping effector-independent? Similarities and differences in reaching and grasping kinematics between the hand and foot. *Experimental Brain Research*, *240*, 1833–1848. https://doi.org/10.1007/s00221-022-06359-x

Lotze, M., Montoya, P., Erb, M., Hülsmann, E., Flor, H., Klose, U., Birbaumer, N., & Grodd, W. (1999). Activation of cortical and cerebellar motor areas during executed and imagined hand movements: An fMRI study. *Journal of Cognitive Neuroscience*, *11*(5), 491–501. https://doi.org/10.1162/089892999563553

Luo, L. (2016). *Principles of Neurobiology*. Garland Science, Taylor, & Francis Group, LLC.

Makin, T. R., & Bensmaia, S. J. (2017). Stability of Sensory Topographies in Adult Cortex. *Trends in Cognitive Sciences*, *21*(3), 195–204. https://doi.org/10.1016/j.tics.2017.01.002

Matelli, M., Luppino, G., & Rizzolatti, G. (1985). Patterns of cytochrome oxidase activity in the frontal agranular cortex of the macaque monkey. *Behavioural Brain Research*, *18*(2), 125–136. https://doi.org/10.1016/0166-4328(85)90068-3

Mcfadyen, J. R., Heider, B., Karkhanis, A. N., Cloherty, S. L., Muñoz, F., Siegel, R. M., & Morris, A. P. (2022). *Robust Coding of Eye Position in Posterior Parietal Cortex despite Context-Dependent Tuning*. https://doi.org/10.1523/JNEUROSCI.0674-21.2022

McGuire, L. M. M., & Sabes, P. N. (2011). Heterogeneous representations in the superior parietal lobule are common across reaches to visual and proprioceptive targets. *The Journal of Neuroscience: The Official Journal of the Society for Neuroscience*, *31*(18), 6661–6673. https://doi.org/10.1523/JNEUROSCI.2921-10.2011

Medendorp, W. P., & Heed, T. (2019). State estimation in posterior parietal cortex: Distinct poles of environmental and bodily states. *Progress in Neurobiology*, *183*. https://doi.org/10.1016/j.pneurobio.2019.101691

Medina, J., Kannan, V., Pawlak, M. A., Kleinman, J. T., Newhart, M., Davis, C., Heidler-Gary, J. E., Herskovits, E. H., & Hillis, A. E. (2009). Neural Substrates of Visuospatial Processing in Distinct Reference Frames: Evidence from Unilateral Spatial Neglect. *Journal of Cognitive Neuroscience*, *21*(11), 2073–2084. https://doi.org/10.1162/jocn.2008.21160

Meier, J. D., Aflalo, T. N., Kastner, S., & Graziano, M. S. A. (2008a). Complex organization of human primary motor cortex: A high-resolution fMRI study. *Journal of Neurophysiology*, *100*(4), 1800–1812. https://doi.org/10.1152/jn.90531.2008

Meier, J. D., Aflalo, T. N., Kastner, S., & Graziano, M. S. A. (2008b). Complex organization of human primary motor cortex: A high-resolution fMRI study. *Journal of Neurophysiology*, *100*(4), 1800–1812. https://doi.org/10.1152/jn.90531.2008

Miller, K. J., Schalk, G., Fetz, E. E., Den Nijs, M., Ojemann, J. G., & Rao, R. P. N. (2010). Cortical activity during motor execution, motor imagery, and imagery-based online

feedback. *Proceedings of the National Academy of Sciences of the United States of America*, *107*(9), 4430–4435. https://doi.org/10.1073/pnas.0913697107

Milner, A. D., & Goodale, M. A. (2008). Two visual systems re-viewed. *Neuropsychologia*, *46*(3), 774–785. https://doi.org/10.1016/j.neuropsychologia.2007.10.005

Mooshagian, E., Yttri, E. A., Loewy, A. D., & Snyder, L. H. (2022). Contralateral Limb Specificity for Movement Preparation in the Parietal Reach Region. *The Journal of Neuroscience*, *42*(9), 1692–1701. https://doi.org/10.1523/JNEUROSCI.0232-21.2021

Mullette-Gillman, O. A., Cohen, Y. E., & Groh, J. M. (2005). Eye-Centered, Head-Centered, and Complex Coding of Visual and Auditory Targets in the Intraparietal Sulcus. *Journal of Neurophysiology*, *94*(4), 2331–2352. https://doi.org/10.1152/jn.00021.2005

Mullette-Gillman, O. A., Cohen, Y. E., & Groh, J. M. (2009). Motor-Related Signals in the Intraparietal Cortex Encode Locations in a Hybrid, rather than Eye-Centered Reference Frame. *Cerebral Cortex*, *19*(8), 1761–1775. https://doi.org/10.1093/cercor/bhn207

Muret, D., & Makin, T. R. (2021). The homeostatic homunculus: Rethinking deprivation-triggered reorganisation. *Current Opinion in Neurobiology*, *67*, 115–122. https://doi.org/10.1016/J.CONB.2020.08.008

Musall, S., Kaufman, M. T., Juavinett, A. L., Gluf, S., & Churchland, A. K. (2019). Single-trial neural dynamics are dominated by richly varied movements. *Nature Neuroscience*, *22*(10), 1677–1686. https://doi.org/10.1038/s41593-019-0502-4

Park, C. hyun, Chang, W. H., Lee, M., Kwon, G. H., Kim, L., Kim, S. T., & Kim, Y. H. (2015). Which motor cortical region best predicts imagined movement? *NeuroImage*, *113*, 101–110. https://doi.org/10.1016/j.neuroimage.2015.03.033

Park, M. C., Belhaj-Saif, A., Gordon, M., & Cheney, P. D. (2001). Consistent Features in the Forelimb Representation of Primary Motor Cortex in Rhesus Macaques. *Journal of Neuroscience*, *21*(8), 2784–2792. https://doi.org/10.1523/JNEUROSCI.21-08-02784.2001

Penfield, W., & Boldrey, E. (1937). Somatic motor and sensory representation in the cerebral cortex of man as studied by electrical stimulation. *Brain*, *60*(4), 389–443. https://doi.org/10.1093/brain/60.4.389

PERENIN, M.-T., & VIGHETTO, A. (1988). OPTIC ATAXIA: A SPECIFIC DISRUPTION IN VISUOMOTOR MECHANISMS: I. DIFFERENT ASPECTS OF THE DEFICIT IN REACHING FOR OBJECTS. *Brain*, *111*(3), 643–674. https://doi.org/10.1093/brain/111.3.643

Pesaran, B., Nelson, M. J., & Andersen, R. A. (2010). A relative position code for saccades in dorsal premotor cortex. *Journal of Neuroscience*, *30*(19), 6527–6537. https://doi.org/10.1523/JNEUROSCI.1625-09.2010

Pons, T. P., Garraghty, P. E., Ommaya, A. K., Kaas, J. H., Taub, E., & Mishkin, M. (1991). Massive cortical reorganization after sensory deafferentation in adult macaques. *Science (New York, N.Y.)*, *252*(5014), 1857–1860. https://doi.org/10.1126/science.1843843

Pouget, A., & Snyder, L. H. (2000). Computational approaches to sensorimotor transformations. *Nature Neuroscience*, *3*(11), 1192–1198. https://doi.org/10.1038/81469

Premereur, E., Janssen, X. P., & Wim Vanduffel, X. (2015). *Behavioral/Cognitive Effector Specificity in Macaque Frontal and Parietal Cortex*. https://doi.org/10.1523/JNEUROSCI.3710-14.2015

Purves, D., Augustine, G. J., Fitzpatrick, D., Katz, L. C., LaMantia, A.-S., McNamara, J. O., & Williams, S. M. (2001). Lesions of the Parietal Association Cortex: Deficits of Attention. In *Neuroscience. 2nd edition*. Sinauer Associates. https://www.ncbi.nlm.nih.gov/books/NBK10998/

Rastogi, A., Vargas-Irwin, C. E., Willett, F. R., Abreu, J., Crowder, D. C., Murphy, B. A., Memberg, W. D., Miller, J. P., Sweet, J. A., Walter, B. L., Cash, S. S., Rezaii, P. G., Franco, B., Saab, J., Stavisky, S. D., Shenoy, K. V., Henderson, J. M., Hochberg, L. R., Kirsch, R. F., & Ajiboye, A. B. (2020). Neural Representation of Observed, Imagined, and Attempted Grasping Force in Motor Cortex of Individuals with Chronic Tetraplegia. *Scientific Reports*, *10*(1). https://doi.org/10.1038/s41598-020-58097-1

Rathelot, J. A., & Strick, P. L. (2006). Muscle representation in the macaque motor cortex: An anatomical perspective. *Proceedings of the National Academy of Sciences of the United States of America*, *103*(21), 8257–8262. https://doi.org/10.1073/pnas.0602933103

Rathelot, J. A., & Strick, P. L. (2009). Subdivisions of primary motor cortex based on cortico-motoneuronal cells. *Proceedings of the National Academy of Sciences of the United States of America*, *106*(3), 918–923. https://doi.org/10.1073/pnas.0808362106

Razmus, M. (2017). Body representation in patients after vascular brain injuries. *Cognitive Processing*, *18*(4), 359–373. https://doi.org/10.1007/s10339-017-0831-8

Rigotti, M., Barak, O., Warden, M. R., Wang, X. J., Daw, N. D., Miller, E. K., & Fusi, S. (2013). The importance of mixed selectivity in complex cognitive tasks. *Nature*, *497*(7451), 585–590. https://doi.org/10.1038/nature12160

Rijntjes, M., Dettmers, C., Büchel, C., Kiebel, S., Frackowiak, R. S. J., & Weiller, C. (1999). A Blueprint for Movement: Functional and Anatomical Representations in the Human

Motor System. *The Journal of Neuroscience*, *19*(18), 8043–8048. https://doi.org/10.1523/JNEUROSCI.19-18-08043.1999

Sadtler, P. T., Quick, K. M., Golub, M. D., Chase, S. M., Ryu, S. I., Tyler-Kabara, E. C., Yu, B. M., & Batista, A. P. (2014). Neural constraints on learning. *Nature*, *512*(7515), 423–426. https://doi.org/10.1038/nature13665

Sanes, J. N., Donoghue, J. P., Thangaraj, V., Edelman, R. R., & Warach, S. (1995). Shared Neural Substrates Controlling Hand Movements in Human Motor Cortex. *Science*, *268*(5218), 1775–1777.

Schieber, M. H. (2001). Constraints on Somatotopic Organization in the Primary Motor Cortex. *Journal of Neurophysiology*, *86*(5), 2125–2143. https://doi.org/10.1152/jn.2001.86.5.2125

Schieber, M. H., & Hibbard, L. S. (1993). How somatotopic is the motor cortex hand area? *Science*, *261*(5120), 489–492. https://doi.org/10.1126/science.8332915

Schmitzer-Torbert, N., Jackson, J., Henze, D., Harris, K., & Redish, A. D. (2005). Quantitative measures of cluster quality for use in extracellular recordings. *Neuroscience*, *131*(1), 1–11. https://doi.org/10.1016/j.neuroscience.2004.09.066

Schwartz, A. B. (2016). Movement: How the Brain Communicates with the World. *Cell*, *164*(6), 1122–1135. https://doi.org/10.1016/j.cell.2016.02.038

Scott, S. H. (2008). Inconvenient Truths about neural processing in primary motor cortex. *Journal of Physiology*, *586*(5), 1217–1224. https://doi.org/10.1113/jphysiol.2007.146068

Seelke, A. M. H., Padberg, J. J., Disbrow, E., Purnell, S. M., Recanzone, G., & Krubitzer, L. (2012). Topographic Maps within Brodmann's Area 5 of Macaque Monkeys. *Cerebral Cortex*, *22*(8), 1834–1850. https://doi.org/10.1093/cercor/bhr257

Snyder, L. H., Grieve, K. L., Brotchie, P., & Andersen, R. A. (1998). Separate body- and world-referenced representations of visual space in parietal cortex. *Nature*, *394*(6696), 887–891. https://doi.org/10.1038/29777

Steinberg, O., Donchin, O., Gribova, A., Cardoso de Oliveira, S., Bergman, H., & Vaadia, E. (2002). Neuronal populations in primary motor cortex encode bimanual arm movements. *European Journal of Neuroscience*, *15*(8), 1371–1380. https://doi.org/10.1046/j.1460-9568.2002.01968.x

Striem-Amit, E., Vannuscorps, G., & Caramazza, A. (2018). Plasticity based on compensatory effector use in the association but not primary sensorimotor cortex of people born without hands. *Proceedings of the National Academy of Sciences of the United States of America*, *115*(30), 7801–7806. https://doi.org/10.1073/pnas.1803926115

Stringer, C., Pachitariu, M., Steinmetz, N., Reddy, C. B., Carandini, M., & Harris, K. D. (2019). Spontaneous behaviors drive multidimensional, brainwide activity. *Science*, *364*(6437), eaav7893. https://doi.org/10.1126/science.aav7893

Taghizadeh, B., Fortmann, O., & Gail, A. (2024). Position- and scale-invariant object-centered spatial localization in monkey frontoparietal cortex dynamically adapts to cognitive demand. *Nature Communications*, *15*, 3357. https://doi.org/10.1038/s41467-024-47554-4

Thier, P., & Andersen, R. A. (1998). Electrical Microstimulation Distinguishes Distinct Saccade-Related Areas in the Posterior Parietal Cortex. *Journal of Neurophysiology*, *80*(4), 1713–1735. https://doi.org/10.1152/jn.1998.80.4.1713

Tibshirani, R., Walther, G., & Hastie, T. (2001). Estimating the Number of Clusters in a Data Set Via the Gap Statistic. *Journal of the Royal Statistical Society Series B: Statistical Methodology*, *63*(2), 411–423. https://doi.org/10.1111/1467-9868.00293

Vallar, G., & Perani, D. (1986). The anatomy of unilateral neglect after right-hemisphere stroke lesions. A clinical/CT-scan correlation study in man. *Neuropsychologia*, *24*(5), 609–622. https://doi.org/10.1016/0028-3932(86)90001-1

Vargas-Irwin, C. E., Feldman, J. M., King, B., Simeral, J. D., Sorice, B. L., Oakley, E. M., Cash, S. S., Eskandar, E. N., Friehs, G. M., Hochberg, L. R., & Donoghue, J. P. (2018). Watch, imagine, attempt: Motor cortex single-unit activity reveals context-dependent movement encoding in humans with tetraplegia. *Frontiers in Human Neuroscience*, *12*. https://doi.org/10.3389/fnhum.2018.00450

Vingerhoets, G. (2014). Contribution of the posterior parietal cortex in reaching, grasping, and using objects and tools. *Frontiers in Psychology*, *5*. https://doi.org/10.3389/fpsyg.2014.00151

Wandelt, S. K., Bjånes, D. A., Pejsa, K., Lee, B., Liu, C., & Andersen, R. A. (2024). Representation of internal speech by single neurons in human supramarginal gyrus. *Nature Human Behaviour*, 1–14. https://doi.org/10.1038/s41562-024-01867-y

Wandelt, S. K., Kellis, S., Bjånes, D. A., Pejsa, K., Lee, B., Liu, C., & Andersen, R. A. (2022). Decoding grasp and speech signals from the cortical grasp circuit in a tetraplegic human. *Neuron*, *110*(11), 1777-1787.e3. https://doi.org/10.1016/j.neuron.2022.03.009

Wardak, C., Olivier, E., & Duhamel, J.-R. (2002). Saccadic Target Selection Deficits after Lateral Intraparietal Area Inactivation in Monkeys. *The Journal of Neuroscience*, *22*(22), 9877–9884. https://doi.org/10.1523/JNEUROSCI.22-22-09877.2002

Wilke, M., Kagan, I., & Andersen, R. A. (2012). Functional imaging reveals rapid reorganization of cortical activity after parietal inactivation in monkeys. *Proceedings of the National Academy of Sciences*, *109*(21), 8274–8279. https://doi.org/10.1073/pnas.1204789109

Willett, F. R., Deo, D. R., Avansino, D. T., Rezaii, P., Hochberg, L. R., Henderson, J. M., & Shenoy, K. V. (2020). Hand Knob Area of Premotor Cortex Represents the Whole Body in a Compositional Way. *Cell*, *0*(0). https://doi.org/10.1016/j.cell.2020.02.043

Wing, A. M. (2000). Motor control: Mechanisms of motor equivalence in handwriting. *Current Biology*, *10*(6), R245–R248. https://doi.org/10.1016/S0960-9822(00)00375-4

Woolsey, C. N., Settlage, P. H., Meyer, D. R., Sencer, W., Pinto Hamuy, T., & Travis, A. M. (1952). Patterns of localization in precentral and "supplementary" motor areas and their relation to the concept of a premotor area. *Research Publications - Association for Research in Nervous and Mental Disease*, *30*, 238–264.

Yeo, B. T. T., Krienen, F. M., Eickhoff, S. B., Yaakub, S. N., Fox, P. T., Buckner, R. L., Asplund, C. L., & Chee, M. W. L. (2014). *Functional Specialization and Flexibility in Human Association Cortex*. https://doi.org/10.1093/cercor/bhu217

Yu, X. J., He, H. J., Zhang, Q. W., Zhao, F., Zee, C. S., Zhang, S. Z., & Gong, X. Y. (2014). Somatotopic reorganization of hand representation in bilateral arm amputees with or without special foot movement skill. *Brain Research*, *1546*, 9–17. https://doi.org/10.1016/J.BRAINRES.2013.12.025

Zhang, C. Y., Aflalo, T., Revechkis, B., Rosario, E., Ouellette, D., Pouratian, N., & Andersen, R. A. (2020). Preservation of Partially Mixed Selectivity in Human Posterior Parietal

Cortex across Changes in Task Context. *Eneuro*, *7*(2), ENEURO.0222-19.2019. https://doi.org/10.1523/eneuro.0222-19.2019

Zhang, C. Y., Aflalo, T., Revechkis, B., Rosario, E. R., Ouellette, D., Pouratian, N., & Andersen, R. A. (2017). Partially Mixed Selectivity in Human Posterior Parietal Association Cortex. *Neuron*, *95*(3), 697-708.e4. https://doi.org/10.1016/j.neuron.2017.06.040